THE UNIVERSITY OF SYDNEY

HONOURS THESIS

STRAIN MEDIATED BAND GAP ENGINEERING OF BENT SEMICONDUCTOR NANOWIRES FROM FIRST PRINCIPLES

Author:
BRYAN LIM
BE Mechanical (Space)

Supervisors:
PROFESSOR SIMON RINGER
DR. CARL CUI

An honours thesis submitted in partial fulfilment of the requirements for the degree of Bachelor of Mechanical Engineering (Space), from the School of Aerospace, Mechanical and Mechatronic Engineering, Faculty of Engineering and Information Technologies, the University of Sydney

November 2018

I hereby declare that this thesis is my own work and that the findings in this thesis were not taken from any other published works. Any assistance I received in my research and in the writing of this thesis was acknowledged in the following contribution statement. All information sources and literature used in this thesis were clearly given reference to.

Bryan Lim

Acknowledgements

I would like to acknowledge the staff of the Australian Centre for Microscopy & Microanalysis (ACMM) for their help and input during the writing of this thesis.

I would like to thank my supervisors, Simon and Carl for giving me the opportunity to conduct this research under their guidance. I would like to specially thank Carl for his expertise and knowledge in the subject matter, and his invaluable support in the writing of this thesis. Furthermore, I would like to acknowledge the invaluable support provided by my friends and family during the preparation of this thesis.

This research could not have been completed without the computing resources from the National Computational Infrastructure (NCI) supported by the Australian Government's National Collaborative Research Infrastructure Strategy (NCRIS).

Contribution Statement

All work in this thesis was the work of Bryan Lim under the guidance of Professor Simon Ringer and Dr. Carl Cui unless stated otherwise. Other contributions to the work if not listed below were given clear reference to within this thesis.

1. Literature survey was conducted by myself.
2. Methodology was designed with the assistance and guidance of Dr. Carl Cui.
3. Methodology was implemented by myself.
4. Convergence tests on all bulk structures were performed by Dr. Carl Cui.
5. Simulations were performed entirely using the VASP code.
6. Calculations on bulk band structures and density of states were performed by myself.
7. Simulation of strain application on all structures were performed by myself.
8. Calculation & plotting of all strain-mediated band structures were done by myself.
9. All tools used for data analysis from the raw outputs of VASP were scripts written by myself in MATLAB.
10. Analysis of results were performed by myself. The conclusions found were my own, influenced by discussion with Dr. Carl Cui.

The above represents an accurate summary of the student's contribution.

Supervisor: _____ Simon Ringer

Student: _____ Bryan Lim

Abbreviations and Nomenclature

ab initio – From first-principles

BZ – Brillouin zone

CBM – Conduction band minimum

DFT – Density functional theory

DOS – Density of States

LDA – Local-density approximation

GGA – Generalised gradient approximation

HF – Hartree-Fock method

HSE – Heyd-Scuseria-Ernzerhof functional

NW(s) – Nanowire(s)

VASP – Vienna *ab initio* Simulation Package

VBM – Valence band maximum

WZ – Wurtzite

ZB – Zinc-blende

Å – Angstrom, 1Å = 10^{-10}m

eV – Electron-volt (energy), 1 eV = 1.60218 x 10^{-19}J

Chemical Elements:

As – Arsenic

Ga – Gallium

Ge – Germanium

In – Indium

N – Nitrogen

O – Oxygen

S – Sulfur

Sb – Antimony

Si – Silicon

Zn – Zinc

Abstract

Semiconductor nanowires (NWs) exhibit both extraordinary mechanical properties and excellent control in the conduction of electrons. NWs present a unique system to explore physical phenomena on a quantum scale and play a critical role in future electronic and optoelectronic devices. The band gaps of semiconductors are commonly tuned to exhibit desired behaviours through means such as alloying or doping. However, a novel method proposed in this work is the use of strain, due to large recoverable elastic strains observed in NWs. Of particular interest is that of strains exhibited in bent NWs; where simultaneous compressive and tensile strains occur along its cross-section. Herein, an *ab initio* investigation on strain-mediated band gap engineering of bent semiconductor nanowires, was performed using density functional theory (DFT). There are difficulties in simulating bent NWs due to symmetry loss in all directions in the bent structure. By considering that compressive and tensile strain occur simultaneously, this thesis proposes a simplified approach to simulating band gap evolution with strain, by using unit cells under tensions and compressions separately. Furthermore, it is well documented that the minute radial dimension of NWs induces solid state phenomena such as the quantum confinement effect and internal strains; which have considerable contributions to band gap modulation. Separation of the effects of these phenomena with external strain application to band gap evolution can be performed using the proposed simplified unit cell model. Both wurtzite (WZ) and zinc-blende (ZB-(111)) polytypes of III-V and II-VI semiconductors were considered in this study. Simulations implementing DFT were performed in the Vienna *ab initio* Simulation Package (VASP), using the hybrid HSE06 functional.

III-V and II-VI semiconductors were considered as a means of alternatives to the short comings of common group IV semiconductors such as silicon, namely its indirect band gap which offers limited use in optoelectronics. These semiconductors have wide

direct band gaps, and high optical absorption/emission coefficients. The semiconductors considered were: GaAs, GaN, GaSb, InAs, InP, ZnO & ZnS. Three main behaviours were observed in the band gap evolution with strain application, named types A, B & C. These were in order: inversely linearly proportional to strain, immediate reduction of band gap with strain and a 'compression shifted peak' reduction of band gap with strain. Representative emission spectra of these behaviours were surmised and were in order, spectra broadening, spectra red shifting, and spectra splitting; resulting in simultaneous red & blue shifting. Furthermore, it was noted that band gap modulation was much more sensitive to tensile strains in all structures par WZ GaSb; where both strains had similar effects. Orbital variation under strain was also analysed to rationalise the band gap behaviours of all semiconductor structures. It was surmised that band gap evolution with strain in III-V & II-VI semiconductors was strongly dependent on both the chemical compositions and specific crystal structures. The implications of the results garnered in this study proposes that strain mediation gives complete control in band gap modulation and hence, emission behaviour of the III-V & II-VI semiconductors considered. The findings of this thesis are applicable to both bulk and NW scales due to the use of unit cells; and pave the way to new novel applications of strain-mediated band gap modulation of semiconductors. This includes fields such as optoelectronics, field emission, flexible piezotronics, and nanoelectromechanical systems (NEMS).

Contents

1.0 Introduction

Semiconductors are perhaps one of the most important materials in modern electronics. Silicon (Si), the most widespread semiconductor material, has fuelled our daily lives for decades; through uses in devices and systems such as sensors, transistors, diodes, and solar panels. Semiconductors are materials with electron conductivity values between that of conductors such as copper & gold, and insulators like glass. Also, unlike metals their resistance decreases with an increase in temperature.

The band gap, a measure of their electron conductivity, is arguably the most critical parameter for applications of semiconductors. It represents the minimum required energy to excite an electron up to a state where it can participate in conduction. Many methods exist to manipulate this property, the most common of which include: introduction of impurities into their crystal structure (doping), modifying the composition of the semiconductor (alloying), layering semiconductors with alternating compositions, or through application of electric fields or light.

Because the electrical properties of semiconductors can be easily manipulated, it makes them great materials to be used in devices for amplification, switching and energy conversion. By changing the morphology of semiconductors to a nanowire (NW) structure, however, begs the question of what significant advances or changes would be present in the semiconductor?

Nanowires (NWs), per their namesake are structures that take the form of wires with diameters in the nano length scale (1nm = 10^{-9}m). Since the advent of NWs there have been many breakthroughs in its use such as its ability to interface with living cells, greatly improving the efficiency of solar cells and frabrication of multicoloured light emitting diodes (LEDs) on a single substrate[1].

There are significant property changes that occur when the size of a semiconductor is reduced to the quantum scale. For instance, at room temperature, bulk Si is considered

to be a good thermal and electron conductor whilst rough Si NWs are good thermal insulators and electron conductors[1]. Within the scope of semiconductors, it is unquestionable the property of main interest is that of the electronic band structure[2][2].

It is well documented that band gap modulation of semiconductors can occur through lattice strain, induced through lattice mismatches in the variation of alloying composition[3]. These lattice mismatches are static; the strains and gap modulation that occur are hence permanent in the resultant semiconductor structure. However, a key advantage for NWs are the significant recoverable elastic strains they have of up to 10%[4–6]. Hence, the elastic nature of NWs give rise to possible novel band gap modulation methods such as actuator applied strain to allow greater control in band gap.

There have been few previous studies on strain application for band gap modulation of bent NWs; with interesting experimental and theoretical results such as direct to indirect gap transitions [7,8] and changes in band gap type (direct band gap in bulk GaSb to indirect as a NW)[9]. However, systematic investigations have yet to be conducted to highlight trends between groups of semiconductors, and to classify possible strain & band gap behaviours.

Particularly of interest when it comes to studying materials on the nanoscale are those of first principles (or *ab initio*) methods; which determines a material's intrinsic properties purely through simulating its interatomic interactions. This makes it a much more powerful and accurate method than others such as molecular dynamics which usually rely on empirical parameters. One such method of interest is density functional theory (DFT), which has been an increasingly popular field of study.

Herein, a first principles study will be conducted to investigate the band gap behaviour of bent semiconductor NWS through hybrid implementations of DFT[10,11] and the Hartree-Fock (HF) method, based on the hybrid Heyd-Scuseria-Ernzerhof (HSE)[12] functional within the Vienna *ab initio* Simulation Package (VASP) [13–16].

2.0 Critical Literature Review

Here, the interest in nanomaterials in the form of NWs is justified and III-V[1] and II-VI[2] semiconductor materials are chosen to be analysed. These materials provide possible solutions and alternatives to the short comings of Si based semiconductors, namely its indirect band gap, as well as novel properties including high optical absorption/emission coefficients & existence of wide direct band gaps[17,18].

2.1 The Rise of Nanomaterials

There is no doubt interest in nanomaterials has significantly increased over the ages, the most well-known of which, graphene, consisting of a two-dimensional (2D) sheet of covalently bonded carbon atoms had its intrinsic strength predicted to exceed that of any material currently known[19]. Comparing this to its common bulk form, graphite, an exceedingly brittle material shows how drastically the material properties can alter.

Nanoscale material provide a promising avenue of research, especially in the electron and thermal transport properties with respect to semiconductors. NWs are a common semiconductor nanomaterial structure and its related topics, have been studied in greater depth over time, as shown in Figure 1.

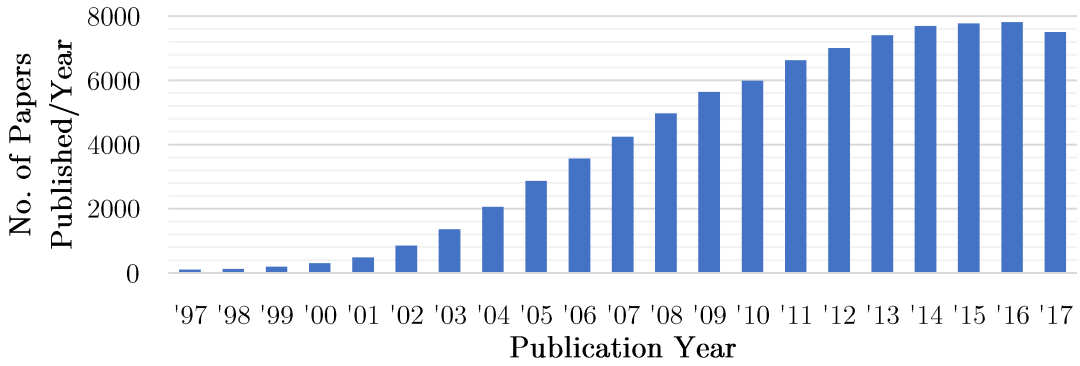

Figure 1 - Increasing number of publications for NW topics. (Source: Web of Science (Oct -2018), keyword: nanowires).

[1] III-V semiconductors refer to materials consisting of group 13 (III) and group 15 (V) elements.
[2] II-VI semiconductors refer materials consisting of group 2 or 12 (II) and group 16 (VI) elements.

The diameter of NWs (1 – 100nm) puts the radial dimension of them at or below the characteristic length scale of various solid state phenomena (see Figure 2) including: exciton bohr radius, mean free photon path, wavelength of light and many others.[2] This results in many physical & electronic properties which differ from their bulk forms, such as a direct band gap in bulk GaSb to indirect as a NW[9].

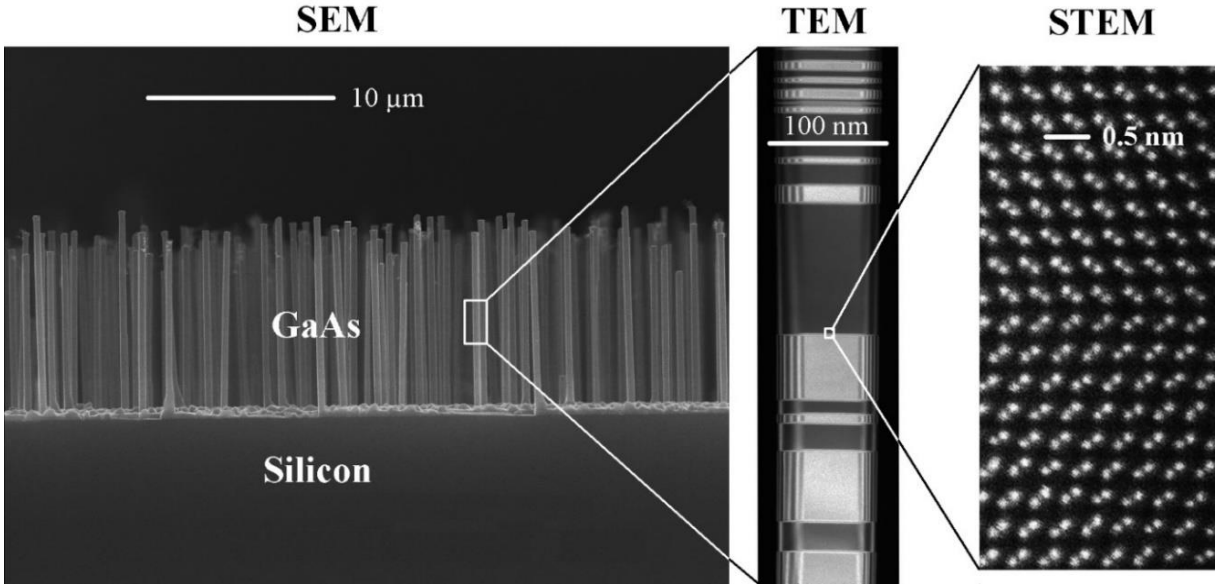

Figure 2 - Comparative size of NWs.[3] *Image (left) shows SEM (Scanning Electron Microscope) of GaAs NWs grown on Si Substrate, (middle) shows TEM (Transmission Electron Microscope) image of single NW, (right) shows STEM (Scanning Transmission Electron Microscope) imaging showing atomic columns.*

For use as a semiconductor structure, a key parameter in NWs is aspect ratio; the proportional relationship between its length and its diameter. NWs have an extraordinary large aspect ratio, and this unique one dimensionality allows for ease in controlling the conduction of quantum particles (electrons) along its length[1,2].

An example of an interesting application of NWs is a nanogenerator based on ZnO NWs; developed to power battery-free wireless nanodevices via a conversion of bending induced movement & ambient vibration to electricity[21]. Furthermore, NWS allow interfacing with living cells due to their minute cross-section and high surface area.

[3] Source: Niels Bohr Institute.[20]

Si NW transistor arrays have been successfully used for the detection, and manipulation of cell neuronal signal propagation[22]. The high aspect ratios of NWs allow for minimal invasiveness whilst maintaining proper cell communication.

The large range of possible novel application of semiconductor NWs make them an avenue of great interest for this thesis.

2.2 III-V and II-VI Semiconductors

Group IV[4] semiconductors such as silicon (Si) and germanium (Ge) have been studied extensively over the last century. Si in particular, due to its abundance, mechanical strength, and great electronic transport properties is currently the most used semiconductor.[23] A large issue however, is the existence of an indirect band gap in Si. This offers limited performance for microwave and optoelectronic applications. As Si does not emit light (indirect band gap), with increased use of semiconductors in light-related applications, such as in light emitting diodes (LEDs), solar photovoltaics & camera sensors, this poor performance in optoelectronics presents a significant challenge for the semiconductor community.

As such, to overcome the shortfalls of Si semiconductors, group II-VI semiconductors such as ZnO have been investigated as alternatives. II-VI materials are direct band gap semiconductors with high optical absorption and emission coefficients[17]. This makes them popular for high energy (short wavelength, high frequency) optoelectronic applications. Similarly, III-V semiconductors are also direct gap semiconductors with wide band gaps, and are widely used in microelectronics and optoelectronics due to their outstanding electronic and optical properties[18] and thermochemical stability[24].

[4] Group IV semiconductors refer to materials containing group 14 (IV) elements.

It is important to note that polytypism occurs in III-V and II-VI materials[25] in the form of either a zinc blende (ZB) lattice structure or wurtzite (WZ)[5] crystal structure. Polytypism is a special form of polymorphism occurring in layered materials; where they have the same chemical composition but differ only in the stacking manner of the layers.

This gives a large variety of stoichiometries to analyse between both semiconductor groups. WZ-ZB polytypism is governed by iconicity[25,26], whereby ZB phase is favoured as the atomic number of the anion constituents increase. Under pressure, the structure of the III-V and II-VI semiconductors however can be changed between WZ and ZB structures[27,28] and hence analysis of the effects of strain on both structural types for each III-V and II-VI material will be conducted. The semiconductors of interest are listed as follows:

- III-V: GaAs, GaSb, GaN, InAs, and InP.
- II-VI: ZnO, and ZnS.

2.2.1 Bulk Properties

A table aggregating current data in literature on bulk III-V and II-VI semiconductors of interest can be seen in Table 1. These results were used to fine tune simulation parameters for VASP calculations and validate computational methods & accuracy. Data from literature is listed alongside the final computed results. Calculation methodology and parameters are more closely explained in Chapter 4.0.

The parameters of interest were: the lattice constants a & c, cohesive energy E_{coh}, and band gap E_g. The total energies of the systems were calculated to determine the lowest energy structural state but not used for direct comparison to literature. Instead

[5] When not explicitly stated, crystallographic orientation of structures can be assumed to be standard; (001) for ZB and (0001) for WZ.

cohesive energy, the energy required to the atoms of a solid into isolated atomic species, was used and can be calculating using Equation 1.

$$E_{coh} = \frac{1}{N}\left(\sum_{n} S_n E_{atom_n} - E_{tot}\right) \quad (1)$$

E_{atom} is the total energy of a single atom of an element (eV), E_{tot} is the total energy of the structure (eV), S is total number of atoms of an element in the structure & N is the total number of atoms in the structure.

		a (Å)	c (Å)	E_{tot} (eV/f.u.)	E_{coh} (eV/f.u.)	E_g (eV)
GaAs $\alpha = 0.26$	**wz**	**3.981** 4.050[d1], 3.955[d2]	**6.575** 6.678[d1], 6.526[d2]	**-4.986**	**6.761**	**1.473** 1.284[d1], 1.861[d2], 1.351[f1], 1.467[f2]
	zb	**5.654** 5.614[d2], 5.632[e], 5.66[q6]		**-5.001**	**6.792** 6.710[e]	**1.436** 1.640[c1], 1.774[d2], 1.43[q6]
GaN $\alpha = 0.30$	**wz**	**3.203** 3.199[a1], 3.189[a4], 3.181[h]	**5.199** 5.226[a1], 5.186[a4], 5.166[h]	**-7.674**	**9.561** 9.265[a1], 9.058[a4]	**3.428** 3.50[q7], 3.320[g]
	zb	**4.522** 3.538[a1], 4.460[a2], 4.500[g]		**-7.664**	**9.541** 10.880[a1], 10.982[a2]	**3.212** 3.299[q7], 2.810[c1], 3.200[c2], 3.070[g]
GaSb $\alpha = 0.23$	**wz**	**4.303** 4.310[j]	**7.079** 8.145[j]	**-4.489**	**6.097**	**0.716** 0.835[b1], 0.503[j]
	zb	**6.102** 6.094[i], 6.096[q2]		**-4.506**	**6.132**	**0.820** 0.783[b1], 0.810[h1], 0.720[h2], 0.820[h3]
InAs $\alpha = 0.26$	**wz**	**4.312** 4.1921[k], 4.256[m]	**7.074** 6.844[k], 7.004[m]	**-4.646**	**6.127**	**0.471** 0.205[k], 0.461[m], 0.458[q3]
	zb	**6.109** 5.921[k], 6.195[l1], 6.030[l2], 6.036[l3]		**-4.656**	**6.147** 5.944[l1], 7.586[l2], 4.487[l3]	**0.405** 0.192[k], 0.400[l1], 0.420[l3]

Table 1 continued on next page

		a (Å)	c (Å)	E_{tot} (eV/f.u.)	E_{coh} (eV/f.u.)	E_g (eV)
InP $\alpha = 0.26$	**wz**	**4.172**	**6.838**	**-5.012**	**6.634**	**1.500**
		4.054[k]	6.625[k]			1.270[k], 1.576[b1]
	zb	**5.908**		**-5.018**	**6.647**	**1.426**
		5.870[n4], 5.729[k]				1.42-1.432[n4], 1.475[a3], 1.232[k]
ZnO $\alpha = 0.38$	**wz**	**3.258**	**5.236**	**-6.370**	**8.174**	**3.408**
		3.286[n3], 3.250[n4]	5.241[n1], 5.205[n4]		7.692[n2], 7.520[n4]	3.400[n2], 3.770[n4]
	zb	**4.581**		**-6.357**	**8.148**	**3.274**
		4.619[o2], 4.463[o3]			7.679[o1]	3.36-3.37[q4], 1.486[p2]
ZnS $\alpha = 0.35$	**wz**	**3.845**	**6.303**	**-4.526**	**6.498**	**3.810**
		3.814[q5]	6.527[q5]			2.232[p1], 2.283[p2], 3.920[q5]
	zb	**5.419**		**-4.528**	**6.502**	**3.808**
						3.660[c1], 3.910[c2]

Table 1 - Bulk Semiconductor Material Properties. Data types listed below:
a1 – GGA, a2 – LDA, a3 – LDA-1/2, a4 – Experimental [29]
b1 – LDA-1/2, b2 – Experimental.[30]
c1 – MBJ-LDA, c2 – Experimental.[31]
d1 – GW-GGA, d2 – GW-LDA[7]
e – LDA.[32] *f1 – GW-LDA, f2 – Experimental.[33]*
g – G0W0.[34] *h1 – B3LYP, h2 – HSE, h3 – Experimental.[35]*
i – Bloch Functions.[36] *j – LDA.[37]* *k – LDA.[38]*
l1 – GGA-EV, l2 – LDA, l3 – Experimental.[39]
m – MBJ-LDA.[40]
n1 – SIC-LDA, n2 – LDA, q3 – HF, n4 – Experimental.[41]
o1 – GGA, o2 – HF, o3 – Experimental.[42]
p1 – GGA, p2 – LDA+U.[43]
q – Experimental. q1;[44], q2;[45], q3;[46], q4;[47], q5;[48] q6; [49], q7; [50].

Bolded entries are values calculated in this study using the HSE06 functional[51] in VASP, and values listed underneath were found in the literature. Data types for values found in literature are also shown however, explicit comparison upon the merits of each calculation method was omitted; as data was used purely for tuning the computational parameters in this thesis. The HF fraction, α, for the hybrid exchange-correlation was

also denoted and the underlined lattice structure represents the lowest energy structural state found. All semiconductors were found to be direct band gap semiconductors in agreement with the literature.

2.3 Strain-Mediated Band Gap Engineering

The effects of strain on semiconductors and its physical mechanisms has been well documented and researched since the early 1950s. The earliest of those, was the development of variable strain transducers developed to exploit the piezoresistive effect in Si and Ge[52]. Manipulation of electronic properties using strain can be traced to an early predecessor of strained Si to enhance metal-oxide-semiconductor field-effect transistor (MOSFET) performance, where researchers showed enhanced electron mobility in n-type Si/Ge_xSi_{1-x} multilayer heterostructures[53] and hole mobility in p-type Si/Ge_xSi_{1-x} double-heterostructures[54]. One of the leading factors for this was attributed to strain caused by lattice mismatch.

Effects of strain on band structures are well understood. Taking Si as an example, hydrostatic strain reduces its atomic bond lengths. Reduced interatomic distances enhances the interatomic electronic wave function[6] overlap and its interactions are strengthened[55]. This results in increased splitting between bonding and antibonding orbitals; widening the band gap. As such, strain effects on band structures are governed by bond stretching and rotation[55]. Though the mechanism allowing strain-mediated band gap modulation is understood, the behaviour of strain on the interactions between differing orbitals are not necessarily the same within different system. Hence, a reduction

[6] In atomic theory and quantum mechanics, an atomic orbital can be described using a wave function. This electronic wave function describes the behaviour of an electron or pair of electrons in an atom. It can be used to calculate the probability of finding any electron of an atom in any specific region around the nucleus.

of band gap with compressive strains (hydrostatic) and the inverse effect with tensions may not be ubiquitous and will be a target of focus in this thesis.

For clarity, Figure 3 show an example of an electronic band structure for ZB GaAs. The electronic band structure of semiconductors describes the range of energies than an electron may have (energy bands) and ranges of energy that it may not have (band gaps). The usage of the term band gap, with respect to the conductivity of a semiconductor, refers to the energy difference between the conduction band minimum (CBM) and valence band maximum (VBM). This energy difference represents the minimum amount of energy required for a valence electron to transition to the conduction band and be used for conduction.

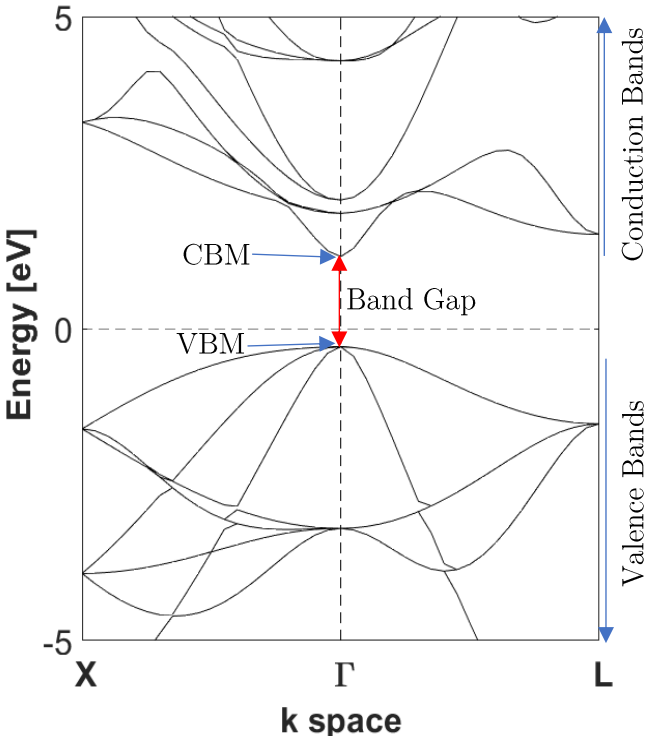

Figure 3 - Electronic Band Structure for ZB GaAs.

Interest in the use of a mechanical mechanism (strain) to modulate an electronic property (band gap) with bent semiconductor NWs, stems from their large recoverable strains; which are between 3-10% and elastic in nature [4–6]. Lattice mismatches (for inducing strain) used in bulk studies are a useful and economic way to tune device performance. Large elastic strain limits due to nanoscale dimensions allow for greater control in semiconductor composition and variation; as these band gaps can be widely tuned at the nanoscale without detrimental effects often evident in bulk materials.[3] Understanding the atomic mechanisms and behaviour for strain induced change in the electronic band structure gives way to use in novel flexible piezotronics and nanoelectromechanical systems (NEMS).

Application of strain engineering in modulating band gaps of semiconductor NWs (type IV, III-V and II-VI) have been met with much success both experimentally and theoretically [56–58], showing relation between strain application and gap energy shift.

Currently, experimental & theoretical studies exist for the use of bent NWs in band gap modulation for ZnO, CdS & Si NWs. [4,58–60] However, a systematic theoretical study is currently lacking. Interest in bent NWs also stem from the simultaneous existence of compressive & tensile strains along the cross-section of the NW.

As shown in Figure 4, line intensity profiles of lattice distortions in the bent NW provides evidence for tensile strains along the outer edge transitioning to compressive strains at the inner edge. Strain application on straight NWs allow only compressive or tensile strain effects to be studied individually. Comparatively, bent NWs are advantageous; as it allows for a complete profile of strain & band gap behaviour to be observed and analysed to elucidate possible trends or gap-transition behaviours.

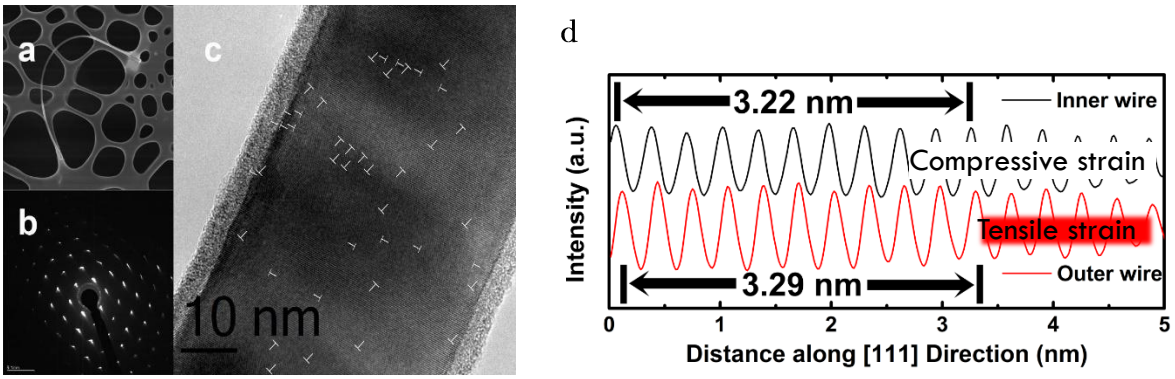

Figure 4 - Micrographs of a Bent GaAs NW.[7] *a – SEM graph, b – SAED pattern, c – HRTEM image, & d – Line intensity profiles of lattice distortion.*

The characteristics of strain & band gap behaviour of semiconductors are heavily orientationally and structurally dependent. In both bulk and NW studies, it was observed that crystallographic orientation, size and structure of material heavily impacts the effects of strain on the band structure[61–63].

[7] Source: Bao et al.[6]

Furthermore, effects of internal strain greatly vary the possible changes in band structure. Internal strains refer to all energy stored within the material when undergoing stresses/strains; these include Van der Waals, torsional, and ring strain. Without internal strain, strain & band gap dependence has very little relation with strain orientation due to isotropic conduction band dispersion around the conduction band minimum (CBM) [61]. Existence of internal strain operates unfavourably for gap transitions which may be a desirable effect.

Alternatively, the size and cross-sectional shape of NWs also effect electronic band behaviour. Due to inducement of the quantum confinement effect, the band gap of a NW reduces with increasing thickness[62]. This effect refers to the change of electronic and optical properties observed when the diameters of a material is of the same magnitude as the de Broglie wavelength of an electron wave function[64,65].

An example of this observation can be seen in WZ & ZB-(111) InAs NWs; where the quantum confinement effect was observed to have a strong effect on the conduction bands with a smaller effect on the valence bands[66]. As such, upon application of strain, separation of strain effects and quantum confinement effects of band gap behaviour need to be quantified. Furthermore, under certain structural conditions or stacking types, semiconductor NWs may no longer behave as a semiconductor[56] and hence coherent directionality of WZ and ZB structures need to be specified.

2.4 WZ-(0001) and ZB-(111) Structure Orientation

The standard orientation of WZ & ZB are WZ-(0001) & ZB-(001). ZB-(001) resembles a face centred cubic (FCC) structure, whilst ZB-(111) and WZ-(0001) are coherent and have a hexagonal closed pack (HCP) structure. This coherency can be seen in their stacking sequence, where ZB-(111) follows a stacking sequence of A-B-C and WZ-(0001) has an A-B stacking order. Each letter represents a bilayer of III-V or II-VI pair, as seen in Figure 5. 3-D unit cell visualisations of these structural orientations were created using the VESTA program[67].

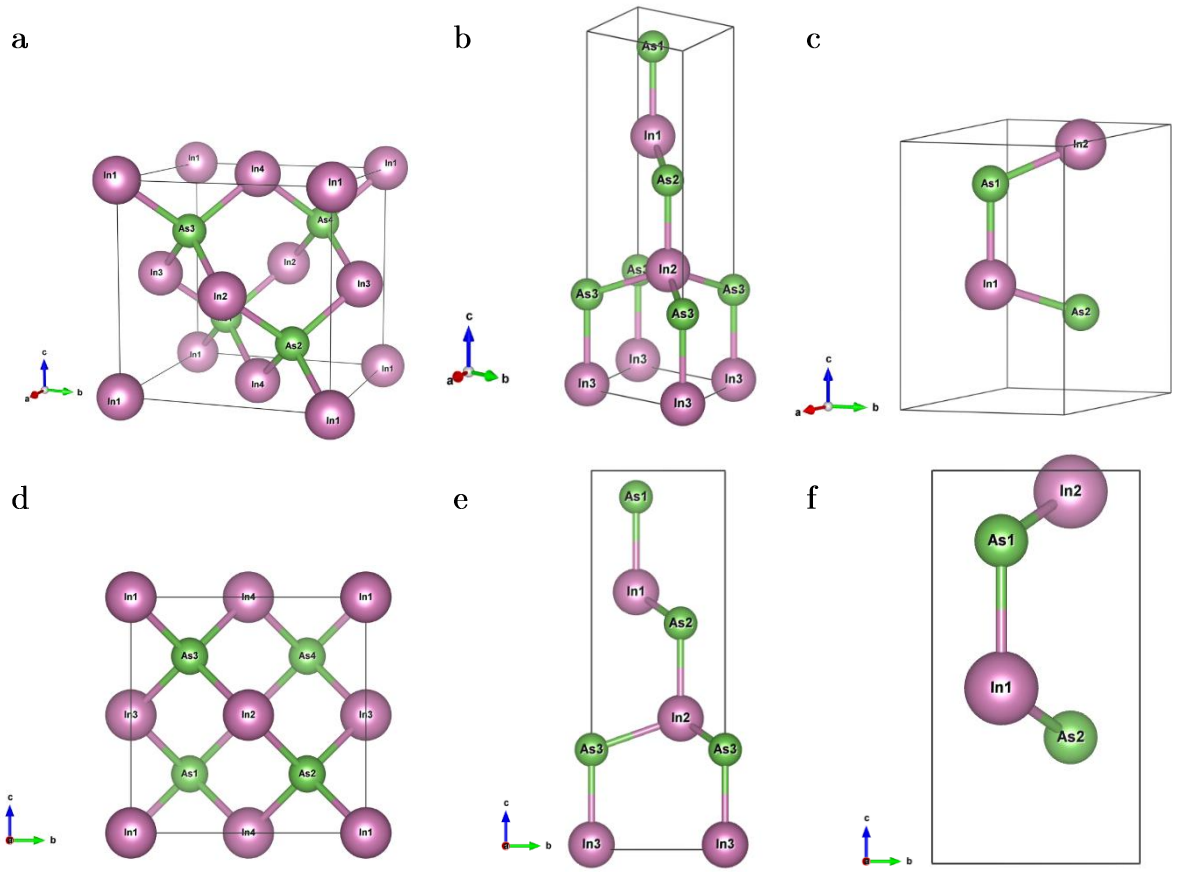

Figure 5 - InAs unit cells of; a – ZB-(001), b – ZB-(111), c – WZ-(0001). d-f show side view of structures respectively.

Unit cells of these orientations consisted of 8 atoms for ZB-(001), 6 atoms for ZB-(111), & 4 atoms for WZ-(0001), with equal part constituents of each element. Experimental growth of III-V & II-VI semiconductor NWs have also been shown to have a tendency to grow in the WZ-(0001) and ZB-(111) orientations.[68,69] Hence, focusing on

these orientations within this *ab initio* study would allow results to be comparable between the 2 structures as well as allow reproduction of results in an experimental framework.

There are challenges in simulating bent NWs due to the loss of symmetry conditions in all dimensions. A simplified bulk unit cell model was considered to mimic strain behaviour on a bent NW; as interest stems from the profile of strains along the cross-section of the NW as opposed to the length of the NW. As simultaneous compressions and tensions occur along the cross-section, a simplified approach was implemented by using unit cells under tensile and compressive strains separately to simulate this strain behaviour.

This proposed model can be examined in Figure 6. Along the cross-section of a bent NW, strain (tension toward outer edge or compression toward inner edge) would only be applied on the ***c*** axis of the NW. This would result in the other 2 lattice constants relaxing accordingly to the strain application to the ***c*** axis. Hence, the difficulties in simulating bent NWs can be validly overcome with a simplified bulk model of various strains applied to the c axis.

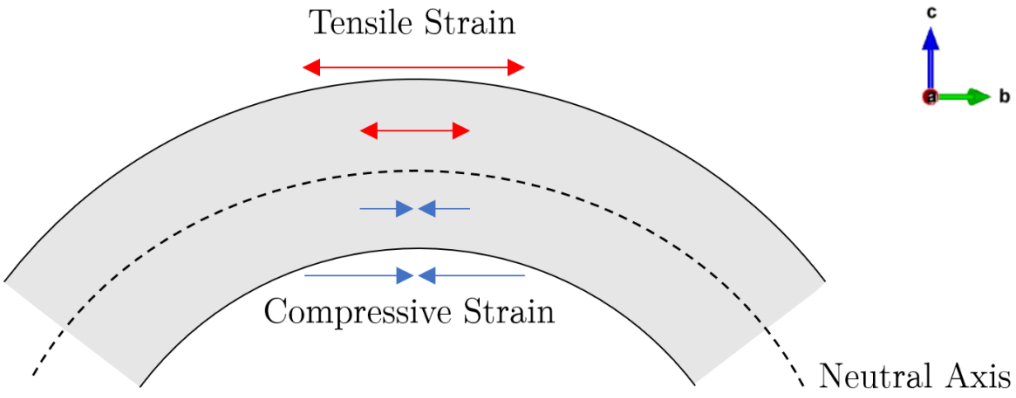

Figure 6 - Strain applied on a bent NW.

Furthermore, the use of a bulk unit cell in this study eliminates external effects on the band structure. As aforementioned, it is well understood that internal strains and the quantum confinement effect have large contributions to the modulation of band gaps

in NWs. The use of unit cells eliminates these external factors as well as possible surface effects on the NW structure itself which too has significant effects on band gap.

2.5 Strain-Mediated Band Gap Modulation

Previous investigations into the application of strain on band gap modulation for III-V and II-VI semiconductor NWs of interest are analysed in the succeeding subsections.

2.5.1 III-V Nanowires

GaAs

A noteworthy result found in literature for WZ GaAs NWs was a direct-indirect band gap transition occurring when the diameter of the NW was reduced to less than 28Å.[70] The same *ab initio* study also discovered that this indirect band gap could be tuned to be direct under external uniaxial strain (both compressive and tensile). This study was furthered by Peng et al.[71] where the same indirect WZ NW structure was analysed alongside a ZB-(111) structure. For the WZ GaAs NW, there was an observed indirect-direct transition at strains of 2.8% and -0.8%[8]. It was also observed that the band gap decreased under both compressive or tensile strain. The ZB-(111) structure was reported as a direct gap semiconductor following the same trends, though the existence of a direct-indirect transition upon application of strain was not evident.

GaN

WZ GaN NWs display an interesting behaviour with application of uniaxial strain. A first principles study found that application of strains within bounds of ±9% causes band gap to increase with compression and decrease with tension linearly.[8] Increasing compressions from 6% to 9%, resulted in a direct to indirect band gap transition; causing band gap to rapidly decrease upon transition. These results were also found to be evident

[8] Per convention, positive strains refer to tension and negative strains refer to compression.

experimentally using x-ray diffraction (XRD); whereby under tensile and compressive loading, a red shift or blue shift of band gap was found, respectively.[72] It was also noted that effects of tensile stress were much more profound than compressive on the band gap. Currently, there were no previous investigations on ZB-(111) GaN.

GaSb

Both the WZ & ZB-(111) NW structures of GaSb acts as an indirect gap semiconductor as opposed to direct band gap in its bulk morphology.[9] In an *ab initio* study by Li-Ming et al., strains of ±4% was applied on both polytypes. Application of tensile strain decreases band gap and compressive strains increases band gap in the ZB-(111) structure. There was also an immediate indirect-direct gap transition due to application of tensile strain. The WZ NW experienced a decrease in band gap and indirect-direct gap transition upon both strain applications.[9]

InAs

In an *ab initio* study, ZB-(111) InAs had a linear reduction of direct band gap from application of -2.4 to 2.4GPa uniaxial stress; with an increase in band gap with compression and decrease with tension.[73] Application of stress has proportional relation to strain within the elastic limits of a material, with respect to Hooke's law; hence similar behaviour with strain application is expected. Another key finding reported was a direct to indirect transitions in the ZB-(110) structure when uniaxial stress was applied though this behaviour was not evident in the (111) orientation. Studies on WZ InAs were lacking.

InP

Currently no investigation has been performed for the strain-gap behaviour of InP NWs. However, in a strain-free context, there has been research performed by Wallentin et al. detailing the suitability of a ZB/WZ mixture of InP NWs as an alternative material to solar cell arrays, capable of achieving efficiencies of up to 13.8%.[74] It was found that NW

diameter and tip length directly affected cell performance. Application of strain to said NWs would be of interest as the combined effects of band gap modulation and volume change from this has yet to be explored.

2.5.2 II-VI Nanowires

ZnO

In a first principles study performed by Han et al.[4] theoretical and experimental results were obtained for strain effects on electronic behaviour of bent WZ ZnO NWs of varying diameters and also in its bulk form. Results concluded that compressive strain increases band gap whilst tensile strain decreases it. However, when diameters of the NW were reduced to <1nm, an application of compressive strain also caused a reduction of band gap. A reduction in diameter of the NW caused the strain effects to become lesser on gap-energy behaviour. Furthermore, it was found that significant band gap reduction occurs with decreased radius of curvature.

Experimentally, these results were confirmed [4,60,75] whereby, ZnO NWs were bent into different shapes of strain ranges showing significant deformation induced reduction in band gap (red shift) on outer tensile side and a blue shift on the inner compressive side; supporting theoretical findings that tensile strains are the main contributor to band gap reduction. Studies on ZB-(111) ZnO NWs were lacking however.

ZnS

Like InP, there still lacks an investigation in strain-mediated band gap engineering of ZnS NWs. However, ZnS NW arrays have been synthesised, unveiling optical and field emission properties of interest. In a study performed by Biswas et al., ZB-ZnS NW arrays were grown in the (111) direction and found to exhibit UV and blue light emission peaks at wavelengths of 350 and 397nm respectively, from room temperature photoluminescence (PL) measurements[76]. This gives rise to possible use as a field emitter

material, and by ascertaining the band gap behaviour upon strain application, these emission wavelengths can be manipulated.

2.5.3 Data Trends

An overall trend for strain & band gap behaviour for III-V & II-VI semiconductor NWs has not been produced prior to the work of this paper. Considerations classifying semiconductors as III-V, II-VI or within structural states as WZ or ZB-(111) do not elucidate a common trend like behaviour from the literature.

However, a pertinent finding was that the band gap transitions of the III-V semiconductors considered, were all due to a shift in the symmetry of the CBM in their band structures. [8,9,71] This would be a key area of consideration within this paper.

3.0 Aim

This thesis aims to investigate distinct correlations between external strain and band gap behaviour of group III-V & II-VI semiconductor NWs. This was conducted through *ab initio* implementations of strain on a simplified unit cell model, to simulate the behaviour of strain along the cross-section of a bent semiconductor NW. This was done with a focus to determine a common trend between coherent structures, semiconductor groups or specific orbitals.

Scope

WZ-(0001) and ZB-(111) polytypes of III-V & II-VI semiconductors.

- III-V: GaAs, GaSb, GaN, InAs and InP.
- II-VI: ZnO and ZnS.

4.0 Methodology

A key differing factor with this *ab initio* study to previous bent NW studies would be the application of strain on bulk unit cells to mimic strain effects on a bent NW. This alleviates possible surface effects, internal strains and quantum confinement effect on the band structure; as interactions between atoms are purely due to internal ionic interactions. This also allows results to be applicable to both bulk and NW scales.

4.1 Density Functional Theory

For this first principles study, VASP was used to perform implementations of density functional theory (DFT) using the HSE06 hybrid functional[51] based on the Perdew, Burke and Ernzerhof generalised gradient approximations (GGA) exchange correlation functional[77,78] to simulate molecular behaviour for strain applications. HSE06 functional was utilised over the standard HSE functional due to improvements in thermochemical results whilst allowing for accurate band gaps and lattice constants in solids[51].

This thesis delves heavily into DFT and assumes firm knowledge of solid-state physics with respect to materials engineering. The succeeding subsections covers a brief introduction into DFT, however if unfamiliar, further readings in references[79–81] are recommended.

4.1.1 Brief Overview

Density functional theory is a computational quantum mechanical method capable of deriving material properties through simulating the interatomic interactions in structures. It does so by approximating a solution to the Schrödinger equation with a one-electron approximation, using the Kohn-Sham assumption[11].

It is pertinent to understand that all aspects of material properties originate from its energetics and electronic structure. Fundamentally, solving for the allowed energy levels (of electrons) in a structure and the effects on the energy levels when atoms are

manipulated, allows its intrinsic properties to be determined[80]. To do this, one must be able to describe the many body interactions between the electrons and nuclei within the structure.

The form of the equation in mention is the time independent, non-relativistic Schrödinger equation: $H\psi = E\psi$. Whereby, H is the Hamiltonian operator and ψ is a set of eigenstates for the operator. As Hamiltonian operators are system dependent, many body interactions between electrons and nuclei can be defined explicitly as follows[80]:

$$\left[-\frac{\hbar^2}{2m}\sum_{i=1}^{N}\nabla_i^2 + \sum_{i=1}^{N}V(\boldsymbol{r}_i) + \sum_{i=1}^{N}\sum_{j<i}U(\boldsymbol{r}_i,\boldsymbol{r}_j)\right]\psi = E\psi \qquad (2)$$

Whereby, $\mathbf{m}$ is the electron mass, $\hbar$ is Planck's constant and $\mathbf{r}$ is the position vector of the electrons[80]. The 3 terms in the bracket, in sequence, define the: kinetic energy of each electron, interaction energy between each electron and the atomic nuclei and interaction energy between different elections.

For the Hamiltonian describing the many body interactions between nuclei and electrons, ψ is the electronic wave function for $\mathbf{N}$ number of electrons, $\psi = \psi(\boldsymbol{r}_1, \boldsymbol{r}_2, \dots, \boldsymbol{r}_N)$ and E is the ground energy state of the electrons.[80] For a single-molecule, defining and solving this eigenvalue equation would require a large multidimensional function. For instance, applying this to H_2O would require a 60-dimensional function (3 dimensions for each of its 20 electrons). When looking at a large nanocluster of atoms, the full wave function would scale equivalently large.

The defining quality of DFT however, is the many body wave function $\psi(\mathbf{r})$ is replaced by a system of single particle wavefunctions, $\phi(\mathbf{r})$, that only interact via electron density, $n(\boldsymbol{r})$, which is a function of only 3 spatial co-ordinates.[81] In doing so, within the Kohn-Sham scheme, the problem is reduce to solving a scheme of single-electron Schrödinger equations. The Kohn-Sham equations have the form shown in Equation 3.

$$\left[-\frac{\hbar^2}{2m}\nabla^2 + V(\boldsymbol{r}) + V_h(\boldsymbol{r}) + V_{XC}(\boldsymbol{r})\right]\phi_i = \epsilon_i\phi_i \tag{3}$$

These equations are superficially similar to Equation 2, where the key difference is the absence of summations that appear in the full Schrödinger equations. On the left-hand side, there are 3 potentials: V, V_h, and V_{XC}. The first potential is the same as that of the full Schrödinger and defines the interaction energy between each electron and atomic nuclei. The second potential is called the Hartree potential and defines the Coulomb repulsion between the current electron being considered and the total electron density defined by all electrons in the system. V_h contains a self-interaction contribution as the electron currently being considered is part of the total electron density. This is an unphysical phenomenon and is corrected for with the exchange – correlation potential, V_{XC}, the functional derivative of the exchange – correlation energy, E_{XC}.

$$V_{XC}(\boldsymbol{r}) = \frac{\delta E_{XC}(\boldsymbol{r})}{\delta n(\boldsymbol{r})} \tag{4}$$

The exact value of the exchange correlation energy, E_{XC}, is unknown and must be approximated to allow for this self-correction.

4.1.2 The Exchange Correlation Functional

A common approximation to E_{XC} used is the generalised gradient approximation (GGA) exchange correlation functional proposed by Perdew, Burke & Ernzerhof [80], and will be used in this thesis. In comparison to other exchange – correlation functionals such as local density approximation (LDA) and local spin density approximations (LSD), GGA tends to improve total energies & atomisation energies as it goes beyond LDA and LSD; by including density gradients which improve calculated results significantly.[77,82]

GGA and LDA are among the most popularly used functionals however, 2 key issues are evident with these exchange-correlation functionals; the first being a self-interaction error where the electron both contributes to the density and interacts with the density of the system[81]. The second is a consistent underestimation of band gaps of

systems, typically within orders of 50% or predicting metallicity in semiconductors[81]. This is caused in LDA due to the overbinding of a molecule; that is, lattice parameters are typically underpredicted, whilst cohesive energies, phonon frequencies, and elastic moduli are overpredicted.[83] On the other hand, GGA has a tendency to overcorrect LDA and underbinds molecules[84]; overestimating band gaps and underestimating binding energies[81]. Although GGA has improvements over LDA, there remains no improvement with respect to the band-gap problem.

A method to overcome this effect was first proposed by Becke in 1993[85], known as the hybrid functional method, where the exchange – correlation potential (V_{XC}) used can be calculated by mixing exchange correlation potentials from a DFT calculation (LDA or GGA) with a fraction of an exchange potential from Hartree-Fock (HF) methods.

$$V_{XC} = V_{XC}^{DFT} + \alpha(V_X^{HF} - V_X^{DFT}) \quad (5)$$

$V_{XC}^{DFT}$is the exchange correlation potential from a DFT calculation, V_X is the exchange potential contribution from HF or DFT. The term α is the fraction of HF used in the calculation of the exchange potential. Qualitatively, this equation mixes the contribution of these 2 differing methods to overcome the band-gap problem.

HF, another *ab initio* method, tends to overestimate band gap whilst DFT underestimates band gap;[86] hence a combination of the 2 can be used to counter each effects. The exact HF/DFT ratio, α, is entirely system dependent and requires convergence tests and comparison to experimental data to determine the exact ratio required. A common exchange – correlation functional that implements this is that of the Heyd, Scuseria & Ernzerhof (HSE) functional which utilises an error function screened Coulomb potential to calculate the exchange portion of the energy.[12]

Hence, for this thesis the HSE06 functional, which improves upon the HSE functional is used for all calculations. This uses a hybrid combination of the GGA exchange-correlation functional, with a fraction of HF as described in Equation 5.

4.2 Computational Details

Following the preceding outline and justification of DFT and hybrid functionals, the explicit computational details of this thesis shall be examined.

4.2.1 Initial Bulk Relaxation

The experimental structures for the aforementioned III-V and II-VI semiconductors were made available and obtained from the American Mineralogist Crystal Structure Database (AMCSD), courtesy of the Mineralogical Society of America and the University of Arizona[87]. Both WZ-(0001) and ZB-(001) polytypes of the semiconductors were obtained, being the standard crystallographic orientation of said structures, and full volumetric relaxation was performed using the hybrid HSE06 functional.

Unit cells of these bulk structures were used (as visualised in Figure 5) as opposed to creation of NW structures; in order to account for varying effects of quantum confinement with size of NWs, existence of internal strains and any possible surface effects on the behaviour of the electronic band structure.

A **Γ**-centred **k** mesh was utilised to sample the reciprocal lattice within the irreducible Brillouin zone (BZ) with sizes 6 x 6 x 4 and 6 x 6 x 6 respectively for WZ & ZB. These mesh sizes were chosen due to previous convergence tests[9], which found them to be of satisfactory accuracy. Energy convergence criteria for electronic and ionic iterations were 10^{-4} eV and 0.01 eV/Å, respectively for all calculations. It should also be noted that GGA based projector augmented wave method (PAW) potentials[88,89] were

[9] By supervisor X.Y. Cui.

used in the implementations of the DFT calculations in VASP to calculate the electronic structures. PAW allows DFT calculations to be performed with greater efficiency.

From initial relaxations, the lattice constants of the relaxed structures were found to be of sufficient accuracy when compared to literature however, comparison of band gaps and cohesive energies showed these initial values were found to be insufficient. To correct for this, the relaxed volumes (lattice constants) were fixed and further DFT calculations were performed wherein the HF fraction of calculations, α, was incrementally varied from the default value of 0.25 until sufficient accuracy was achieved. The final parameters of the fully relaxed bulk structures are shown in Table 1. These bulk parameters were used only to tune simulation parameters, and resultant α values were used in strained simulation parameters.

4.2.2 Convergence Test

A representative **k** mesh convergence test was conducted on InAs polytypes which were found to be in accordance with previous convergence test performed[10]. Alongside this, a convergence test for cut-off energy for plane wave basis sets, **ENCUT**, was performed. These results are tabulated in Appendix 9.2. The **k** mesh convergence tests for InAs WZ & ZB in terms of total energy, E_{tot}, and volume are shown in Figure 7 & Figure 8.

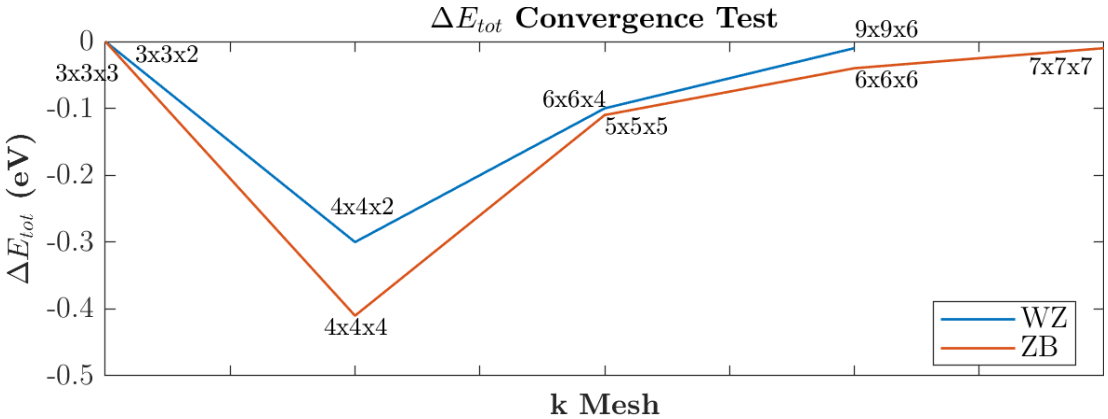

Figure 7 - Total Energy (E_{tot}) convergence test for WZ & ZB InAs.

[10] By supervisor X.Y. Cui.

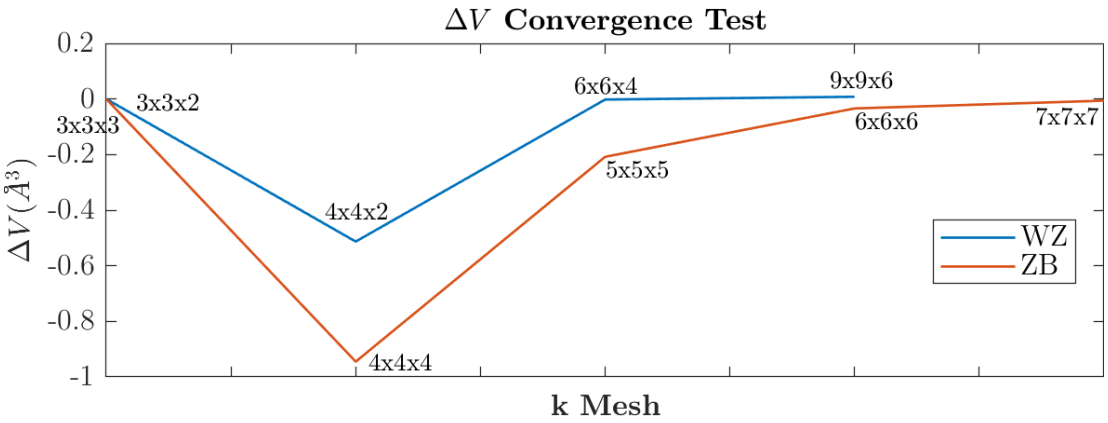

Figure 8 - Volume (V) convergence test for WZ & ZB InAs.

A summary of these convergence tests can be seen in Table 2, whereby the computational times, T, drastically increase with very minute gains in accuracy with increasing **k** mesh size. From a cost-benefit analysis, a 6 x 6 x 4 and 6 x 6 x 6 sized **k** mesh was justified in these representative convergence tests for WZ & ZB structures. A pertinent point is that **ENCUT** was not a fixed value and was system dependent; as PAW potentials are defined for individual elements. Hence **ENCUT** was set as approximately 2 times the default cut-off energy specified in the supplied PAW potentials for all calculations. Convergence tests shown in Appendix 9.2 show sufficient accuracy with this setting.

k mesh	ΔE_{tot}	ΔV	T (s)	T/T_0
3 x 3 x 2	0	0	2530.62	1
4 x 4 x 2	-0.3	-0.513	5838.76	2.31
6 x 6 x 4	-0.1	-0.002	76021.5	30.04
9 x 9 x 6	-0.01	0.008	150159	59.34

k mesh	ΔE_{tot}	ΔV	T (s)	T/T_0
3 x 3 x 3	0	0	5235	1
4 x 4 x 4	-0.41	-0.945	32667.9	6.24
5 x 5 x 5	-0.11	-0.208	44781.9	8.55
6 x 6 x 6	-0.04	-0.034	141710	27.07
7 x 7 x 7	-0.01	-0.006	151490	28.94

*Table 2 – InAs **k** mesh convergence results; WZ (left) & ZB (right). V = Volume (Å³).*

4.2.3 Unit Cell Transformation

The standard ZB-(001) and WZ-(0001) orientations of the semiconductor polytypes have an FCC and HCP structure, respectively. These have primitive lattice vectors ($\boldsymbol{a_{1,2,3}}$) as shown in Equation 6.[80]

$$\begin{bmatrix}\boldsymbol{a}_1\\ \boldsymbol{a}_2\\ \boldsymbol{a}_3\end{bmatrix}_{FCC} = a\begin{bmatrix}\frac{1}{2} & \frac{1}{2} & 0\\ 0 & \frac{1}{2} & \frac{1}{2}\\ \frac{1}{2} & 0 & \frac{1}{2}\end{bmatrix} \quad , \quad \begin{bmatrix}\boldsymbol{a}_1\\ \boldsymbol{a}_2\\ \boldsymbol{a}_3\end{bmatrix}_{HCP} = a\begin{bmatrix}\frac{1}{2} & -\frac{\sqrt{3}}{2} & 0\\ \frac{1}{2} & \frac{\sqrt{3}}{2} & 0\\ 0 & 0 & \frac{c}{a}\end{bmatrix} \tag{6}$$

The ZB-(111) orientation of the semiconductors was hence obtained from the relaxed ZB structures through the following magnitude relation and decomposed into the HCP primitive lattice vector:

$$\begin{bmatrix}\boldsymbol{a}_1\\ \boldsymbol{a}_2\\ \boldsymbol{a}_3\end{bmatrix}_{ZB_{(111)}} = \frac{1}{\sqrt{2}}\begin{bmatrix}1\\ 1\\ \sqrt{6}\end{bmatrix}\begin{bmatrix}\boldsymbol{a}_1 & 0 & 0\\ 0 & \boldsymbol{a}_2 & 0\\ 0 & 0 & \boldsymbol{a}_3\end{bmatrix}_{ZB_{(001)}} \tag{7}$$

With this step, the final structures and parameters were obtained for the strain-free and coherent WZ & ZB-(111) structures. All calculations for WZ-(0001) & ZB-(111) structures were performed using a **Γ**-centred 6 x 6 x 4 **k** mesh using the HSE06 functional unless explicitly stated otherwise. The same mesh was used for ZB-(111) due to lattice coherency with the WZ structure.

4.2.4 Strain Simulation

WZ and ZB-(111) lattice vectors can also be written in the form:

$$\boldsymbol{a_1} = a\left(\frac{1}{2}, -\frac{\sqrt{3}}{2}, 0\right),\ \boldsymbol{a_2} = a\left(\frac{1}{2}, \frac{\sqrt{3}}{2}, 0\right),\ \boldsymbol{a_3} = a\left(0, 0, \frac{c}{a}\right) \tag{8}$$

These lattice vectors represent the lattice constants: $\boldsymbol{a}$, $\boldsymbol{b}$ & $\boldsymbol{c}$ respectively in the unit cells. To simulate strain behaviour on bent NWs, for the given WZ and ZB-(111) structures (as exemplified in Figure 4), a strain, $\boldsymbol{\varepsilon}$, is applied on the $\boldsymbol{c}$ axis. Hence the

strain free lattice vector $\boldsymbol{a_3}$ was fixed and multiplied by a desired strain; where, $\boldsymbol{a_{3_\varepsilon}} = \varepsilon \cdot \boldsymbol{a_3}$. An HSE06 calculation was then run, allow geometric relaxation of only the remaining unknown strained vectors $\boldsymbol{a_{1_\varepsilon}}$ & $\boldsymbol{a_{2_\varepsilon}}$. In doing so, instead of applying a blanket volumetric strain on the structure, it was possible to mimic the behaviour of strain along the cross-section of a bent NW.

Although it was possible to perform atomic relaxations in 3 dimensions in VASP, a caveat was that it was not possible to fix a single lattice vector whilst allowing full volumetric relaxation. This was non-ideal with the method proposed to simulate strain along the cross-section of a bent a NW.

As the original strain-free lattice constant magnitude, $\boldsymbol{a}$, was known, the initial strained lattice constant was set as $\boldsymbol{a_{i_\varepsilon}} = (1+\varepsilon) \cdot \boldsymbol{a}$. The new strained lattice vectors are hence set as $|\boldsymbol{a_{1_\varepsilon}}| = |\boldsymbol{a_{2_\varepsilon}}| = \boldsymbol{a_\varepsilon}$ and calculations are run <u>without</u> allowing volumetric relaxation, and the total energy, $\boldsymbol{E_{tot}}$, of the system is found.

To fully relax the remaining lattice vectors, $\boldsymbol{a_\varepsilon}$ was then incremented by ±0.05Å and this process was repeated, obtaining a parabolic curve showing $\boldsymbol{a_\varepsilon}$ versus $\boldsymbol{E_{tot}}$. With the resultant curve, a 4th order polynomial curve fit was applied to determine the value of $\boldsymbol{a_\varepsilon}$ which results in the local minimum $\boldsymbol{E_{tot}}$. This correspond to the relaxed strained lattice vectors $\boldsymbol{a_{1_\varepsilon}}$ & $\boldsymbol{a_{2_\varepsilon}}$ and hence the lattice constants $\boldsymbol{a}$ & $\boldsymbol{b}$. Figure 9 shows an example of a fitted graph for application of 6% compressive strain on WZ GaAs.

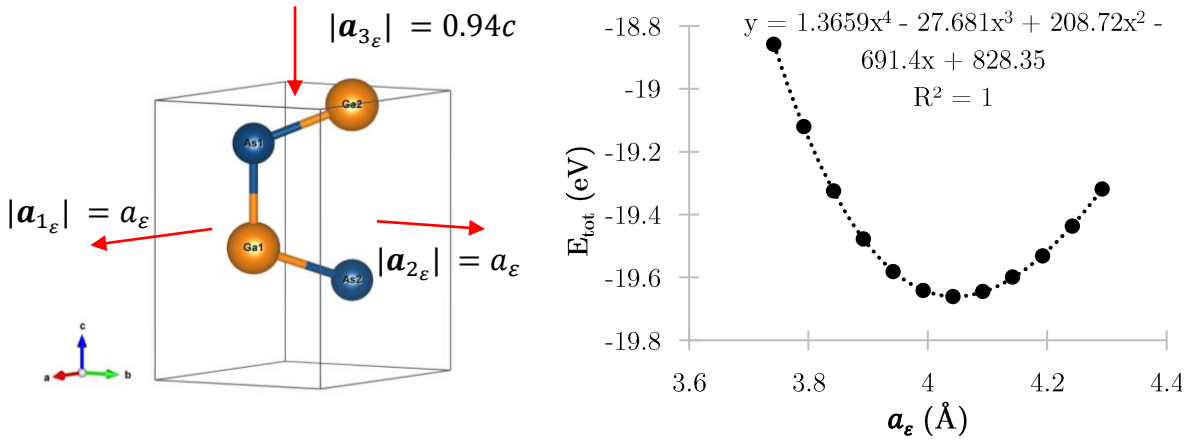

Figure 9 - Applying 6% compressive strain on WZ-GaAs. Strain application (left), curve – fit (right).

To reduce computational cost, the **k** meshes were reduced to 4 x 4 x 2 during this step and the plane wave energy cut-off parameter, **ENCUT**, was set to default values. As convergence tests showed very low sensitivity between lattice constants & **k** mesh size and **ENCUT**. For accuracy, it was ensured that $R^2 > 0.99$ and the residual sum of squares, $SSE < 10^{-4}$ for all curve-fitted data.

4.2.5 Band Structures and Density of States

After self-consistent hybrid HSE06 calculations of the final structures were completed, electronic band structure plots were obtained by plotting the Kohn-Sham eigenvalues along paths of high-symmetrical points in the Brillouin zone (BZ) of the reciprocal lattice of the structures. These eigenvalues represent the energies of the band at a particular **k** point.

The BZ of the structures were visualised using the SeeK-path code by Hinuma et al.[90,91] and corresponding high-symmetry **k** points & paths chosen. WZ & ZB-(111) have a primitive HCP lattice and ZB-(001) has a primitive FCC lattice. The BZ of the lattices is shown in Figure 10.

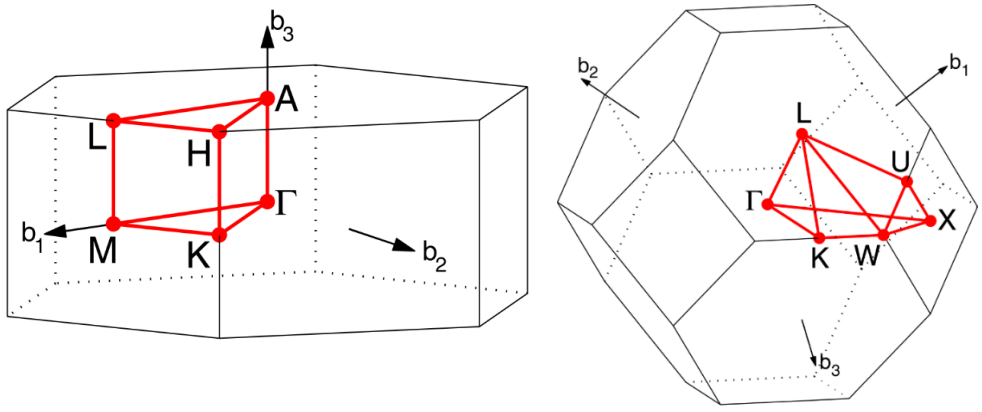

Figure 10 - Irreducible BZ of an HCP Lattice (left) & FCC Lattice (right). [11]

[11] Source: W. Setywan et al.[92]

41 **k** points were used to plot along the chosen paths. For WZ and ZB-(111), a path from **A**(0, 0, 0.5) → **Γ**(0, 0, 0) → **M**(0.5, 0, 0) was chosen, with fractional co-ordinated specified in brackets. For ZB-(001) a path from **X**(0.5, 0, 0.5) → **Γ**(0, 0, 0) → **L**(0.5, 0.5, 0.5) was chosen.

The density of states (DOS) were also calculated for the bulk strain-free calculations, alongside with the projected density of states (PDOS). DOS describes the number of states at each energy level available for occupation. The PDOS is a breakdown of the DOS, showing specific orbital contributions to each energy level available for occupation.

All calculations performed were non-spin polarised and results would show accordingly. The choice of non-spin polarisation had little consequence on results as magnetisation properties and phenomena were outside the scope of this thesis.

As reference, it was found that all WZ and ZB-(111) structures had an extended Bravais lattice symbol of hP2 and ZB structures had a Bravais lattice symbol of cF2. For reproducibility, key VASP input parameters for the band structure calculations are shown in Appendix 9.1.

5.0 Results & Analysis

5.1 Strain-Free Band Structures & Density of States

To analyse the relation between strain and band gap, first the strain-free band structures and DOS were considered. Namely, the PDOS would highlight which orbital has the most prominent effect on the CBM & VBM[12] of each structure and allow analysis in the behaviour of the orbitals upon application of strain. The effects of strain contribution on the band gap, E_g, could hence be attributed to specific orbital behaviours.

DOS of all 3 structures; WZ, ZB-(001) & ZB-(111), were calculated for each semiconductor. First, the WZ & standard ZB-(001) structures were considered to compare CBM & VBM orbital attributions to literature; to validate computational methods. Then the DOS of the WZ & ZB-(111) orientations were considered to analyse orbital behaviour of the strain mediated band structures in this study.

The absolute energies of each **k** point in the energy bands of the band structure yields little information. However, the energy difference between the highest valence band and lowest conduction band yields the band gap at various **k** points. Hence the band gap, E_g, was defined as the difference between the CBM & VBM of the band structure; that is,

$$E_g = \text{CBM} - \text{VBM} \ \ (\text{eV}) \tag{9}$$

DOS plots for all structures can be seen in Appendix 9.3. All calculations were non-spin polarised, hence the DOS reflects this accordingly. For all these figures, the Fermi-level was shifted to 0eV. All strain-free structures were found to be direct gap ($\mathbf{\Gamma}_{\text{VBM}}$-$\mathbf{\Gamma}_{\text{CBM}}$) semiconductors, in accordance to literature; as shown in Table 1. As a representative, Figure 11 shows the band structure, DOS & PDOS for WZ GaAs.

[12] Unless specified otherwise, mention of CBM & VBM herein refer to the CBM & VBM at **Γ** in the BZ.

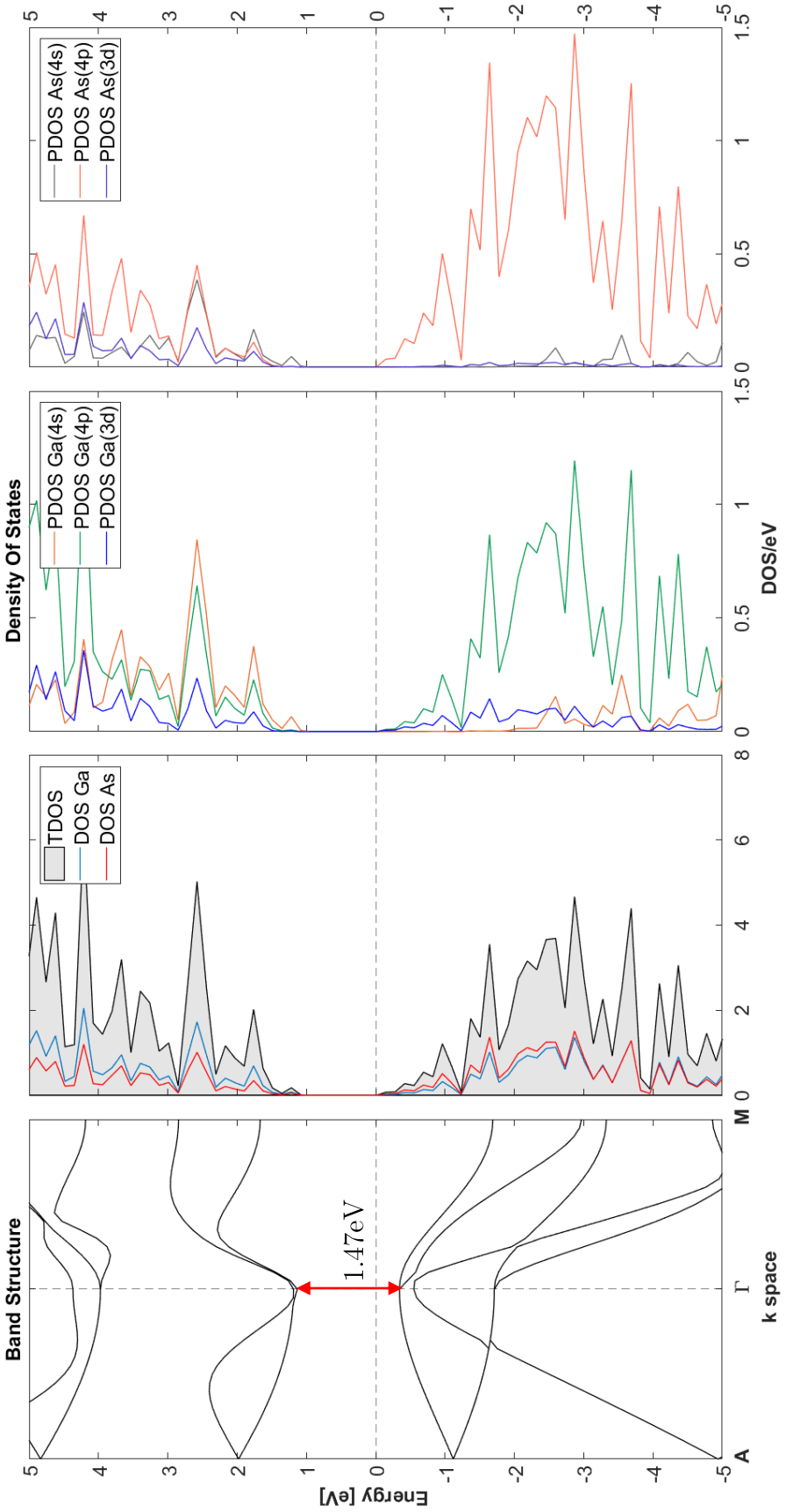

Figure 11 - WZ GaAs Band structure, DOS & PDOS.

5.2 Strain-Mediated Band Structures

For strain simulations, WZ and ZB-(111) structures were analysed; due to coherency and NW experimental growth tendency in these orientations. Strains considered were initially within bounds of ±6% to be within the elastic limit of nanowires[4–6] however, compression was increased to 10% to investigate homogenous behaviours in band gap evolution with strain application between WZ & ZB-(111) structures in: WZ- InP, ZnO, and ZnS, as well as in both GaN structures to compare results with literature.

Band structures were hence obtained for strains intervals of 2%, as shown in Figure 12 for ZB-(111) GaAs. Like the strain free band structures, a path from $\mathbf{A} \rightarrow \mathbf{\Gamma} \rightarrow \mathbf{M}$ using 41 $\mathbf{k}$ points in the irreducible BZ was used for both WZ & ZB-(111) polytypes. For all band structures, the Fermi-level was shifted to 0eV.

All strain-mediated band structures can be found in Appendix 9.4 along tabulated data of the relaxed latticed constants and the VBM & CBM energies at the $\mathbf{k}$ points of high symmetry. A sample of said data can be in Table 3 for GaAs ZB-(111). Similarly, per convention, $\varepsilon < 0$ refer to compressions and $\varepsilon > 0$ refer to tensions.

$\boldsymbol{\varepsilon}$	**a** (Å)	**c** (Å)	$\mathbf{A}_{\mathbf{VBM}}$ (eV)	$\mathbf{A}_{\mathbf{CBM}}$ (eV)	$\mathbf{\Gamma}_{\mathbf{VBM}}$ (eV)	$\mathbf{\Gamma}_{\mathbf{CBM}}$ (eV)	$\mathbf{M}_{\mathbf{VBM}}$ (eV)	$\mathbf{M}_{\mathbf{CBM}}$ (eV)
-6%	4.067	9.205	-0.912	0.972	-0.241	1.243	-2.129	1.559
-4%	4.048	9.401	-0.841	1.135	-0.241	1.227	-2.104	1.672
-2%	4.031	9.597	-0.806	1.259	-0.288	1.140	-2.109	1.739
0	3.998	9.792	-0.709	1.506	-0.295	1.158	-2.075	1.819
2%	4.003	9.988	-0.667	1.564	-0.305	0.939	-2.038	1.823
4%	3.991	10.184	-0.581	1.723	-0.257	0.818	-1.979	1.810
6%	3.982	10.380	-0.602	1.767	-0.310	0.582	-2.022	1.682

Table 3 - ZB-(111) GaAs strain mediated lattice constants & energies at $\mathbf{k}$ points of high symmetry.

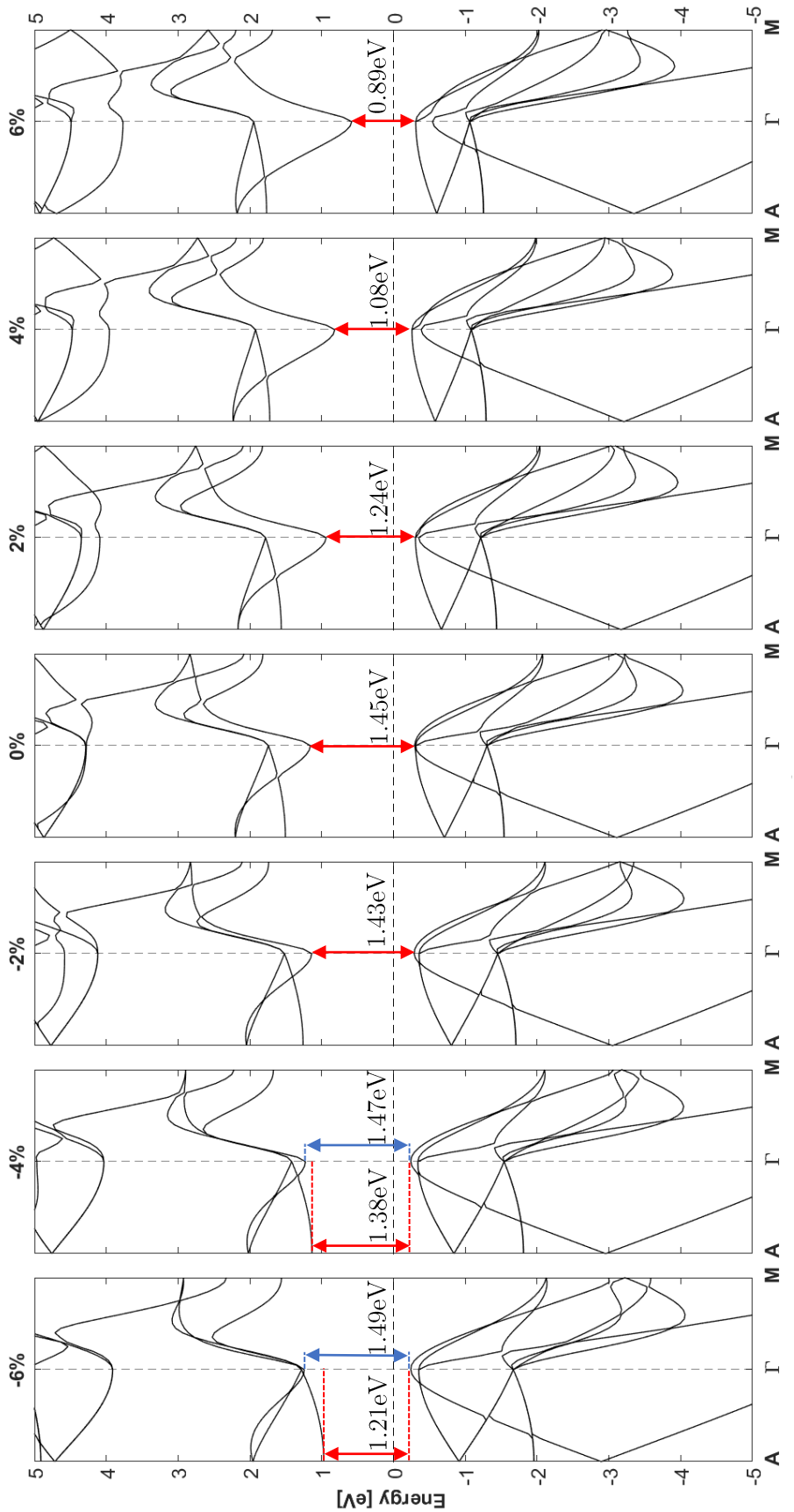

Figure 12 - ZB-(111) GaAs strain mediated band structures. Strains are displayed above subplots. x-axis represents **k** *path in the BZ. Fermi-level shifted to 0eV. Band gaps are explicitly annotated with red arrows.*

5.3 Band Gap Evolution with Strain

From the strain-mediated band structures shown in Appendix 9.4 and corresponding tabulated data, the behaviour of the band gap of semiconductor NWs upon application of strain were determined. Figure 13 & Figure 14 show the strain & band gap behaviour of all the III-V and II-VI semiconductors in their WZ and ZB-(111) structures respectively. ΔE_g refers to the change in band gap energy from initial strain-free value.

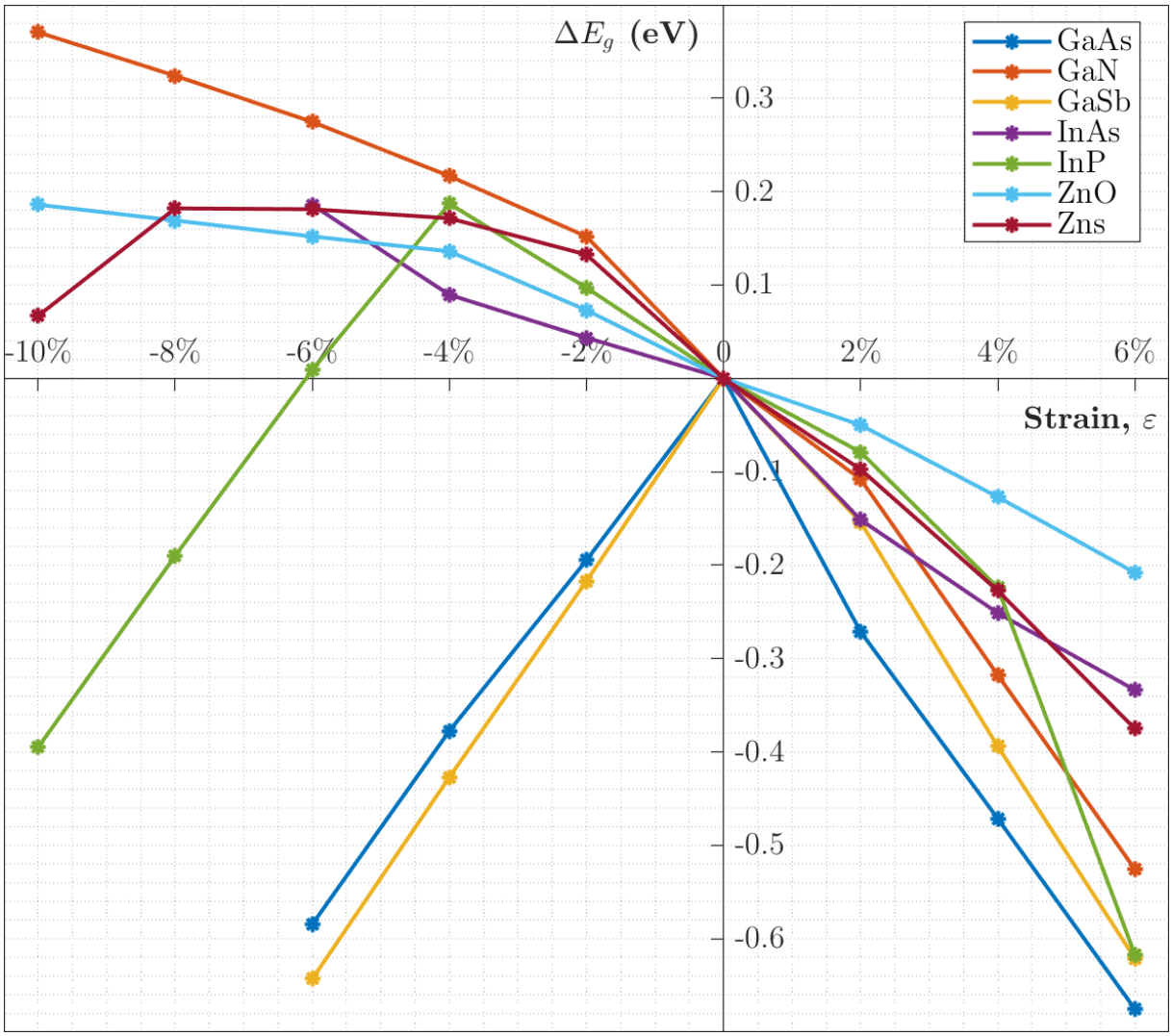

Figure 13 - WZ Strain & Band Gap behaviour.

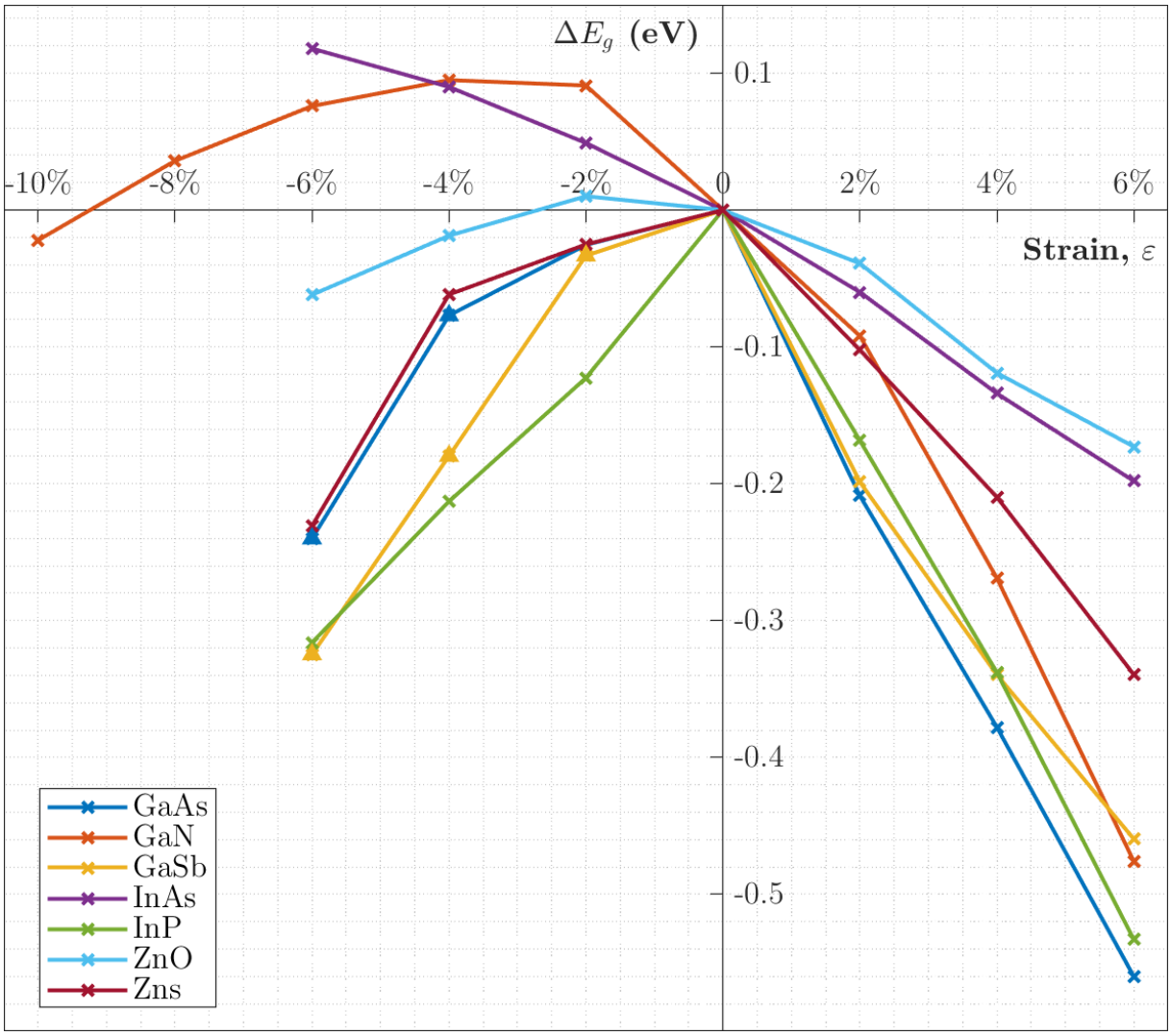

Figure 14 - ZB-(111) Strain & Band Gap behaviour. Triangles represent indirect band gaps.

There were 3 main behaviours in band gap modulation with strain observed: inversely linearly proportional, reduction in band gap and a 'compression shifted peak' reduction. These are henceforth defined as Types A, B and C.

The same trends between WZ & ZB-(111) structures of the same semiconductor was not always observed, as evidenced by GaN, InP, ZnO & ZnS. Furthermore, a salient feature observed in ZB-(111) GaAs & GaSb were the indirect band gap transitions at 4% and 2% compressive strains respectively.

The following sections show the strain & band gap behaviour of each individual semiconductor in both coherent polytypes to allow further analysis of trends.

For the tabulated band gap data, all band gaps listed, E_g, were found to be direct ($\mathbf{\Gamma}_{VBM}$-$\mathbf{\Gamma}_{CBM}$) band gaps and where relevant, band gaps listed in brackets represent indirect band gaps ($\mathbf{\Gamma}_{VBM}$-$\mathbf{A}_{CBM}$). Cases where direct-indirect band gap transition occurs, the 'correct' band gap is that of the indirect variant ($\mathbf{\Gamma}_{VBM}$-$\mathbf{A}_{CBM}$), as it gives the true minimum gap energy value. The Fermi-level of all graphs was set at 0eV.

Furthermore, plots of CBM & VBM energy at **k** points of high symmetry (**A**, **Γ** & **M**) were shown to elucidate contributions from specific orbitals to band gap modulation with strain. Like the preceding graphs, data for all figures and tables were taken from their corresponding band structures shown in Appendix 9.4.

5.3.1 GaAs

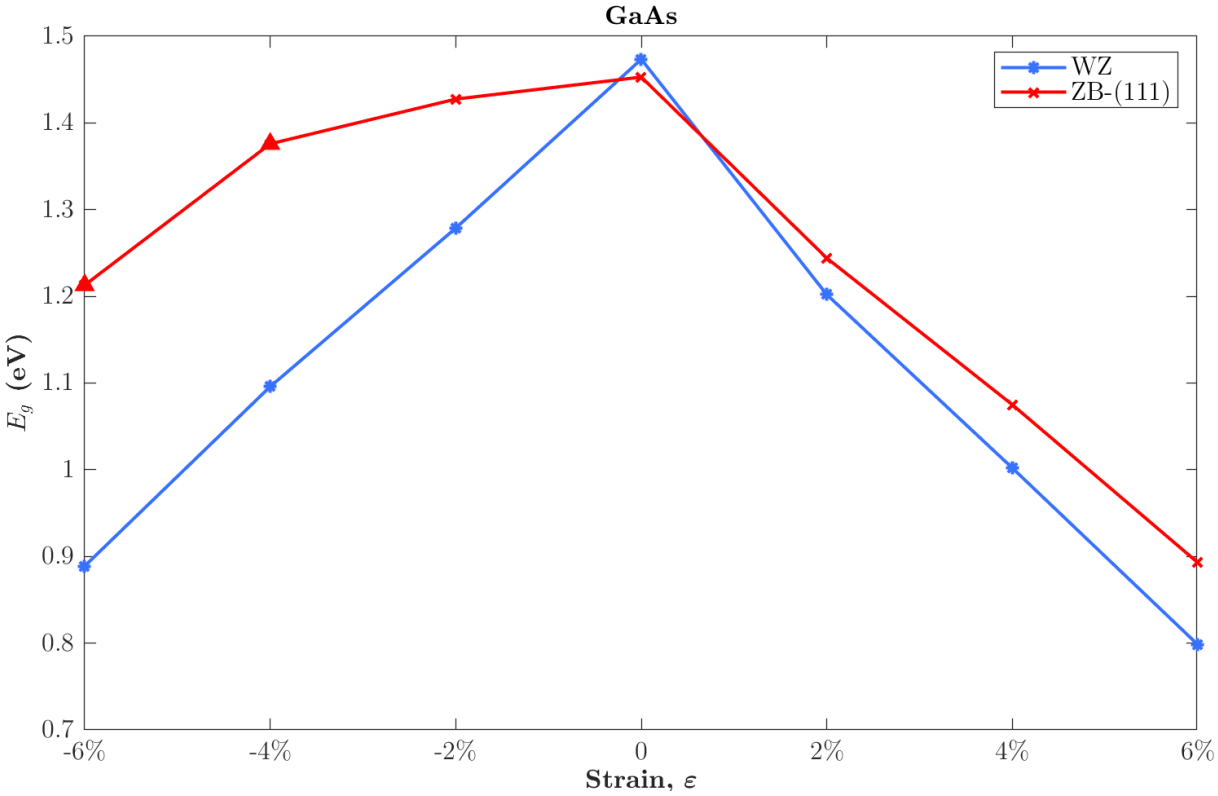

Figure 15 - GaAs Strain & Band Gap behaviour. Triangles represent Indirect Band Gaps.

ε	E_g (eV)	ΔE_g (eV)
-6%	0.889	-0.585
-4%	1.096	-0.378
-2%	1.279	-0.195
0	1.473	-
2%	1.202	-0.271
4%	1.002	-0.471
6%	0.798	-0.675

ε	E_g (eV)	ΔE_g (eV)
-6%	1.485 (1.213)	$-0.240_{(\Gamma\text{-}A)}$
-4%	1.468 (1.376)	$-0.077_{(\Gamma\text{-}A)}$
-2%	1.428	-0.025
0	1.453	-
2%	1.244	-0.209
4%	1.075	-0.378
6%	0.893	-0.560

Table 4 - GaAs Strain & Band Gap values. WZ (left) & ZB-(111) (right).
Values in brackets indicate indirect (Γ_{VBM}-A_{CBM}) band gaps.

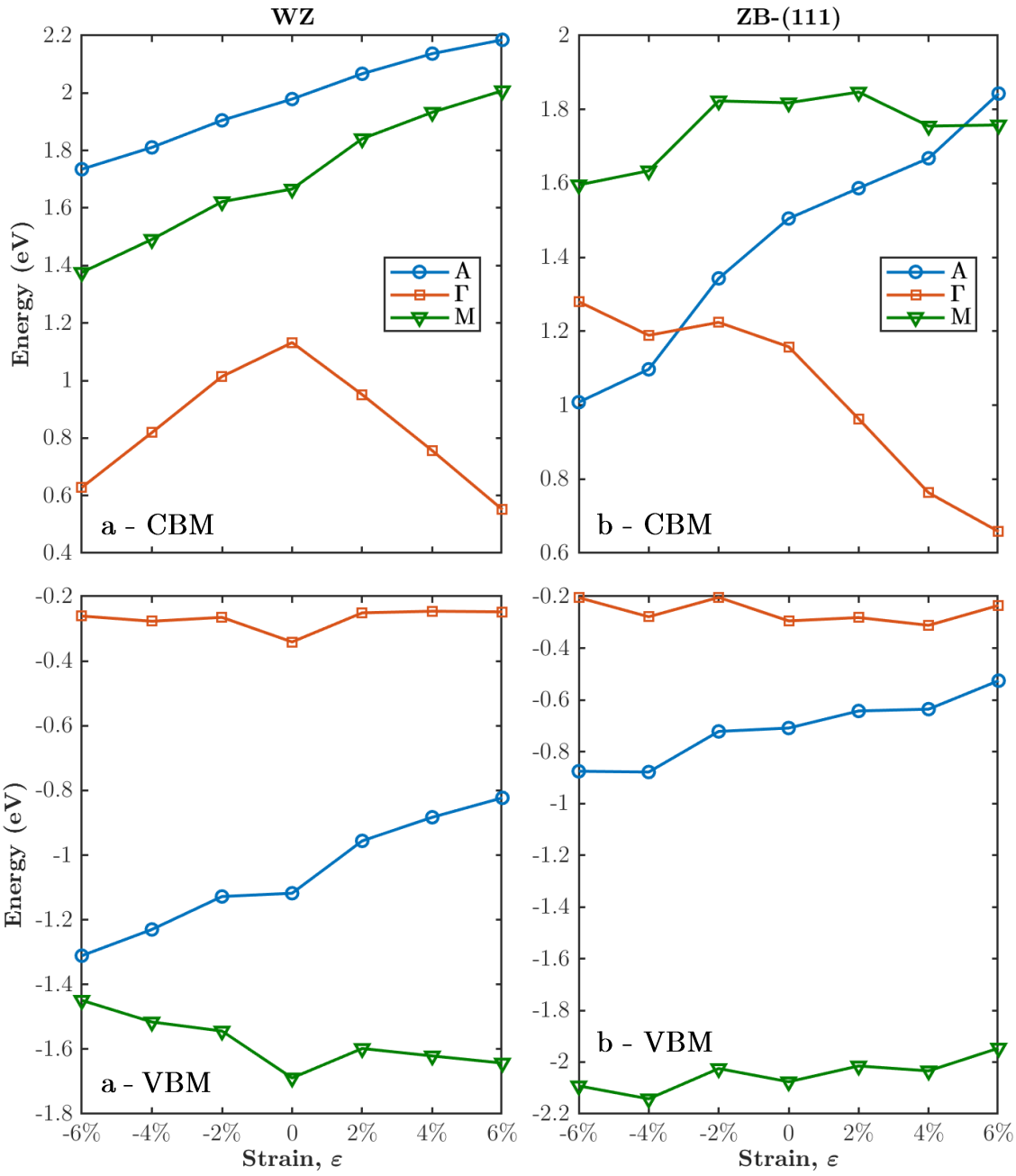

Figure 16 - GaAs CBM (top) & VBM (bottom) Strain & Energy behaviours. WZ (left, a) & ZB-(111) (right, b). In ZB-(111), Indirect $\Gamma \rightarrow A$ *transition occurs at ~3.1% compressive strain in the CBM.*

5.3.2 GaN

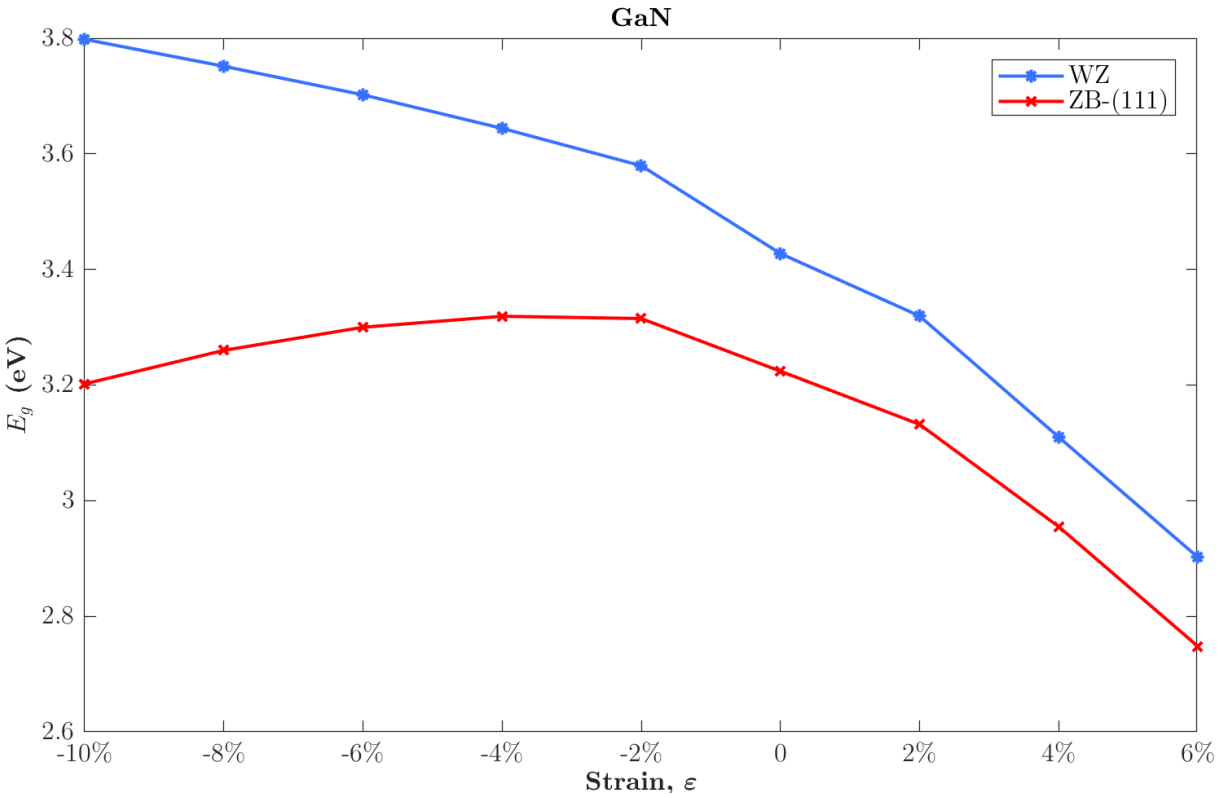

Figure 17 - GaN Strain & Band Gap behaviour.

$\boldsymbol{\varepsilon}$	E_g (eV)	ΔE_g (eV)
-10%	3.798	0.371
-8%	3.752	0.324
-6%	3.702	0.275
-4%	3.644	0.217
-2%	3.579	0.152
0	3.428	-
2%	3.320	-0.108
4%	3.110	-0.318
6%	2.902	-0.526

$\boldsymbol{\varepsilon}$	E_g (eV)	ΔE_g (eV)
-10%	3.202	-0.022
-8%	3.260	0.036
-6%	3.300	0.076
-4%	3.319	0.095
-2%	3.315	0.091
0	3.224	-
2%	3.132	-0.092
4%	2.955	-0.269
6%	2.748	-0.476

Table 5 - GaN Strain & Band Gap values. WZ (left) and ZB-(111) (right).

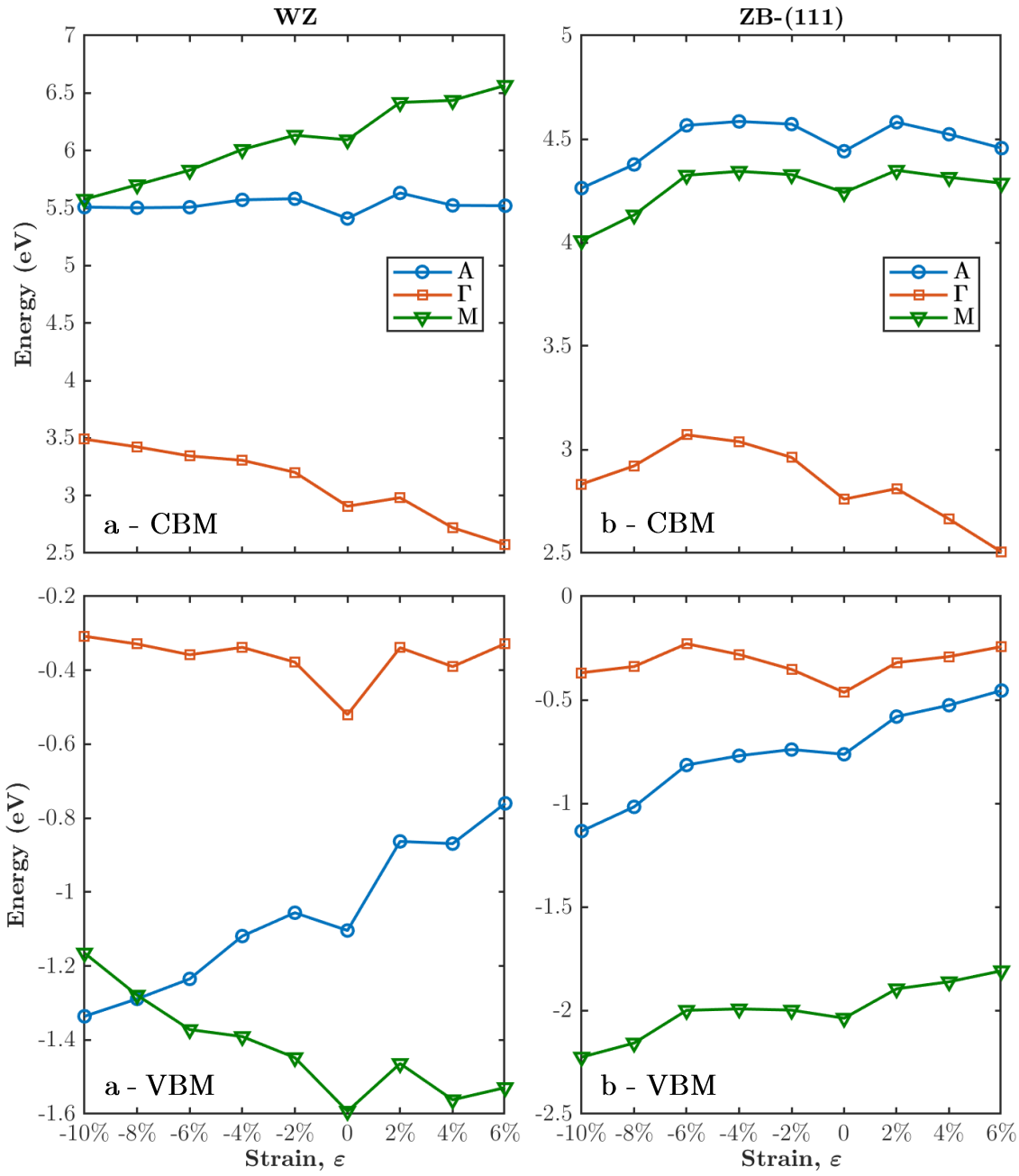

Figure 18 - GaN CBM (top) & VBM (bottom) Strain & Energy behaviours. WZ (left, a) & ZB-(111) (right, b).

5.3.3 GaSb

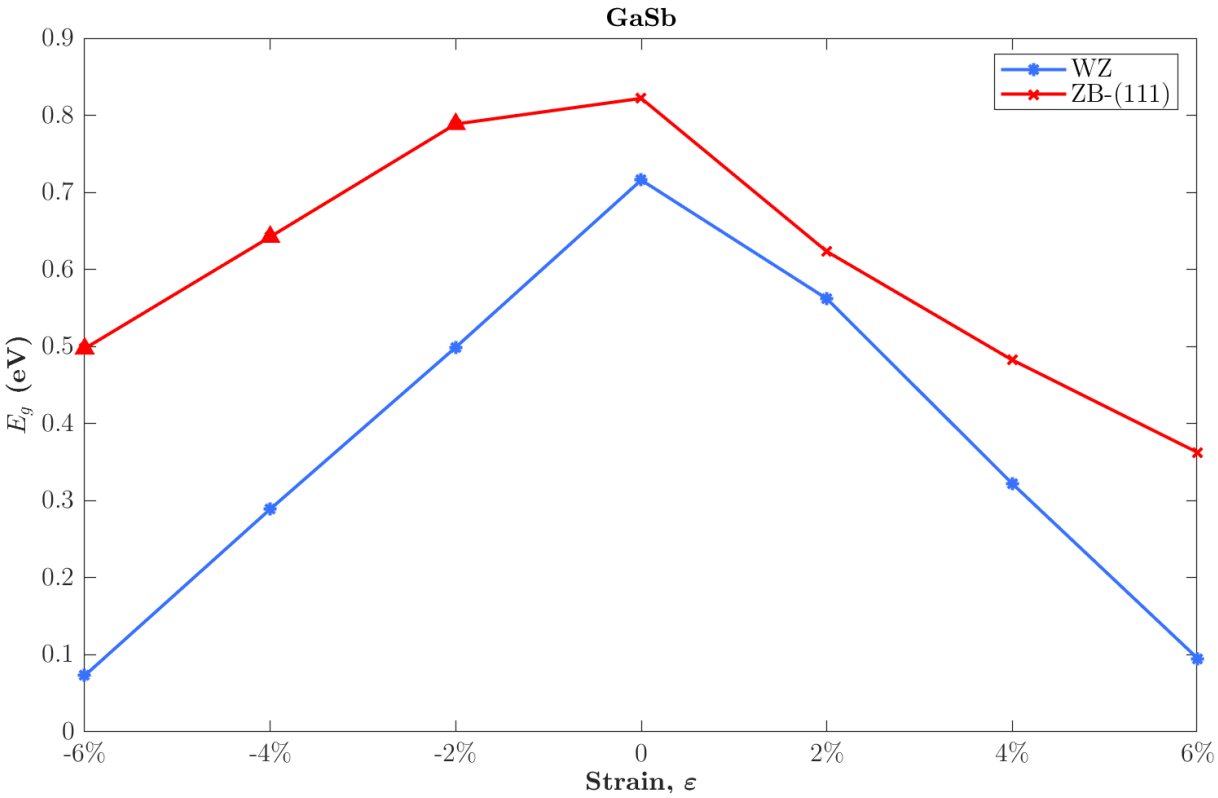

Figure 19 - GaSb Strain & Band Gap behaviour. Triangles represent Indirect Band Gaps.

$\boldsymbol{\varepsilon}$	E_g (eV)	ΔE_g (eV)
-6%	0.073	-0.643
-4%	0.289	-0.427
-2%	0.499	-0.217
0	0.716	-
2%	0.562	-0.154
4%	0.322	-0.394
6%	0.095	-0.621

$\boldsymbol{\varepsilon}$	E_g (eV)	ΔE_g (eV)
-6%	0.830 (0.497)	$-0.325_{(\Gamma\text{-}A)}$
-4%	0.954 (0.642)	$-0.180_{(\Gamma\text{-}A)}$
-2%	0.813 (0.789)	$-0.033_{(\Gamma\text{-}A)}$
0	0.822	-
2%	0.623	-0.199
4%	0.482	-0.340
6%	0.362	-0.460

Table 6 - GaSb Strain & Band Gap values. WZ (left) and ZB-(111) (right).
Values in brackets indicate indirect (Γ_{VBM}-A_{CBM}) band gaps.

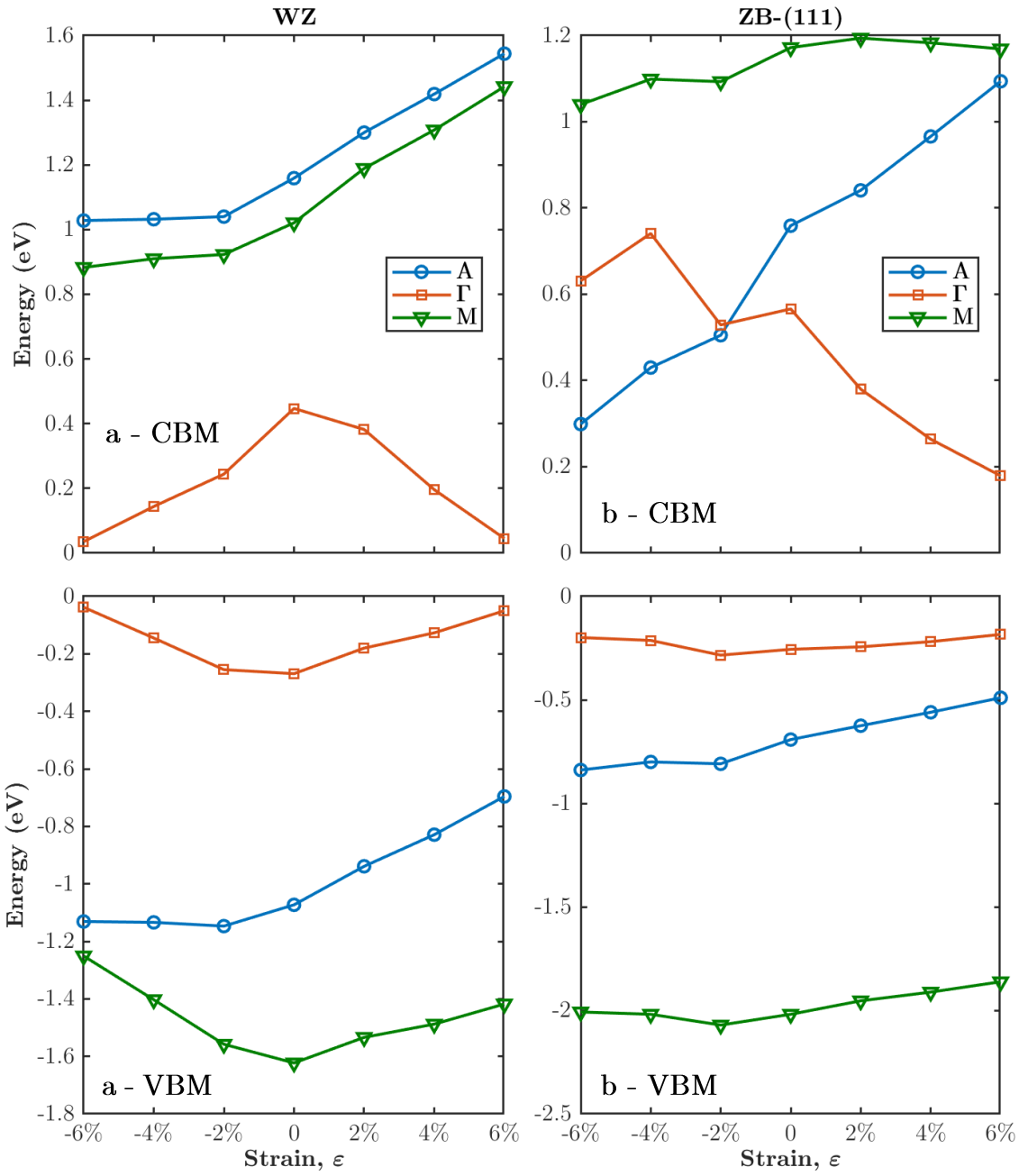

Figure 20 – GaSb CBM (top) & VBM (bottom) Strain & Energy behaviours. WZ (left, a) & ZB-(111) (right, b). In ZB-(111), Indirect $\Gamma \rightarrow A$ transition occurs at ~1.8% compressive strain in CBM.

5.3.4 InAs

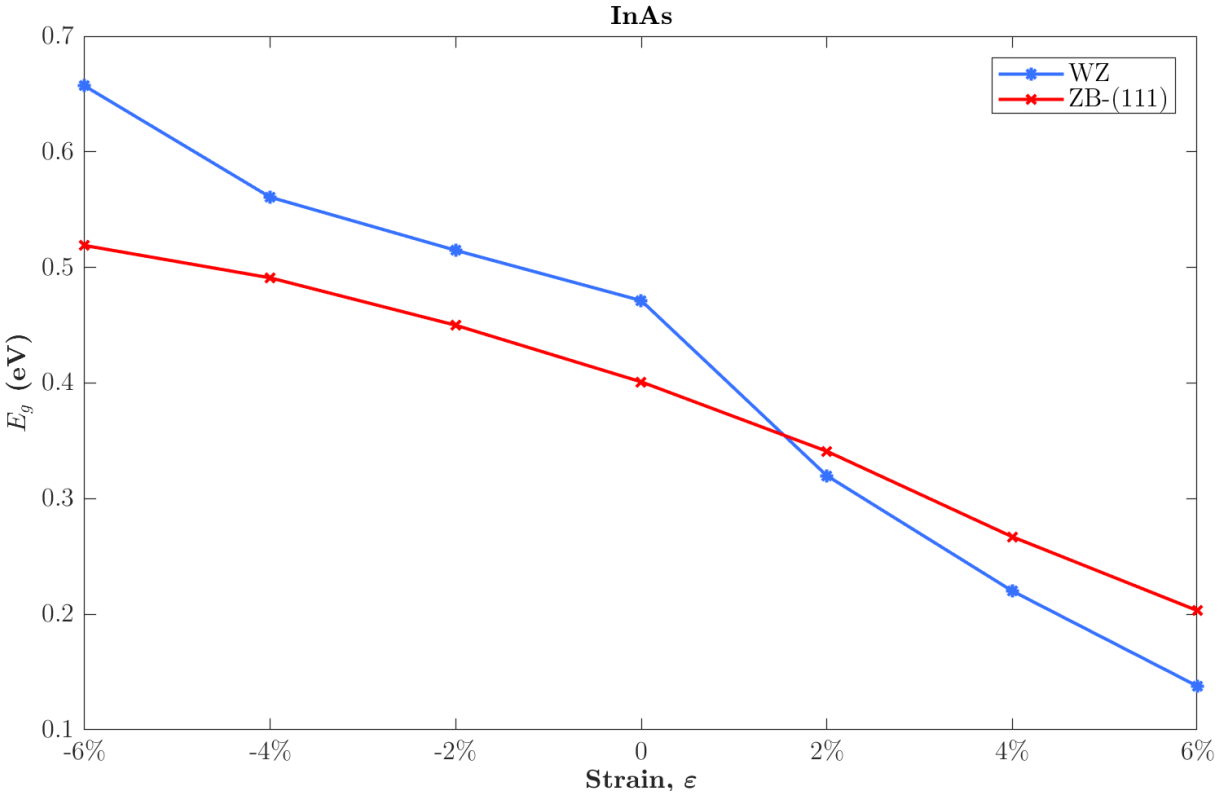

Figure 21 - InAs Strain & Band Gap behaviour.

ε	E_g (eV)	ΔE_g (eV)
-6%	0.657	0.186
-4%	0.561	0.090
-2%	0.515	0.044
0	0.471	-
2%	0.320	-0.151
4%	0.220	-0.251
6%	0.138	-0.334

ε	E_g (eV)	ΔE_g (eV)
-6%	0.519	0.118
-4%	0.491	0.090
-2%	0.450	0.049
0	0.401	-
2%	0.341	-0.061
4%	0.267	-0.134
6%	0.203	-0.199

Table 7 - InAs Strain & Band Gap values. WZ (left) and ZB-(111) (right).

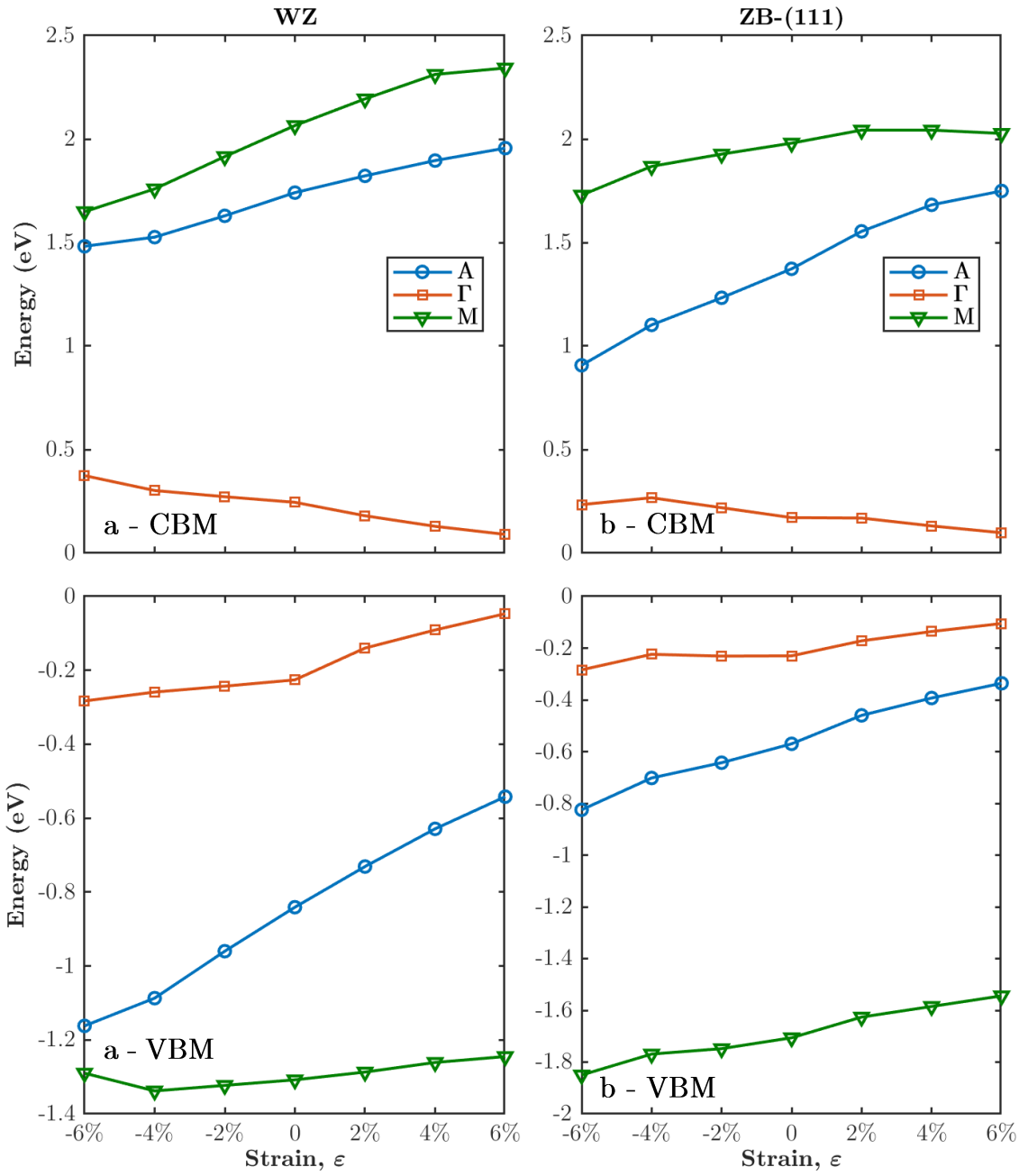

Figure 22 - InAs CBM (top) & VBM (bottom) Strain & Energy behaviours. WZ (left, a) & ZB-(111) (right, b).

5.3.5 InP

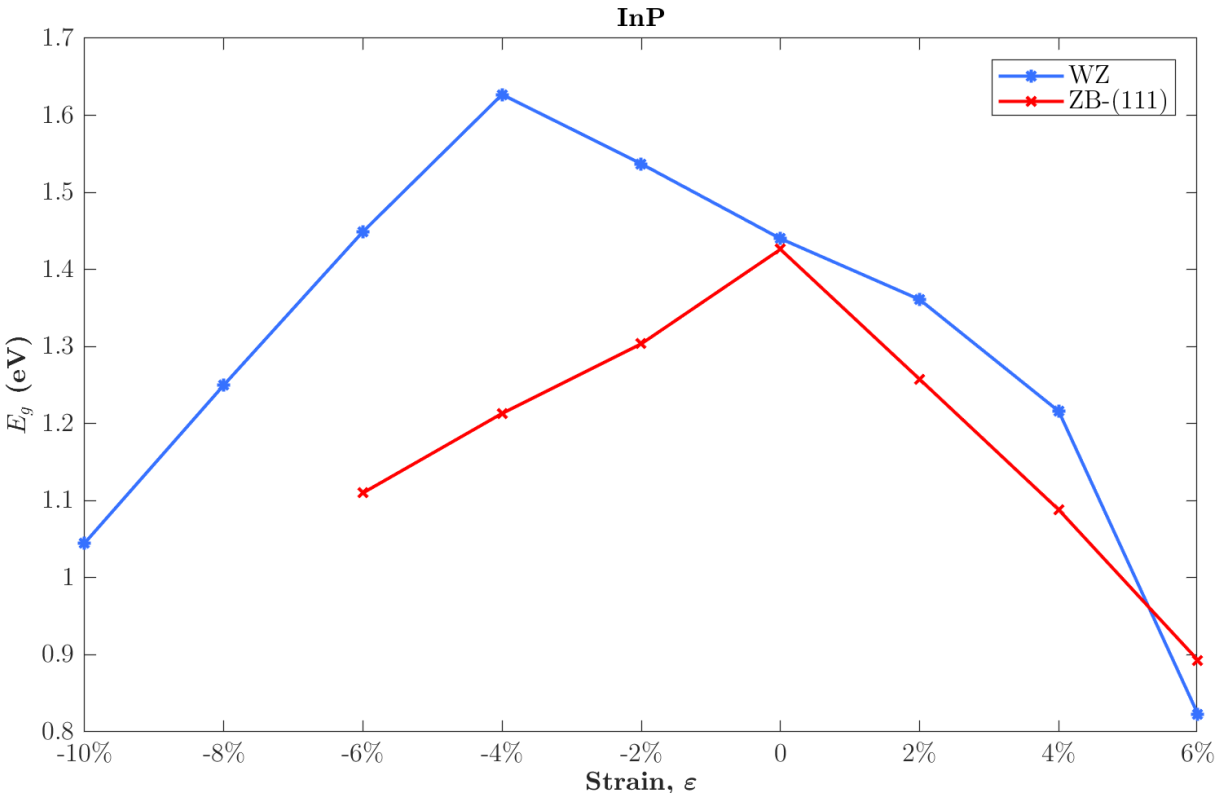

Figure 23 - InP Strain & Band Gap behaviour.

ε	E_g (eV)	ΔE_g (eV)
-10%	1.045	-0.394
-8%	1.250	-0.190
-6%	1.449	0.009
-4%	1.627	0.187
-2%	1.537	0.097
0	1.440	-
2%	1.361	-0.079
4%	1.216	-0.224
6%	0.823	-0.617

ε	E_g (eV)	ΔE_g (eV)
-6%	1.110	-0.316
-4%	1.213	-0.213
-2%	1.304	-0.123
0	1.426	-
2%	1.258	-0.169
4%	1.088	-0.338
6%	0.893	-0.533

Table 8 - InP Strain & Band Gap values. WZ (left) and ZB-(111) (right).

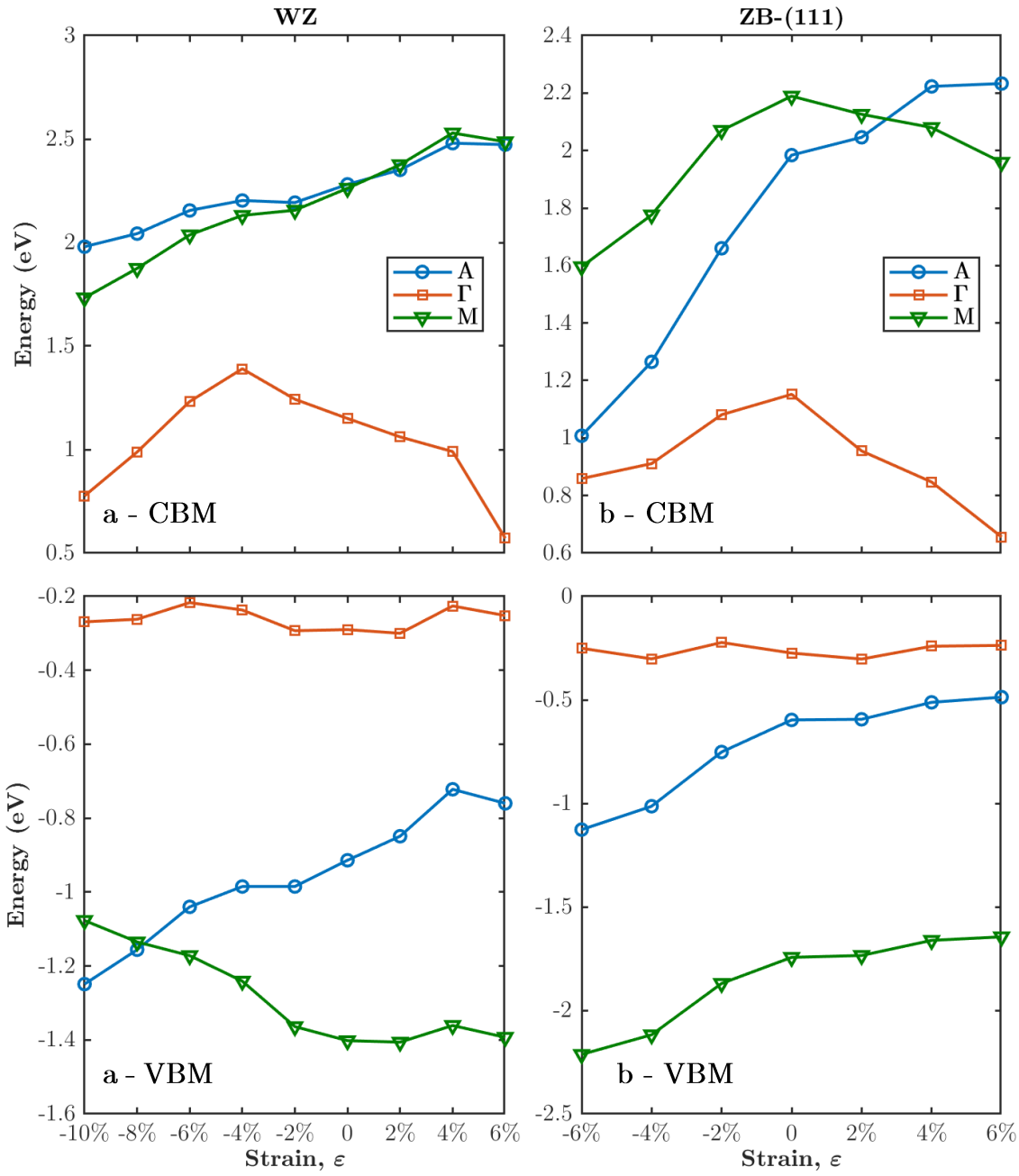

Figure 24 - InP CBM (top) & VBM (bottom) Strain & Energy behaviours. WZ (left, a) & ZB-(111) (right, b).

5.3.6 ZnO

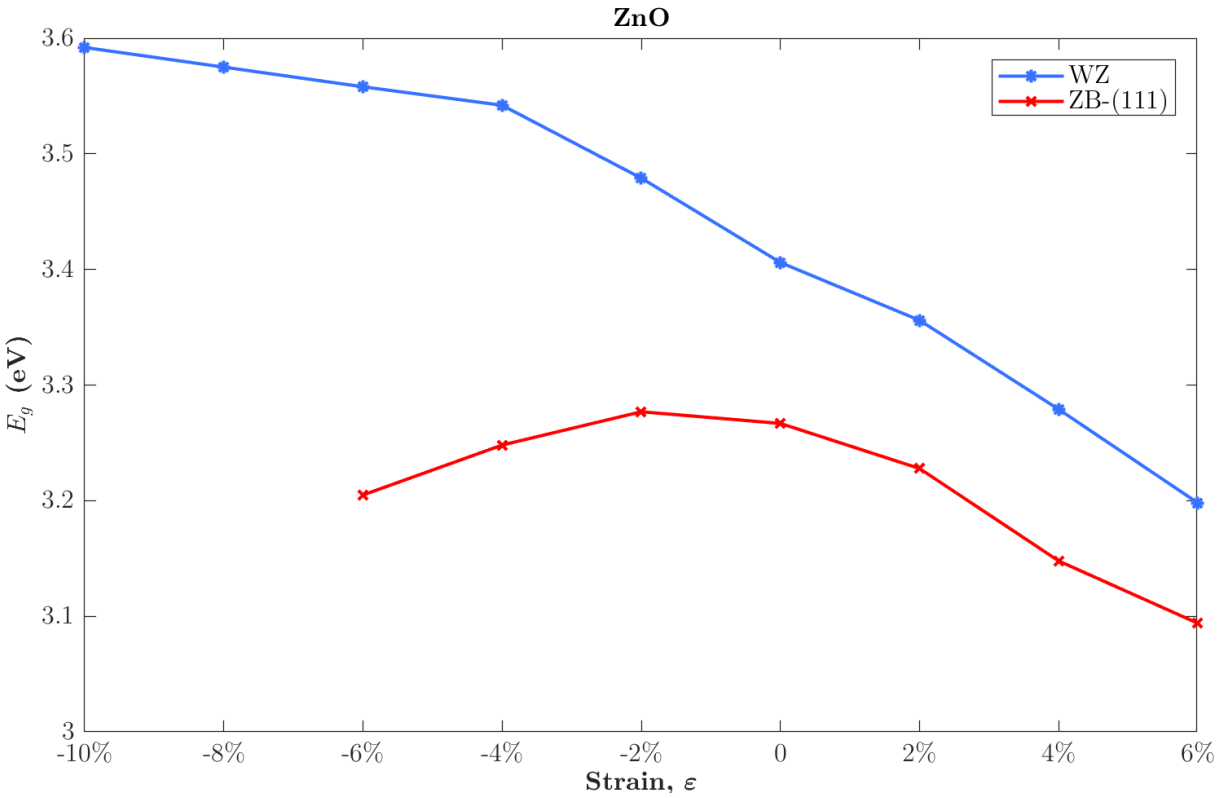

Figure 25 - ZnO Strain & Band Gap behaviour.

ε	E_g (eV)	**Δ**E_g (eV)
-10%	3.591	0.185
-8%	3.575	0.168
-6%	3.558	0.152
-4%	3.542	0.136
-2%	3.479	0.072
0	3.406	-
2%	3.356	-0.050
4%	3.279	-0.127
6%	3.198	-0.211

ε	E_g (eV)	**Δ**E_g (eV)
-6%	3.205	-0.062
-4%	3.248	-0.019
-2%	3.277	0.010
0	3.267	-
2%	3.228	0.039
4%	3.148	0.119
6%	3.094	0.173

Table 9 - ZnO Strain & Band Gap values. WZ (left) and ZB-(111) (right).

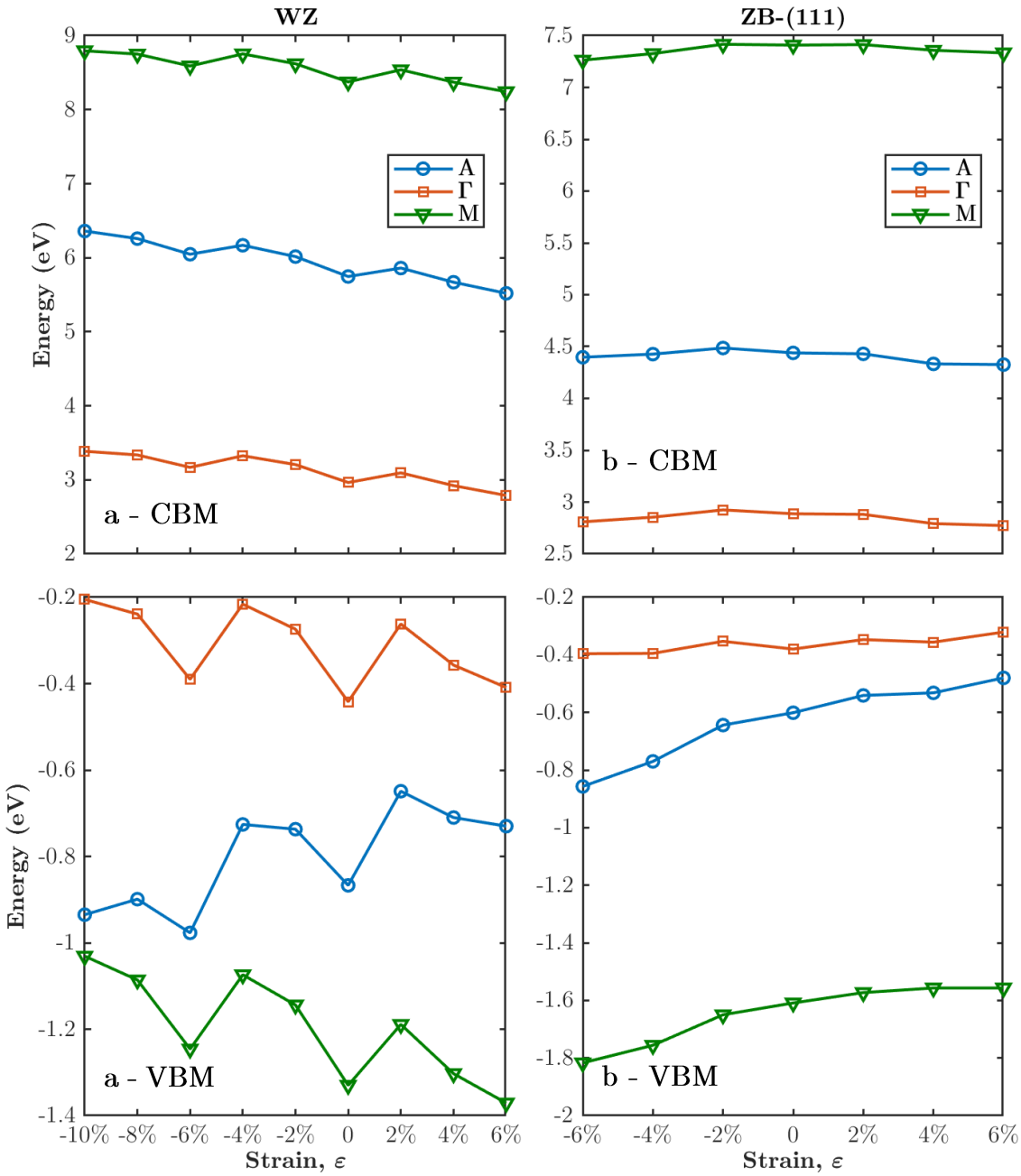

Figure 26 - ZnO CBM (top) & VBM (bottom) Strain & Energy behaviours. WZ (left, a) & ZB-(111) (right, b).

5.3.7 ZnS

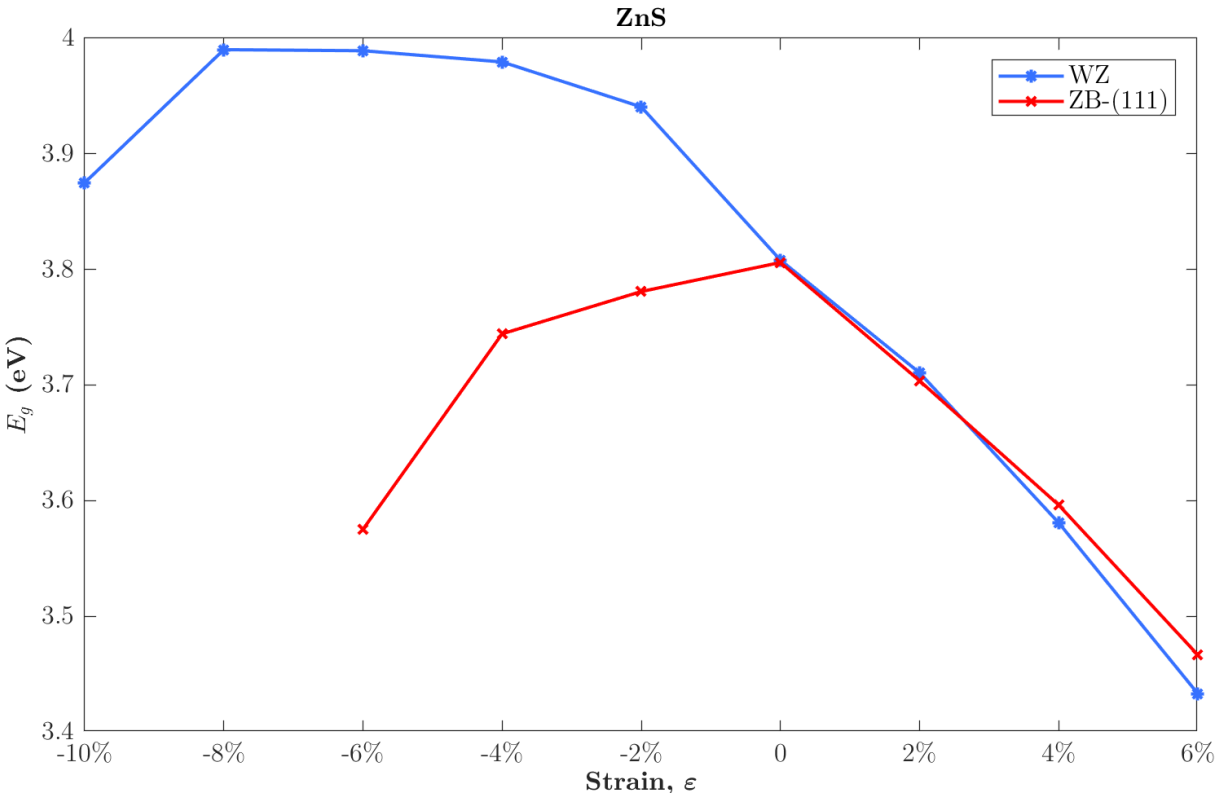

Figure 27 - ZnS Strain & Band Gap behaviour.

ε	E_g (eV)	ΔE_g (eV)
-10%	3.875	0.067
-8%	3.990	0.182
-6%	3.989	0.181
-4%	3.980	0.171
-2%	3.941	0.133
0	3.808	-
2%	3.711	-0.098
4%	3.581	-0.227
6%	3.433	-0.375

ε	E_g (eV)	ΔE_g (eV)
-6%	3.575	-0.231
-4%	3.744	-0.062
-2%	3.781	-0.025
0	3.806	-
2%	3.704	-0.102
4%	3.596	-0.210
6%	3.467	-0.340

Table 10 - ZnS Strain & Band Gap values. WZ (left) and ZB-(111) (right).

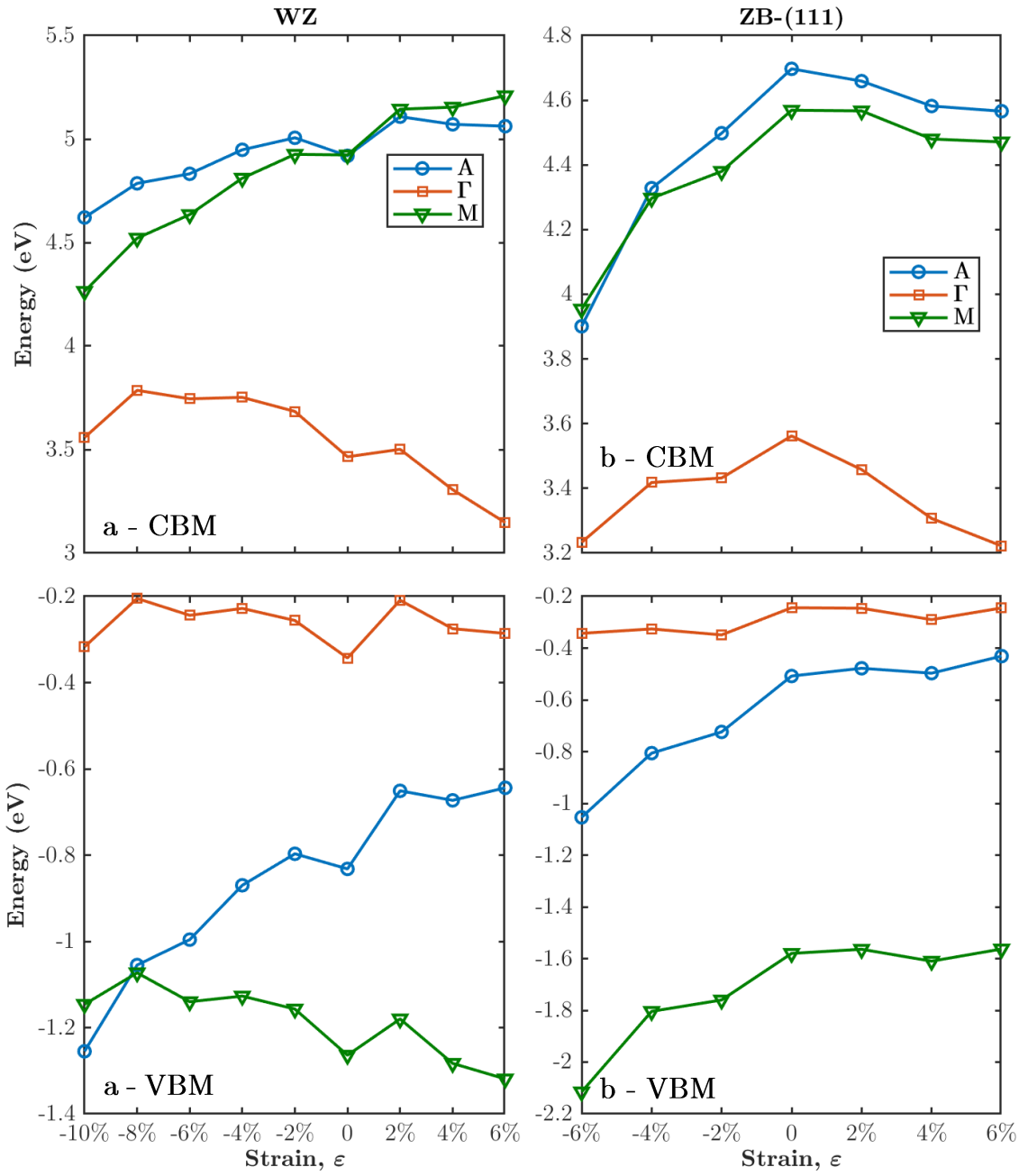

Figure 28 - ZnS CBM (top) & VBM (bottom) Strain & Energy behaviours. WZ (left, a) & ZB-(111) (right, b).

6.0 Discussion

A simplified bulk model was successfully implemented in this study to investigate the behaviour of band gap with external strain application in bent semiconductor nanowires. To reiterate, strain along the cross-section of a bent NW results in simultaneous compressions and tensions; with tension toward the outer edge and compression toward the inner edge (Figure 29). Hence, results were considered from 2 differing frameworks; firstly, in terms of band gap behaviour of a bent semiconductor NW and secondly, with individual analysis of material behaviour.

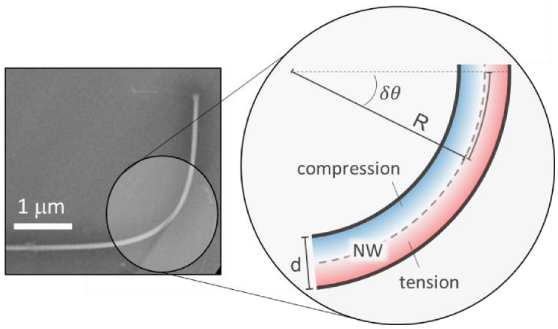

Figure 29 - Bent nanowire experiencing compression along the inner edge and tension along the outer edge.[13]

6.1 Overall Behaviours

There were three main behaviours observed in band gap evolution with strain; inversely linearly proportional, reduction in band gap and a 'compression shifted peak' reduction. These were defined as types A, B and C, as seen in Figure 30, and the representative emission spectra behaviour of these behaviours were also denoted similarly. Type C behaviour was split into 2 regions; C(i) where the band gap behaviour with strain was the same as Type A, and C(ii) which refers to the overall behaviour of the semiconductor, encompassing the C(i) region. In the C(ii) region, tensions reduced band gaps and compressions increased band gaps until reaching a peak and then immediately degrading.

To ascertain representative emission spectra of these band gap behaviours, the concept of band gap needs to be first reaffirmed. Band gap, E_g, refers to the amount of

[13] Source: Grumstrup Research Group.[93]

energy to excite an electron from the valence band to the conduction band; allowing for its 'application' in devices. After excitation, when the electron returns to the valence band from the conduction band, it releases energy in the form of a photon. The energy and hence wavelength of the photon can be described via the Planck-Einstein relationship, $E_\gamma = \frac{\hbar c}{\lambda}$. Where $\hbar$ is Planck's constant, c is the speed of light and λ is the wavelength of the photon. The energy released by the photon has a magnitude proportional to the band gap, hence, $E_g = E_\gamma$. In this manner, semiconductors can emit a spectrum of wavelengths of light, with a peak corresponding to their band gaps.

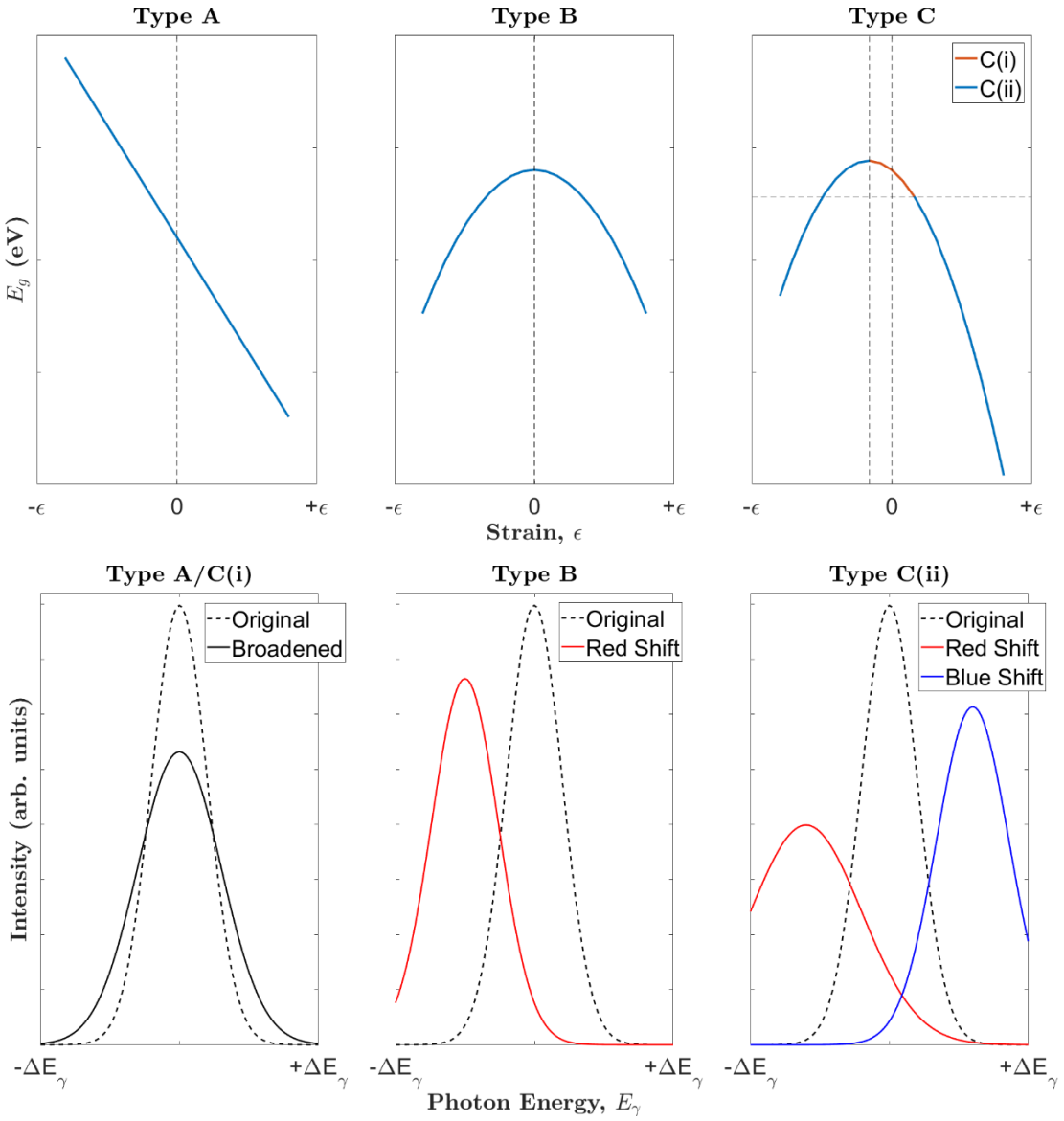

Figure 30 - Strain & Band Gap behaviours (top) & Corresponding Emissions Spectra behaviour (bottom).

As seen in Figure 30, strain on type A semiconductor NWs results in spectra broadening. Bent NWs experience both compressive and tensile strains occurring simultaneously. Strain in these NWs cause E_g to increase towards the compressive side and decrease the toward tensile. This increase in E_g range corresponds directly to a proportional broadening in emission spectrum.

Similarly, type B NWs have an increase in E_g range with strain application, also resulting in spectra broadening. However, as the application of strains cause a reduction in band gap throughout the NW, from the Planck-Einstein relationship, this will result in a red shift in the spectrum; increasing photon wavelength and hence decreasing photon energy. This red shifting would be the prominent behaviour observed.

Type C NWs experience 2 effects with strain applications. Like type A NWs, small strains within region C(i) results only in the broadening of spectra. For larger strains, past region C(i), type C(ii) behaviour occurs which results in spectra splitting. Blue and red shifting of the spectrum occurs; with the blue shift attributed to strains causing a reduction of E_g range; equal to the increase previously imparted by the C(i) region. Red shifting simultaneously occurs during all ranges of strain due to the tensile reduction of band gap. The corresponding broadening of the spectra at these shifts were proportional to the increase/decrease of E_g range that occurs with these 2 effects.

Qualitatively, type B and C band gap behaviours can be typified as homogenous; as both result in a net reduction of band gap however, effects on the emission spectra would differ however. Classification of strain & band gap behaviour for all III-V and II-VI semiconductors is summarised in Table 11. The main orbital contributors to the CBM & VBM were also listed along with a short description of CBM/VBM behaviour upon strain application. Analysis of the orbital behaviours under strain in this manner was used to rationalise the observed band gap changes.

		E_g Behaviour	CBM	VBM	CBM/VBM Behaviour
GaAs	WZ	Type B	Ga(4s)	As(4p)	E_g behaviour was attributed to larger CBM contributions. Application of strains reduced CBM & increased VBM.
	ZB-(111)	Type B	$Ga(4s)_{\Gamma,A}$	As(4p)	E_g behaviour was attributed to larger CBM contributions. Application of strains increased the VBM. Tensions reduced the CBM and compressions increased the CBM at **Γ**. Inverse was true for CBM at **Λ**, resulting in **Γ-Λ** indirect gap transition at ~3.1% compressive strain.
GaN	WZ	Type A	Ga(4s) & N(2s)	N(2p)	CBM had larger contributions to E_g. Strains increased the VBM whilst reducing the CBM with tension and increasing the CBM with compressions.
	ZB-(111)	Type C	Ga(4s) & N(2s)	N(2p)	CBM had larger contributions to E_g with tensile strains, whilst VBM had larger contributions with compressions. Strains resulted in reduction of the CBM & VBM however, this effect was more pronounced in tensile strains applied to the CBM. Compressions had negligible effects on the CBM although resulting in a net reduction.
GaSb	WZ	Type B	Ga(4s)	Sb(5p)	CBM decreased with strains and VBM increased with strains. Contribution of both were equally significant to Eg evolution with strain, although CBM contributed more.
	ZB-(111)	Type B	$Ga(4s)_{\Gamma,A}$	Sb(5p)	VBM had little sensitivity to strains; resulting in a minute increase. CBM at **Γ** experienced a reduction of VBM with tensions and increase with compressions. This was inversely true for the CBM at **Λ**, resulting in an indirect gap transition at ~1.8% compressive strain.
InAs	WZ	Type A	In(5s)	As(4p)	CBM decreased with tension and increased with strain, inversely true for VBM. Contributions were skewed in favour of the CBM for Eg modulations. Tensions had a more profound effect on the band structures than compressive strains.
	ZB-(111)	Type A	In(5s)	As(4p)	Exact same behaviour as WZ.

Table 11 continued on next page

		E_g Behaviour	CBM	VBM	CBM/VBM Behaviour
InP	WZ	Type C	In(5s) & P(3s)	P(3p)	Strains had a more prominent effect on the CBM. Tensile strain reduced CBM and compressive strain increased CBM until 4% compression. Compressive strains greater than this reduced the CBM. This was seen accordingly in the Eg behaviour. VBM remained relatively unchanged; though strains resulted in a net reduction.
	ZB-(111)	Type B	In(5s) & P(3s)	P(3p)	Like WZ, there were more pronounced effects on the CBM. Applications of strains caused a reduction of CBM and a minor increase in the VBM. Eg evolution was attributed to CBM.
ZnO	WZ	Type A	Zn(4s) & O(2s)	O(2p)	Tensions caused a reduction in CBM and VBM. VBM reduced with all strains. CBM reduced with tension but had negligible changes with compression. Attribution Eg behaviour was to VBM with compression, and both CBM & VBM with tension
	ZB-(111)	Type C	Zn(4s) & O(2s)	O(2p)	Strain behaviour on both CBM & VBM were identical. Application of compressive strains initially increased CBM/VBM at 2% compression then reduced with greater compressions. Tensions resulted in a reduction in CBM and an increase in the VBM. Contributions of both CBM & VBM were significant to Eg.
ZnS	WZ	Type C	Zn(4s) & S(3s)	S(3p)	VBM and CBM had the same behaviour with compressive strains; resulting in an overall increase. VBM & CBM reduced at 10% compression, correlating to the observed drop in Eg. tensions netted an increase in VBM and reduction in CBM. Evolution of Eg with strain was prominently contributed by CBM.
	ZB-(111)	Type B	Zn(4s) & S(3s)	S(3p)	Reduction of CBM occurred with strain application. Tensions increased VBM and compressions reduced VBM. Attribution of Eg behaviour with strain to larger CBM

Table 11 - Strain & Band Gap behaviours, CBM/VBM main orbital contributors, and Strain & CBM/VBM behaviours

For all the semiconductors, it was observed that attribution to the VBM was from the anion p-orbitals. Furthermore, the CBM was governed by the s-orbitals of the cations, which were in many cases hybridised with the s-orbitals of the anions. It was noticed that hybridisation did not occur in Ga compounds with heavier anions; though this nature was not repeated for InAs; as degeneracy[14] did not occur between In and the lighter As element. These conclusions were drawn from the DOS of all the structures, as seen in Appendix 9.3, and the CBM & VBM behaviours shown in Section 0.

From Table 11 it was clear that commonalities in band gap behaviour within III-V or II-VI semiconductors was not present. Furthermore, from Figure 13 & Figure 14, common behaviours between WZ & ZB-(111) polytypes were not present either. This surmises that strain & band gap behaviours are both strongly chemically and structurally dependent; effects of strain on orbital interactions differ vastly between semiconductors as well as between coherent polytypes of the same semiconductor.

Grouping of the band gap behaviours in terms of their expected emission spectra allows for the results in this study to be comparable to those found in an experimental framework. Hence, the following sections provide analyses of individual semiconductors as well as comparisons of trends found to past investigations.

[14] Degenerate or degeneracy in this context refers to differing states (orbitals) that give the same value upon measurement.

6.2 III-V & II-VI Semiconductor Behaviour

Although classifications of band gap behaviours with strain could not be performed within various functional groups, common trends in behaviour were apparent. Homogeneity in strain & band gap behaviour between WZ & ZB-(111) structures of individual semiconductors were adhered to in most cases par GaN & ZnO. The behaviours of InP & ZnS were considered homogenous despite differing band gap behaviours (types B & C) between polytypes, as strain applications resulted in a net reduction in band gap. Analyses of semiconductors sharing orbitals ('Ga-', 'In-', '-As' & 'Zn-') showed inconsistent behaviours between CBM/VBM behaviours of the orbitals with strain application, affirming the strong chemical and structural dependence of strain & band gap behaviour. It was also noted that tensile strains had a larger effect on band gap modulation except for WZ GaSb where both strains had similar effects.

In the succeeding analyses, the absolute values of band gap upon strain application was not considered, however the trends were investigated. There was particular interest in rationalising the band gap evolution with strain with respect to orbital behaviours and sensitivity to strains. Nevertheless, band gaps for all strains applied are readily available in relevant subsections of Section 0.

6.2.1 GaAs

As seen in Figure 15, application of both tensile and compressive strain in both WZ & ZB-(111) structures caused a decrease in band gap, E_g (Type B). An interesting feature in GaAs was the observed direct ($\mathbf{\Gamma}_{VBM}$-$\mathbf{\Gamma}_{CBM}$) to indirect ($\mathbf{\Gamma}_{VBM}$-$\mathbf{A}_{CBM}$) band gap transition in the ZB-(111) structure upon application of -4% compressive strains. Analysis of the ZB-(111) CBM & VBM as shown in Figure 16b, shows $\mathbf{\Gamma}\rightarrow\mathbf{A}$ transition of the CBM occurs at ~3.1% compressive strain.

The reduction in band gap upon strain application was supported by past *ab initio* investigations [70,71]. However, a factor of note was the use of an indirect gap GaAs NWs

in literature. It was found that indirect to direct gap transitions occurred upon application of strains in both WZ & ZB-(111) structures. Although results between a NW and bulk were not directly comparable, trends were expected to remain consistent between both structures; and a lack of direct to indirect gap transition in the WZ structure in this study was of interest. An important note was that previous investigations analysed a **k** path from $\mathbf{\Gamma} \rightarrow \mathbf{X}$ in the BZ, however, as the fractional co-ordinates for **X** was listed as (0, 0, 0.5), this would be the same as point **A** in this thesis.

The DOS of GaAs in Appendix 9.3.1 reveals that the main orbital contributor to the CBM at **Γ** was Ga(4s) for both polytypes. There was a high degree of hybridisation present between Ga(4p) & As(4p) orbitals at the VBM, however, As(4p) was the main contributor. This was found to be in agreement with a past study[94].

Analysis of the CBM & VBM behaviour of both structures shown in Figure 16 reveals that valence band sensitivity to strain was comparatively smaller to the conduction band; surmising that the major contributor to band gap modulation was the CBM at **Γ**, attributed to Ga(4s). Analysis of the ZB-(111) DOS in Appendix 9.3.1 shows that the CBM at **Γ** & **A** are both attributed to the Ga(4s) orbital, hence the direct-indirect transition observed was not due to a shift in orbital contribution but an increase in the asymmetry of the conduction band with compressive strains, as seen in Appendix 9.4.1.

6.2.2 GaN

GaN orbitals overlap in a degenerate manner at the VBM. As seen in Appendix 9.3.2, in both structures, N(2p) had the highest contribution to the VBM. Unlike GaAs, there was a strong overlap in the Ga(4s) & N(2s) orbital at the CBM highlighting strong hybridisation at the **Γ** point. This was found to be in accordance to literature.[95]

The band gap behaviour of GaN upon strain application showed different effects between WZ & ZB-(111) structures. Evidenced in Figure 17, tensile strains caused

degradation of E_g in both structures however, WZ structure had a linear relationship with strain; increasing with tension and decreasing with compression (Type A). The ZB-(111) structure had an initial increase in band gap with compressive strain, however past 2% compressions the band gap dropped (Type C).

Strain had more pronounced effects on the conduction bands in both structures, as seen in Figure 18. This suggests that variation of E_g with respect to strain was dependent on the evolution of the CBM, due to the Ga(4s) & N(2s) orbitals. This conclusion was also supported in a previous *ab initio* HSE06 study[95].

Findings on the linear nature of strain & band gap behaviour of the WZ structure was found to be in support of past work on uniaxially strained GaN NWs[8]. Strains were applied up to the elastic limit of 10% in GaN in this thesis for direct comparison to this *ab initio* GGA study by Xia et al. It was reported that under compressive strains of greater than 6%, a direct-indirect gap transition would occur from $\mathbf{\Gamma}_{VBM}$-$\mathbf{\Gamma}_{CBM}$ to $\mathbf{F}_{VBM}$-$\mathbf{\Gamma}_{CBM}$. However, as **F** was not a standard denotation of high symmetry points in the BZ and the co-ordinates of **F** was not provided, a direct comparison to this work was not possible. Furthermore, a lack of electronic band structures in the literature made further investigation into this phenomenon not possible.

As the only Ga- based structure in this study that did not have a reduction in E_g upon strain application was WZ GaN, a further increase in compressive strains on the WZ structure was proposed to investigate this effect. However, for feasible application to NWs, superseding the elastic limit of ~10% strain in NWs was deemed to be outside the scope of this study.

A past experimental investigation into uniaxially stained WZ GaN NWs[72] also agreed with these findings. In this, x-ray diffraction (XRD) data demonstrated that application of tensile strains reduced band gap and applications of compressive strains reduce band gap.

6.2.3 GaSb

A salient feature in gap-strain behaviour of GaAs was the immediate introduction of a direct-indirect ($\mathbf{\Gamma}_{\text{VBM}}$-$\mathbf{A}_{\text{CBM}}$) gap transition upon compression in the ZB-(111) structure. As shown in Figure 19, like GaAs, application of strains caused a reduction of E_g in both structures (Type B). However, the trends in their valence and conduction bands were contrastingly different.

Both the CBM & VBM in the WZ structure were sensitive to strain applications at $\mathbf{\Gamma}$ (see Figure 20); with an increase in the VBM and a reduction in the CBM upon strain implementation. Although the CBM showed greater sensitivity to strain, this surmises that E_g behaviour was dependent on both bands. Alternatively, the VBM of ZB-(111) was insensitive to strain application. The behaviour of the band gap in this case was attributed to the CBM, contributed by the Ga(4s) orbital at both $\mathbf{\Gamma}$ and $\mathbf{A}$ points. The $\mathbf{\Gamma}\rightarrow\mathbf{A}$ CBM transition occurred at compressions of ~0.18%.

The DOS of both GaSb structures show strong hybridisation at the $\mathbf{\Gamma}$ point at both the CBM & VBM (see Appendix 5.3.3). These were Ga(4s) & Sb(5s) for the CBM, and Ga(4p) & Sb(5p) for the VBM. Furthermore, the p-orbitals were degenerate at the VBM. However, slightly larger contributions were observed from Ga(4s) & Sb(5p), making them the main orbital contributors to the CBM & VBM, respectively. Such findings were found to be in accordance to past work.[96]

Similar to GaAs NWs, an *ab initio* LDA study by Li-Ming et al. determined that the NW morphology of GaSb acts as an indirect gap semiconductor[9]. Strains in both WZ & ZB-(111) structures were determined to also result in a reduction of the band gap, in agreement with the results found in this thesis. There was, also immediate indirect-direct gap transitions reported upon application of strains in the WZ structure and tensile strains in the ZB-(111) structure. The occurrence of a gap transition only in the ZB-(111) structure with compression in this study highlights a key difference in the findings.

6.2.4 InAs

A strong degree of hybridisation at the CBM occurred in the ZB morphologies between the In(5s) & As(4s) orbitals. This was not as evident in the WZ structure however, In(5s) remained as the largest contributor in all structures. Hence, As(4p) and In(5s) were determined to be the main orbital contributors to the VBM & CBM respectively for all structures (as seen in Appendix 9.3.4). These results were in agreement to past literature on WZ InAs; where the major orbital contributors to the VBM and CBM were the p-orbitals and s-orbitals, respectively[40].

InAs experienced an inversely linearly proportional relationship with strain (Type A); where compressive strains caused an increase in E_g and tension resulted in a decrease in E_g (as seen in Figure 21). The WZ structure experienced greater changes in E_g with strain application in comparison to the ZB-(111) structure.

Application of tensile strain had similar effect on the CBM and VBM in WZ InAs however, compressive strains caused a larger evolution in the CBM (see Figure 22a). Nonetheless, the stronger resultant change in band gap, ΔE_g, was caused by tensions, suggesting modulation of E_g was governed by similar effects of strain on both the In(5s) orbital & As(4p) orbital in the CBM & VBM respectively. The favouring of tensile strains was also evident in the ZB-(111) structure, with the CBM & VBM behaviour mimicking the WZ behaviour indistinguishably (see Figure 22b). These findings were found to be consistent to an *ab initio* investigation in the uniaxial stress application on ZB-(111) InAs NWs, where this linear trend was observed between stress and band gap[73]. This also surmises that strain and stress applications should yield the same band gap behaviour in structures.

In WZ InAs, there was also an observed VBM shift in the band structures from $\mathbf{\Gamma}$ to the adjacent $\mathbf{k}$ point with co-ordinates (0, 0, 0.025) upon application of all strains (see Appendix 9.4.4). Similarly, there was an observed VBM shift from $\mathbf{\Gamma}$ to adjacent $\mathbf{k}$

point co-ordinates (0.025, 0, 0) upon application of 4% & 6% compressive strains in the ZB-(111) structure.

As the location of both VBM & CBM by nature always occurs at points of high symmetry in the BZ, this was attributed to technical errors of VASP. A range of methods were implemented to alleviate this effect to no avail, including: changing the electronic minimisation algorithm (between 'Normal', 'All' & 'Damped'[15]), increasing the **k** mesh size to up to 12 x 12 x 8 and increasing the convergence criteria of ionic and electronic iterations by up to a factor of 10^2 in calculations. Hence, the energies found at said **k** points were listed as that of the **Γ** point for these strains. Further investigation into this effect will be of interest in future work.

6.2.5 InP

Strain application on InP structures were initially considered within bounds of ±6% however, compressive strains on the WZ structure was increased to 10% to further investigate homogeneity in band gap evolution with strain between the coherent ZB-(111) & WZ lattice structures. In both structures, strains resulted in an overall reduction in band gap (Type B for ZB-(111)). However, compressive strains up to 4% first increased E_g before a linear reduction occurred in WZ InP (Type C), as depicted in Figure 23.

In both structures, the s-orbitals were degenerate at the CBM, showing equal contributions between In(5s) & P(3s). The hybrid nature at the VBM showed similar effects between In(5p) & P(3p) however, the P(3p) orbital was found to be the main contributor at this point (see Appendix 9.4.5). These findings were consistent with literature where the CBM state was attributed to the s-orbitals and VBM state to the p-orbitals. [97]

[15] This refers to the 'ALGO' tag in the VASP input file, INCAR.

As evidenced in Figure 24, E_g modulation with strain in both polytypes was attributed to the behaviours of the s-orbitals in the CBM at **Γ**. The behaviour of the CBM in both structures were homogenous upon strain application; resulting in a decrease upon compressions and tensions.

To understand this shift in band gap maxima from strain-free to 4% compressive strain in WZ InP despite similar CBM behaviour, the strain-mediated band structures were considered (see Appendix 9.4.5). Application of compressive strains in the WZ structure caused an overlap of the bands at the VBM in a degenerate manner. In contrast, this resulted in the separation of overlapping orbitals in the VBM of the ZB-(111) structure, with the 'heavy hole' band rising to the VBM.

Furthermore, relative symmetry in the conduction band was still maintained at the **Γ** point, for up to 4% compressive strains in the WZ structure. Exceeding this resulted in asymmetry of the conduction band. Tensile strains on the other hand increased symmetry in the conduction bands, which was consistent with the CBM behaviour of the ZB-(111) structure. Although compressive strains also reduced symmetry in the ZB-(111) CBM, the strain free conduction band was initially asymmetrical. As a reduction in band gap remained in compressive strains despite differing VBM behaviours, the band gap maxima shift to -4% strain in WZ InP was surmised to be promoted by the behaviour of the In(5s) & P(3s) orbitals at the CBM.

Investigations into strain application for band gap modulation of InP were lacking and hence no comparisons to the trends found in this study could be made. However, comparison of the strain-free band structures and lattice constants to literature affirms the methodology proposed by this study was sound and results determined to be correct.[29,30,38,41]

6.2.6 ZnO

The trends found in ZnO were homologous with those found in GaN. Like InP, compressive strains on the WZ structure were increased to 10% to investigate homogeneity between strain and E_g nature of both polytypes. Both WZ and ZB-(111) morphologies had a linear reduction of E_g with tensions however, effects compressive strains differed between the two.

The band gap of the WZ structure decreased with tension and increased with compression (Type A), as seen in Figure 25. Tensions had a larger effect on band gap modulation, suggesting the band gap of WZ ZnO was more sensitive to tensile strains. These findings were consistent with previous theoretical investigations[4]. There were little noticeable changes in the band structures seen in Appendix 9.4.6; where the only detail of note would be the separation of overlapping bands at the VBM with compressive strains. Analysis of the CBM & VBM in Figure 26a suggests that the evolution of E_g with strain was dependent on both CBM and VBM during tensions whilst the major contributor during compression was the VBM.

The CBM can be attributed to the Zn(4s) & O(2s) orbitals in both polytypes, as evidenced in the DOS in Appendix 9.3.6. Past literature on the WZ structure suggests strong hybridisation at Γ for both p-orbitals at the VBM[98]. This was also evident in this work however, the lighter O(2p) orbitals showed much greater contributions to the VBM, in agreement to a separate ZB study[99].

Alternatively, the ZB-(111) structure had an initial increase in E_g with compressive strains, however, compressions of more than 2% yielded an immediate reduction in E_g. Evidently in Figure 26b, the conduction bands were also more sensitive to strains, thus attributing the band gap modulation to the behaviour of Zn(4s) & O(2s) at the CBM. The strain-mediated band structures of ZB-(111) showed little changes in band behaviours upon application of strains (see Appendix 9.4.6). Of note however, was

the separation of degenerate bands at the VBM with compressions, with a noticeable rise in the 'heavy' band. However, this splitting of overlapping bands occurred in both structures during compression. Hence, it would be presumptuous in correlating the rise of the heavy valence band to a reduction of band gap; as this did not occur in the WZ polytype.

A PDOS of each strained band structure to determine the mechanism of this gap-strain behaviour would hence be desired in further investigations into the ZB-(111) structure. A further break down of the PDOS in the p-orbitals to (p_z, p_x & p_y) and d-orbitals to (d_{z2}, d_{xz}, d_{yz}, d_{xy} & d_{x2-y2}) would be also desired to more clearly attribute the behaviour of the band structure to specific orbitals. However, due to large computational costs and time restraints, this data was not able to be included in this work.

Expected spectra broadening of ZnO NWs, as proposed in Table 11, was affirmed by previous experimental investigations into bent WZ ZnO NW. These studies proposed that red shift occurs in regions of tension[4,60] and blue shift[60] occurs in regions of compression in the bent NW. These findings agreed with this study; as tensions reducing the band gap would cause a redshift and compressions increasing the band gap would cause a blueshift. As seen in Figure 31, the emission spectrum would thus be broadened to include the spectra of both the red and blue shifted regions; confirming the proposed emission spectrum behaviour.

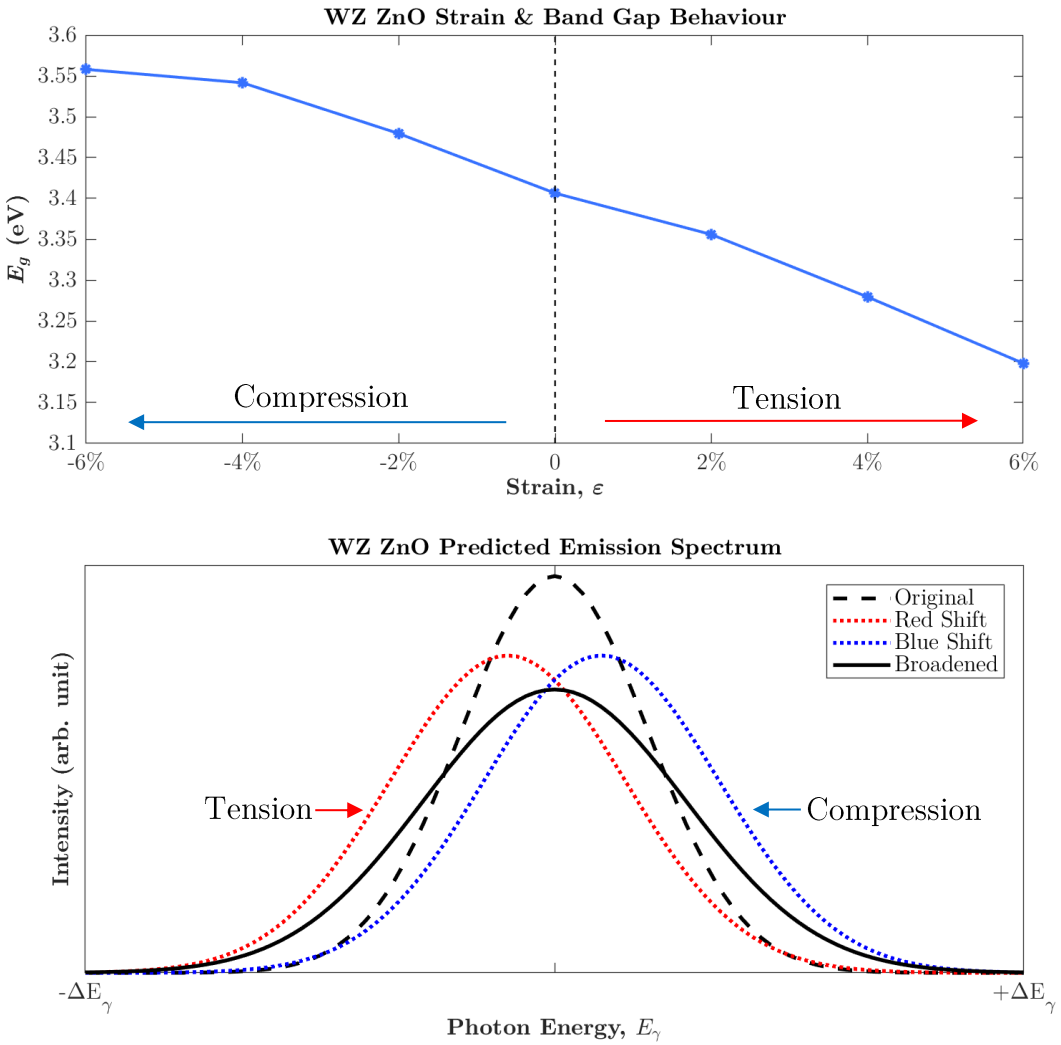

Figure 31 - WZ ZnO; Strain & Band Gap behaviour (top), Predicted Emission Spectrum (bottom).

6.2.7 ZnS

Band gap behaviour upon strain application in ZnS structures were analogously similar to InP. Strains for ZnS were initially considered within bounds of 6%; within the elastic limit of NWs. However, due to dissimilar band gap behaviour between the polytypes with compression, compressive strains were increased to 10% in the WZ structure.

Tensile strains in both WZ and ZB-(111) polytypes resulted in linear deterioration of E_g. As displayed in Figure 27, application of compressive strains ensued different responses; resulting in E_g reduction in the ZB-(111) structure, and E_g promotion in the WZ structure up to 8% compressive strains. Compression applied past 8% resulted in an immediate drop in E_g. In this manner, consistency in strain & E_g behaviour was maintained between the ZnS polytypes.

Like ZnO, the lighter S(3p) orbital displayed much larger attribution to the VBM. There was also a large hybridisation between the Zn(4s) & S(3s) orbital in the CBM which was not present in the VBM, as shown in Appendix 9.3.7. This was consistent with findings in previous work on ZB ZnS[99].

Analysis of the CBM and VBM behaviours of both structures determined that the conduction bands were comparatively more sensitive to strain applications than the valence bands, (see Figure 28), hence surmising that E_g behaviour was attributed to effects of strain on the s-orbitals in the CBM. A prominent feature displayed was an almost indistinguishable trend between the CBM and VBM behaviours of both WZ & ZB-(111) structures.

Band structure behaviours however, were contrastingly different between the polytypes, with respect to compressive strains on the conduction bands (see Appendix 9.4.7). Compressive strains in the ZB-(111) structure resulted in a reduction in symmetry of the lowest conduction band. This behaviour also occurred in the WZ polytype however, there was also a progressive overlapping of the bottom 2 conduction bands with

compressions. The lowest conduction band in the strain free band structure will be referred to as CB_1 and the 2nd lowest as CB_2. The position of CB_2 relative to CB_1 progressively reduced toward the band gap with compression, with CB_2 overtaking CB_1 at a compressive strain of 10%. The CBM location had shifted from the **Γ** point on CB_1 to the **Γ** point in CB_2, correlating with the reduction in band gap in the WZ structure. This strongly suggests that the evolution of the band gap in the WZ structure was dependent on the orbitals attributed to the CBM at both CB_1 and CB_2.

Analysis of the DOS of WZ ZnS in Appendix 9.3.7, shows that the **Γ** point in CB_2 was similarly contributed by the Zn(4s) & S(3s) orbital. This suggests that the reduction in band gap was not due to orbital separations. As DOS for the individual strained band structures were not obtained due to computational costs and time restrictions, further investigation into the DOS of the strained band structures for WZ ZnS would be a noteworthy interest. Past investigations into ZnS were also lacking hence direct comparison of data could not be made. However, comparison of the strain free band structures to literature showed similar band behaviours and band gaps, affirming the methodology implemented was valid.[31,43,48]

6.3 Applications

There are profound applications of the findings in this thesis with respect to III-V and II-VI semiconductors. Wide direct band gap semiconductors, such as those of III-V & II-VI materials, present significant advantages over indirect Si- based compounds in optoelectronic applications. Their wide direct band gaps causes the photon energy emitted by electron transitions between the conduction and valence band to be within the visible spectrum, and hence are commonly used in light emitting devices such as: light emitting diodes (LEDs), and laser diodes (LDs)[100].

Current LED technology uses semiconductors of varying band gaps to produce differing spectrum of visible light. To achieve a range of colours, commonly 3 LEDs are used in parallel; red, green and blue (RGB). [100] Varying the intensity of each RGB LED allows for a broad visible spectrum to be emitted. With strain mediation, the capability to modulate the band gap of semiconductors allows for the use of a single LED to produce a whole spectrum of colours. Taking GaAs as an example, it has a wide direct band gap and emits blue light. From the findings in this thesis, strain application will result in a reduction in band gap (Type B), which causes a red shift in light emitted; allowing the spectrum of visible light emitted to be the entire range from blue to red.

These implications can be applied to many other optoelectronic and field emissive applications. The method of strain proposed in this thesis gives complete control in band gap modulation and hence, emission behaviour of the III-V & II-VI semiconductors considered. The results and behaviours garnered in this study are applicable to both future NW and bulk studies. The use of bulk unit cells eliminated external factors to band gap modulation par applied strain. Future investigations using strain as a mechanism to modulate band gap, including commonly used lattice mismatches in bulk semiconductors[3], have both theoretical and expected experimental emission spectra benchmarks.

6.4 Limitations

As aforementioned, the use of a bulk model to mimic the behaviour of strain on a bent NW led to differences in gap transition behaviour; as seen in the Ga- based III-V semiconductors. Although the behaviours of band gap evolution with strain remained consistent between the bulk model used and previous investigations using NW models, findings in this thesis cannot be used to engineer band gap transition in these respective semiconductor NWs. Numerous factors come into play with respect to band gap transitions, the most prominent of which are the existence of internal strains, surface effects and quantum confinements effect in NWs. Replication of these factors were not considered in this thesis as interest was purely in understanding the behaviour of band gap evolution with strain. In doing so, separation of band gap modulation effects could be made between these external factors and applied strain.

Furthermore, as classifications of trends could not be performed between coherent polytypes (WZ & ZB-(111)), semiconductor groups (III-V & II-VI) or orbitals (Ga-, In-, -As, Zn-); results garnered can only be applied to the specific III-V and II-VI semiconductors studied.

Comparisons of emission spectra surmised to previous experimental investigations was limited to WZ ZnO. This was due to a lack of previous bent NW investigations of materials within the scope of this thesis. Nonetheless, the predicted spectra of WZ ZnO was affirmed by 2 past investigations, endorsing the validity of the computational methods implemented.

Lastly, the irregular InAs VBM shift behaviour would introduce sources of error into the absolute band gap values. The source of the introduction of technical error by VASP could not be determined; though a range of methods were employed to investigate these occurrences. However, comparison of InAs behaviours observed in this study to literature surmised that the results obtained were minimally affected by these errors.

7.0 Conclusion

This investigation found that there were 3 distinct behaviours observed between external strain application and band gap behaviours of bent semiconductor nanowires. These were named Types A, B & C, and were in order: inversely linearly proportional to strain, immediate reduction in band gap, and 'compression shifted peak' reduction in band gap.

- Type A systems included: WZ GaN, WZ & ZB-(111) InAs, and WZ ZnO.
- Type B systems included: WZ & ZB-(111) GaAs, WZ & ZB-(111) GaSb, ZB-(111) InP, and ZB-(111) ZnO.
- Type C systems included: ZB-(111) GaN, WZ InP, ZB-(111) ZnO, and WZ ZnS.

Corresponding emission spectra of these behaviours were also surmised detailing expected behaviour in an experimental framework. The predicted spectra behaviour of type A was confirmed in WZ ZnO though lack of studies in bent NWs meant comparisons of other behaviours could not be made. These predictions provide a benchmark for future experimental work on band gap behaviour of bent NWs. Analyses showed that common trends in strain & band gap behaviour between coherent polytypes (WZ & ZB-(111)), semiconductor groups (III-V & II-VI) or orbitals (Ga-, In-, -As & Zn-) were not apparent. This strongly suggests chemical and structural dependence of strain & band gap behaviour. It was also observed that band gap modulation was much more sensitive to tensile strains in all systems, par WZ GaSb where both compressions and tensions has similar effects.

Results found in this study with respect to band gap modulation of NWs were in support of past investigations however, occurrences of band gap transitions were not in agreement. The application of a bulk model to simulate strain behaviour in bent NWs removed external effects on the band gap, including; quantum confinement effect, internal strains and surface effects. These have been shown in literature to contribute

significant effects to band gaps of semiconductor NWs. Trends found in this thesis were attributed purely to strain mediation, allowing the separation of behaviours found in previous studies to where these external factors were considered.

Continuing work on this thesis would first begin with further break downs of the PDOS into specific p-orbitals (p_z, p_x & p_y) & d-orbitals (d_{z2}, d_{xz}, d_{yz}, d_{xy} & $d_{x2\text{-}y2}$). Doing so would better attribute CBM and VBM to specific orbitals and allow further insight into orbital behaviours with strain application. As the behaviour of band gap evolution with strain was surmised to be strongly chemically and structurally dependent, this would be an avenue to discover trend like behaviours between similar orbitals. This would also allow greater insight to inhomogeneous behaviour of strain and band gap evolution between GaN & ZnS polytypes.

The observed VBM shift in InAs simulations would also be further investigated in future work. This irregular behaviour was not observed in any other calculations hence, to ensure reliability in the results and conclusions drawn on InAs polytypes, computational parameters that could have caused this would be investigated with much higher scrutiny. This would be also accompanied by further analysis of more III-V & II-VI semiconductors; to both investigate individual behaviours of the semiconductors, and to discern if other band gap behaviours occur with strain application; apart from types A, B & C surmised in this thesis.

Lastly, replication of this study using more complex NW models as opposed to bulk unit cells would be of interest; to perceive if the behaviours of band gap evolution with strain observed remains consistent between both models. This would also elucidate band gap transitions that were noted in past investigations of strain-mediated NWs which were not apparent in this study; allowing greater understanding upon the individual contributions from internal strains, quantum confinement effect, surface effects, and applied strain to band gap transitions in NWs.

Experimental work on bent NWs would also be of interest; to corroborate conclusions drawn on proposed emission spectra behaviour. Results of this thesis can be reproduced in an experimental framework with NWs as the polytypes chosen were of the orientations III-V and II-VI NWs tend to grow in.

The findings of this thesis can be applied to both bulk and NW scales, and pave the way to new novel applications of strain-mediated band gap modulation of semiconductors. The method of strain proposed in this thesis gives complete control in band gap modulation and hence, emission behaviour of the III-V & II-VI semiconductors considered. This includes fields such as optoelectronics, field emission, flexible piezotronics, and nanoelectromechanical systems (NEMS).

8.0 Bibliography

[1] P. Yang, R. Yan, M. Fardy, *Nano Lett.* **2010**, *10*, 1529.

[2] A. I. Hochbaum, P. Yang, *Chem. Rev.* **2010**, *110*, 527.

[3] C.-Z. Ning, L. Dou, P. Yang, *Nature Reviews Materials* **2017**, *2*, 17070.

[4] X. Han, L. Kou, X. Lang, J. Xia, N. Wang, R. Qin, J. Lu, J. Xu, Z. Liao, X. Zhang, et al., *Advanced Materials* **2009**, *21*, 4937.

[5] Y.-B. Wang, L.-F. Wang, H. J. Joyce, Q. Gao, X.-Z. Liao, Y.-W. Mai, H. H. Tan, J. Zou, S. P. Ringer, H.-J. Gao, et al., *Advanced Materials* **2011**, *23*, 1356.

[6] P. Bao, Y. Wang, X. Cui, Q. Gao, H.-W. Yen, H. Liu, W. Kong Yeoh, X. Liao, S. Du, H. Hoe Tan, et al., *Appl. Phys. Lett.* **2014**, *104*, 021904.

[7] T. Cheiwchanchamnangij, W. R. L. Lambrecht, *Phys. Rev. B* **2011**, *84*, 035203.

[8] S. Xia, L. Liu, Y. Kong, M. Wang, *Superlattices and Microstructures* **2016**, *97*, 327.

[9] L. Li-Ming, N. Feng, T. Li-Ming, *Acta Physica Sinica* **n.d.**, *64*, 227303.

[10] P. Hohenberg, W. Kohn, *Phys. Rev.* **1964**, *136*, B864.

[11] W. Kohn, L. J. Sham, *Phys. Rev.* **1965**, *140*, A1133.

[12] J. Heyd, G. E. Scuseria, M. Ernzerhof, *The Journal of Chemical Physics* **2003**, *118*, 8207.

[13] G. Kresse, J. Furthmüller, *Phys. Rev. B* **1996**, *54*, 11169.

[14] G. Kresse, J. Furthmüller, *Computational Materials Science* **1996**, *6*, 15.

[15] G. Kresse, J. Hafner, *Phys. Rev. B* **1993**, *47*, 558.

[16] G. Kresse, J. Hafner, *Phys. Rev. B* **1994**, *49*, 14251.

[17] M. Afzaal, P. O'Brien, *Journal of Materials Chemistry* **2006**, *16*, 1597.

[18] L. Sirleto, G. Coppola, M. Iodice, M. Casalino, M. Gioffrè, I. Rendina, in *Optical Switches*, Woodhead Publishing, **2010**, pp. 61–96.

[19] C. Lee, X. Wei, J. W. Kysar, J. Hone, *Science* **2008**, *321*, 385.

[20] R. Bøyesen, "Nanowire solar cells raises efficiency limit," can be found under http://www.nbi.ku.dk/english/news/news13/nanowire-solar-cells-raises-efficiency-limit/, **2013**.

[21] Z. L. Wang, J. Song, *Science* **2006**, *312*, 242.

[22] F. Patolsky, B. P. Timko, G. Yu, Y. Fang, A. B. Greytak, G. Zheng, C. M. Lieber, *Science* **2006**, *313*, 1100.

[23] W. C. O'Mara, R. B. Herring, L. P. Hunt, in *Handbook of Semiconductor Silicon Technology*, William Andrew Publishing/Noyes, **1990**.

[24] J. Wang, C. Youtsey, R. McCarthy, R. Reddy, N. Allen, L. Guido, J. Xie, E. Beam, P. Fay, *Appl. Phys. Lett.* **2017**, *110*, 173503.

[25] T. Ito, *Jpn. J. Appl. Phys.* **1998**, *37*, L1217.

[26] C.-Y. Yeh, Z. W. Lu, S. Froyen, A. Zunger, *Phys. Rev. B* **1992**, *46*, 10086.

[27] C. J. M. Rooymans, *Journal of Inorganic and Nuclear Chemistry* **1963**, *25*, 253.

[28] S. Froyen, M. L. Cohen, *Phys. Rev. B* **1983**, *28*, 3258.

[29] A. Zoroddu, F. Bernardini, P. Ruggerone, V. Fiorentini, *Phys. Rev. B* **2001**, *64*, 045208.

[30] F. Bechstedt, A. Belabbes, *J. Phys.: Condens. Matter* **2013**, *25*, 273201.

[31] F. Tran, P. Blaha, *Phys. Rev. Lett.* **2009**, *102*, 226401.

[32] K. Albe, K. Nordlund, J. Nord, A. Kuronen, *Phys. Rev. B* **2002**, *66*, 035205.

[33] Z. Zanolli, F. Fuchs, J. Furthmüller, U. von Barth, F. Bechstedt, *Phys. Rev. B* **2007**, *75*, 245121.

[34] P. Rinke, M. Scheffler, A. Qteish, M. Winkelnkemper, D. Bimberg, J. Neugebauer, *Appl. Phys. Lett.* **2006**, *89*, 161919.

[35] S. Tomić, B. Montanari, N. M. Harrison, *Physica E: Low-dimensional Systems and Nanostructures* **2008**, *40*, 2125.

[36] G. A. Sai-Halasz, R. Tsu, L. Esaki, *Appl. Phys. Lett.* **1977**, *30*, 651.

[37] M. Gmitra, J. Fabian, *Phys. Rev. B* **2016**, *94*, 165202.

[38] S. Q. Wang, H. Q. Ye, *J. Phys.: Condens. Matter* **2002**, *14*, 9579.

[39] R. Ahmed, S. Javad Hashemifar, H. Akbarzadeh, M. Ahmed, Fazal-e-Aleem, *Computational Materials Science* **2007**, *39*, 580.

[40] L. C. O. Dacal, A. Cantarero, *Mater. Res. Express* **2014**, *1*, 015702.

[41] I. Vurgaftman, J. R. Meyer, L. R. Ram-Mohan, *Journal of Applied Physics* **2001**, *89*, 5815.

[42] "A comprehensive review of ZnO materials and devices: Journal of Applied Physics: Vol 98, No 4," can be found under https://aip.scitation.org/doi/10.1063/1.1992666, **n.d.**

[43] S. Z. Karazhanov, P. Ravindran, A. Kjekhus, H. Fjellvåg, U. Grossner, B. G. Svensson, *Journal of Crystal Growth* **2006**, *287*, 162.

[44] M. P. Thompson, G. W. Auner, T. S. Zheleva, K. A. Jones, S. J. Simko, J. N. Hilfiker, *Journal of Applied Physics* **2001**, *89*, 3331.

[45] M. E. Straumanis, C. D. Kim, *Journal of Applied Physics* **1965**, *36*, 3822.

[46] M. Möller, M. M. de L. Jr, A. Cantarero, T. Chiaramonte, M. A. Cotta, F. Iikawa, *Nanotechnology* **2012**, *23*, 375704.

[47] D. C. Look, D. C. Reynolds, J. R. Sizelove, R. L. Jones, C. W. Litton, G. Cantwell, W. C. Harsch, *Solid State Communications* **1998**, *105*, 399.

[48] O. Zakharov, A. Rubio, X. Blase, M. L. Cohen, S. G. Louie, *Phys. Rev. B* **1994**, *50*, 10780.

[49] H. Ohno, A. Shen, F. Matsukura, A. Oiwa, A. Endo, S. Katsumoto, Y. Iye, *Appl. Phys. Lett.* **1996**, *69*, 363.

[50] I. Vurgaftman, J. R. Meyer, *Journal of Applied Physics* **2003**, *94*, 3675.

[51] A. V. Krukau, O. A. Vydrov, A. F. Izmaylov, G. E. Scuseria, *The Journal of Chemical Physics* **2006**, *125*, 224106.

[52] W. P. Mason, R. N. Thurston, *The Journal of the Acoustical Society of America* **1957**, *29*, 1096.

[53] D. V. Lang, R. People, J. C. Bean, A. M. Sergent, *Appl. Phys. Lett.* **1985**, *47*, 1333.
[54] H. M. Manasevit, I. S. Gergis, A. B. Jones, *Appl. Phys. Lett.* **1982**, *41*, 464.
[55] Y. Sun, S. E. Thompson, T. Nishida, *Strain Effect in Semiconductors: Theory and Device Applications*, Springer US, **2010**.
[56] S. Cahangirov, S. Ciraci, *Phys. Rev. B* **2009**, *79*, 165118.
[57] Y. Gao, Z. L. Wang, *Nano Lett.* **2007**, *7*, 2499.
[58] M. Nolan, S. O'Callaghan, G. Fagas, J. C. Greer, T. Frauenheim, *Nano Lett.* **2007**, *7*, 34.
[59] Q. Fu, Z. Y. Zhang, L. Kou, P. Wu, X. Han, X. Zhu, J. Gao, J. Xu, Q. Zhao, W. Guo, et al., *Nano Res.* **2011**, *4*, 308.
[60] H. Xue, N. Pan, M. Li, Y. Wu, X. Wang, J. G. Hou, *Nanotechnology* **2010**, *21*, 215701.
[61] T. Inaoka, T. Furukawa, R. Toma, S. Yanagisawa, *Journal of Applied Physics* **2015**, *118*, 105704.
[62] S. Yang, D. Prendergast, J. B. Neaton, *Nano Lett.* **2010**, *10*, 3156.
[63] C. L. dos Santos, P. Piquini, *Phys. Rev. B* **2010**, *81*, 075408.
[64] M. Cahay, *Quantum Confinement VI: Nanostructured Materials and Devices: Proceedings of the International Symposium*, The Electrochemical Society, **2001**.
[65] H. Haug, S. W. Koch, *Quantum Theory of the Optical and Electronic Properties of Semiconductors*, World Scientific, **1994**.
[66] F. Ning, L.-M. Tang, Y. Zhang, K.-Q. Chen, *Journal of Applied Physics* **2013**, *114*, 224304.
[67] K. Momma, F. Izumi, *Journal of Applied Crystallography* **2008**, *41*, 653.
[68] Duan X., Lieber C. M., *Advanced Materials* **2000**, *12*, 298.
[69] H. J. Joyce, J. Wong-Leung, Q. Gao, H. H. Tan, C. Jagadish, *Nano Lett.* **2010**, *10*, 908.
[70] A. Copple, N. Ralston, X. Peng, *Appl. Phys. Lett.* **2012**, *100*, 193108.
[71] X. Peng, A. Copple, *Phys. Rev. B* **2013**, *87*, 115308.
[72] H. W. Seo, S. Y. Bae, J. Park, H. Yang, K. S. Park, S. Kim, *The Journal of Chemical Physics* **2002**, *116*, 9492.
[73] K. Alam, *IEEE Transactions on Electron Devices* **2012**, *59*, 661.
[74] J. Wallentin, N. Anttu, D. Asoli, M. Huffman, I. Åberg, M. H. Magnusson, G. Siefer, P. Fuss-Kailuweit, F. Dimroth, B. Witzigmann, et al., *Science* **2013**, *339*, 1057.
[75] B. Wei, K. Zheng, Y. Ji, Y. Zhang, Z. Zhang, X. Han, *Nano Lett.* **2012**, *12*, 4595.
[76] S. Biswas, T. Ghoshal, S. Kar, S. Chakrabarti, S. Chaudhuri, *Crystal Growth & Design* **2008**, *8*, 2171.
[77] J. P. Perdew, K. Burke, M. Ernzerhof, *Phys. Rev. Lett.* **1996**, *77*, 3865.
[78] J. P. Perdew, K. Burke, M. Ernzerhof, *Phys. Rev. Lett.* **1997**, *78*, 1396.
[79] Georg Kresse, Martijn Marsman, Jürgen Furthmüller, "vasp," can be found under https://cms.mpi.univie.ac.at/vasp/vasp/vasp.html, **2018**.

[80] David S. Sholl, Janice A. Steckel, in *Density Functional Theory*, Wiley-Blackwell, **2009**, pp. 1–33.
[81] L. Weston, First-Principles Theoretical Studies of Bulk, Defect and Interface Properties of Oxide Semiconductors, The University of Sydney, **2015**.
[82] P. Ziesche, S. Kurth, J. P. Perdew, *Computational Materials Science* **1998**, *11*, 122.
[83] A. van de Walle, G. Ceder, *Phys. Rev. B* **1999**, *59*, 14992.
[84] C. Stampfl, C. G. Van de Walle, *Phys. Rev. B* **1999**, *59*, 5521.
[85] A. D. Becke, *The Journal of Chemical Physics* **1993**, *98*, 1372.
[86] A. S. Barnard, S. P. Russo, I. K. Snook, *Philosophical Magazine B* **2002**, *82*, 1767.
[87] R. T. Downs, M. Hall-Wallace, *American Mineralogist* **2003**, *88*, 247.
[88] P. E. Blöchl, *Phys. Rev. B* **1994**, *50*, 17953.
[89] G. Kresse, D. Joubert, *Phys. Rev. B* **1999**, *59*, 1758.
[90] Y. Hinuma, G. Pizzi, Y. Kumagai, F. Oba, I. Tanaka, *Computational Materials Science* **2017**, *128*, 140.
[91] A. Togo, I. Tanaka, *arXiv:1808.01590 [cond-mat]* **2018**.
[92] W. Setyawan, S. Curtarolo, *Computational Materials Science* **2010**, *49*, 299.
[93] Grumstrup Research Group, "Structure-Function Relationships in Nanomaterials," can be found under http://www.montana.edu/grumstruplab/research.html, **2018**.
[94] Y. I. Diakite, S. D. Traore, Y. Malozovsky, B. Khamala, L. Franklin, D. Bagayoko, *arXiv:1601.05300 [cond-mat]* **2016**.
[95] L. Qin, Y. Duan, H. Shi, L. Shi, G. Tang, *J. Phys.: Condens. Matter* **2013**, *25*, 045801.
[96] X. Lin, C. Niu, F. Pan, H. Chen, X. Wang, *Physica B: Condensed Matter* **2017**, *521*, 371.
[97] L. C. O. Dacal, A. Cantarero, *Solid State Communications* **2011**, *151*, 781.
[98] A. G. E. Hachimi, H. Zaari, A. Benyoussef, M. E. Yadari, A. E. Kenz, *Journal of Rare Earths* **2014**, *32*, 715.
[99] H. Dixit, R. Saniz, D. Lamoen, B. Partoens, *J. Phys.: Condens. Matter* **2010**, *22*, 125505.
[100] S. M. Sze, K. K. Ng, *Physics of Semiconductor Devices*, John Wiley & Sons, **2006**.

9.0 Appendix

9.1 VASP Key Calculation Parameters.

Key input parameters for calculations are listed as follows. These 2 steps begin after the assumption geometric relaxation has been already achieved.

Step 1 of 2) Self-consistent GGA calculation to obtain starting WAVECAR, wavefunction file.

INCAR:

```
ISTART = 0
EDIFFG = -0.01; EDIFF = 0.0001
ISMEAR = 0; SIGMA = 0.05
IBRION = 2
PREC = accurate

ISIF = 2; NSW = 0;
ENCUT = a # set a for system, can comment out line for default VASP setting
NBANDS = a # set number of electronic bands dependent on system
```

KPOINTS:

```
Automatic Mesh
0
Gamma-centred
6 6 4
0 0 0
```

Step 2 of 2) Zero – weighted self-consistent HSE06 calculation for band structure

Copy IBZKPT file to KPOINTS file and edit to input **k** points along high symmetry path desired, with 0 weighting at the end of the file. Ensure the total number of **k** points is updated in the header of the file.

Plot resulting band structure with 0 weighting. If eigenvalues between weighted and non-weighted points of high-symmetry are not converged, consider using a larger **k** mesh & a smaller AMIX value.

INCAR:

```
ISTART = 1 # set to 1 to continue from previous WAVECAR file
EDIFFG = -0.01; EDIFF = 0.0001
ISMEAR = 0; SIGMA = 0.05
IBRION = 2
PREC = accurate

ISIF = 2; NSW = 0;
ENCUT = a # set a for system, can comment out line for default VASP setting
NBANDS = a # set number of electronic bands dependent on system

LORBIT = 11 # LORBIT = 11 for projected DOS to be generated

# HSE Tags
LHFCALC = .TRUE. ; HFSCREEN = 0.2
ALGO = Normal; # ALGO = All # If Normal does not converge
IMIX = 1; AMIX = 0.1;  NELMIN = 5
AEXX = a  # set a (default = 0.25), set dependent on convergence test
LWAVE = .FALSE. # set .TRUE. to overwrite current WAVECAR file
```

KPOINTS (Sample path from Γ to M):

```
Automatically generated mesh
      31
Reciprocal lattice
    0.00000000000000    0.00000000000000    0.00000000000000             1
    0.16666666666667    0.00000000000000    0.00000000000000             6
    0.33333333333333    0.00000000000000    0.00000000000000             6
    0.50000000000000   -0.00000000000000    0.00000000000000             3
    0.16666666666667    0.16666666666667    0.00000000000000             6
    0.33333333333333    0.16666666666667    0.00000000000000            12
    0.33333333333333    0.33333333333333    0.00000000000000             2
    0.00000000000000    0.00000000000000    0.25000000000000             2
    0.16666666666667    0.00000000000000    0.25000000000000            12
    0.33333333333333    0.00000000000000    0.25000000000000            12
    0.50000000000000   -0.00000000000000    0.25000000000000             6
    0.16666666666667    0.16666666666667    0.25000000000000            12
    0.33333333333333    0.16666666666667    0.25000000000000            24
    0.33333333333333    0.33333333333333    0.25000000000000             4
    0.00000000000000    0.00000000000000    0.50000000000000             1
    0.16666666666667    0.00000000000000    0.50000000000000             6
    0.33333333333333    0.00000000000000    0.50000000000000             6
    0.50000000000000   -0.00000000000000    0.50000000000000             3
    0.16666666666667    0.16666666666667    0.50000000000000             6
    0.33333333333333    0.16666666666667    0.50000000000000            12
    0.33333333333333    0.33333333333333    0.50000000000000             2
0.00000000 0.00000000 0.00000000 0.000 ! This line and below contains
0.00000000 0.00000000 0.05555556 0.000 ! K-points chosen along the high
0.00000000 0.00000000 0.11111111 0.000 ! symmetry path in the BZ
0.00000000 0.00000000 0.16666667 0.000
0.00000000 0.00000000 0.22222222 0.000
0.00000000 0.00000000 0.27777778 0.000
0.00000000 0.00000000 0.33333333 0.000
0.00000000 0.00000000 0.38888889 0.000
0.00000000 0.00000000 0.44444444 0.000
0.00000000 0.00000000 0.50000000 0.000
```

9.2 Convergence Test

Representative convergence tests performed on WZ & ZB InAs.

InAs WZ-(0001)

Γ-centred **k** mesh convergence test at cut-off energy of 450 eV.

k mesh	E_{tot} (eV)	a (Å)	c (Å)	V (Å^3)	CPU Time (s)	T/T_0
3 x 3 x 2	-18.05	4.3413	7.0108	114.428	2530.62	1.00
4 x 4 x 2	-18.35	4.3198	7.0489	113.915	5838.76	2.31
6 x 6 x 4	-18.45	4.3120	7.0743	113.913	76021.51	30.04
9 x 9 x 6	-18.46	4.3100	7.0814	113.921	150158.58	59.34

Cut-off energy (**ENCUT**) convergence test using 6 x 6 x 4 **Γ**-centred **k** mesh.

ENCUT (eV)	E_{tot} (eV)	a (Å)	c (Å)	V (Å^3)	CPU Time (s)	T/T_0
200 (Default)	-18.4610	4.3098	7.0708	113.741	26168.21	1.00
250	-18.4503	4.3118	7.0739	113.897	32600.75	1.25
300	-18.4491	4.3119	7.0741	113.906	41070.18	1.57
350	-18.4499	4.3118	7.0739	113.898	69251.63	2.65
400	-18.4502	4.3119	7.0740	113.903	69496.61	2.66
450	-18.4502	4.3120	7.0743	113.913	76021.51	2.91
500	-18.4501	4.3121	7.0744	113.918	126259.18	4.82
550	-18.4501	4.3123	7.0742	113.924	183415.68	7.01
600	-18.4502	4.3122	7.0741	113.922	185111.20	7.07

InAs ZB-(001)

Γ-centred **k** mesh convergence test at cut-off energy of 450 eV.

k mesh	E_{tot} (eV)	a (Å)	c (Å)	V (Å^3)	CPU Time (s)	T/T_0
3 x 3 x 3	-27.15	4.3616	10.4471	172.114	5235.00	1
4 x 4 x 4	-27.57	4.3324	10.5304	171.169	32667.91	6.24
5 x 5 x 5	-27.68	4.3228	10.5641	170.961	44781.87	8.55
6 x 6 x 6	-27.72	4.3213	10.5694	170.927	141710.22	27.07
7 x 7 x 7	-27.73	4.3209	10.5713	170.922	151490.13	28.94

Cut-off energy (**ENCUT**) convergence test using 6 x 6 x 6 **Γ**-centred **k** mesh.

ENCUT (eV)	E_{tot} (eV)	a (Å)	c (Å)	V (Å^3)	CPU Time (s)	T/T_0
200 (Default)	-27.7317	4.31902	10.56332	170.648	17782.10	1
250	-27.7155	4.32099	10.56812	170.881	28081.06	1.58
300	-27.7137	4.32110	10.56838	170.894	34362.60	1.93
350	-27.7149	4.32101	10.56815	170.883	58388.81	3.28
400	-27.7154	4.32106	10.56829	170.889	57912.96	3.26
450	-27.7154	4.32118	10.56859	170.904	63696.68	3.58
500	-27.7152	4.32125	10.56874	170.912	94846.22	5.33
550	-27.7153	4.32124	10.56871	170.911	94024.26	5.29
600	-27.7156	4.32122	10.56866	170.908	108599.27	6.11

9.3 Strain-Free Band Structures & Density of States

The following band structures and DOS are displayed for polytypes WZ-(0001), ZB-(001) & ZB-(111). The Fermi-level for all figures was set at 0eV. Subplots per figure are in the order: band structure, DOS, PDOS Element 1, PDOS Element 2.

Within the DOS subplots both the total density of states (TDOS) of the semiconductor as well as the total atomic DOS for each element is shown. All calculations were done using HSE06 functional with a 6 x 6 x 4 or 6 x 6 x 6 $\mathbf{\Gamma}$-centred $\mathbf{k}$ mesh for WZ-(0001)/ZB-(111) and ZB-(001) respectively. Exact HF exchange fractions, α, used are shown in Table 1.

Band structure plots contain 41 $\mathbf{k}$ points plotted along the high symmetrical points in the irreducible BZ. The path for WZ-(0001) & ZB-(111) was $\mathbf{A} \rightarrow \mathbf{\Gamma} \rightarrow \mathbf{M}$ and ZB-(001) was $\mathbf{X} \rightarrow \mathbf{\Gamma} \rightarrow \mathbf{L}$.

9.3.1 GaAs

WZ GaAs

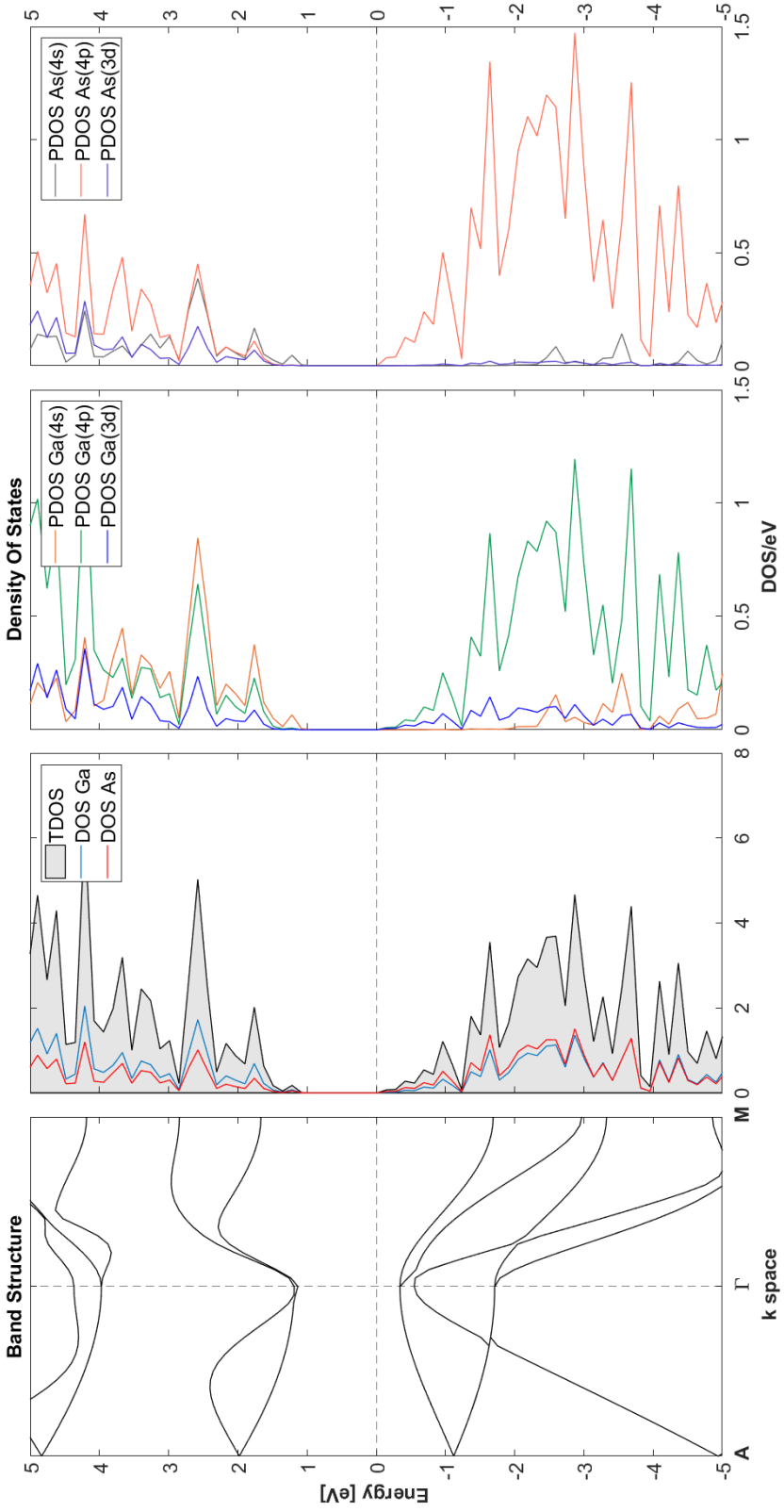

ZB GaAs

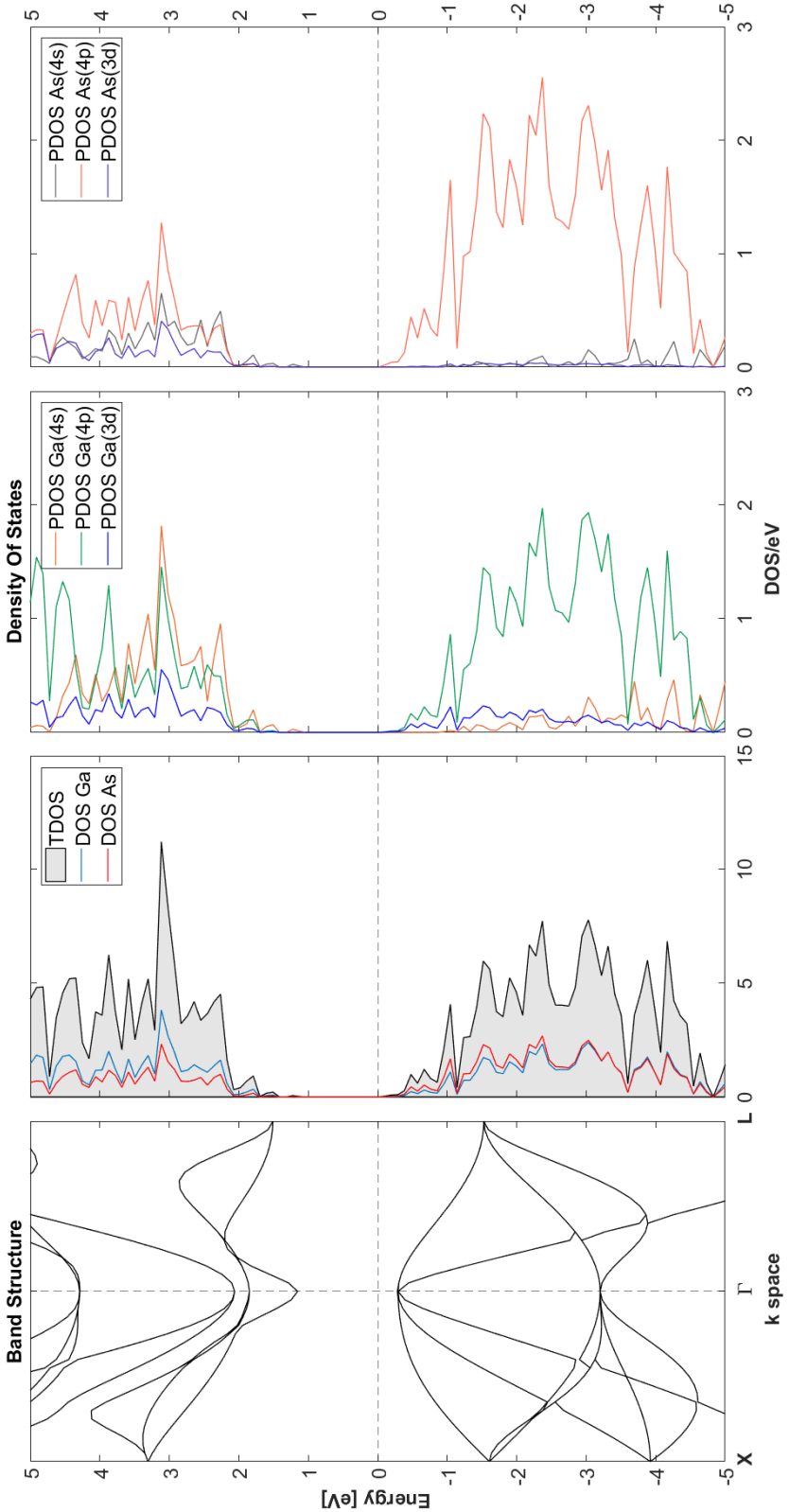
PDOS As(4s)
PDOS As(4p)
PDOS As(3d)
PDOS Ga(4s)
PDOS Ga(4p)
PDOS Ga(3d)
TDOS
DOS Ga
DOS As
Density Of States
DOS/eV
Band Structure
k space
Energy [eV]
X
Γ
L

ZB-(111) GaAs

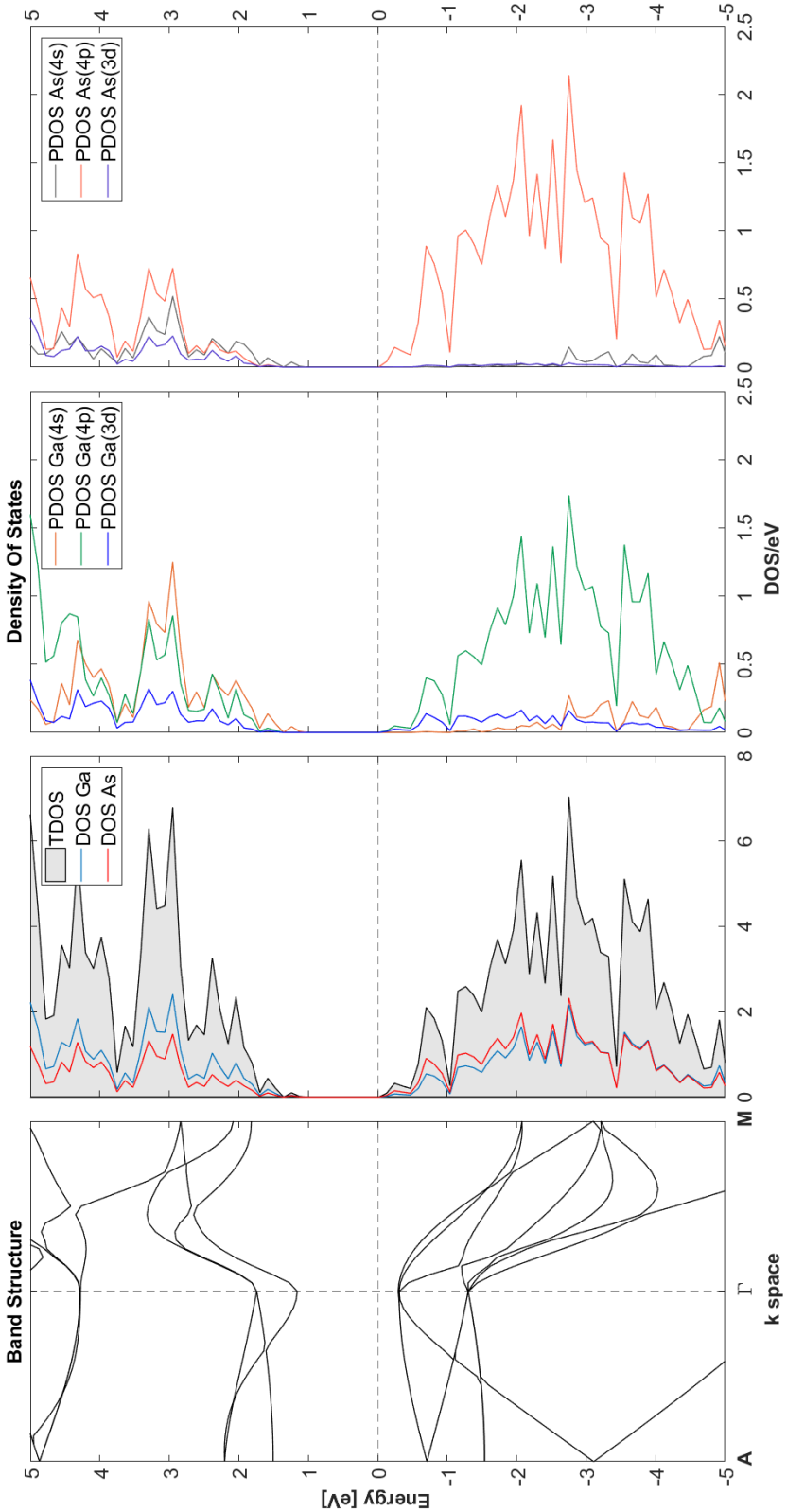
Band Structure
Density Of States
Energy [eV]
k space
A
Γ
M
DOS/eV
PDOS As(4s)
PDOS As(4p)
PDOS As(3d)
PDOS Ga(4s)
PDOS Ga(4p)
PDOS Ga(3d)
TDOS
DOS Ga
DOS As

9.3.2 GaN

WZ GaN

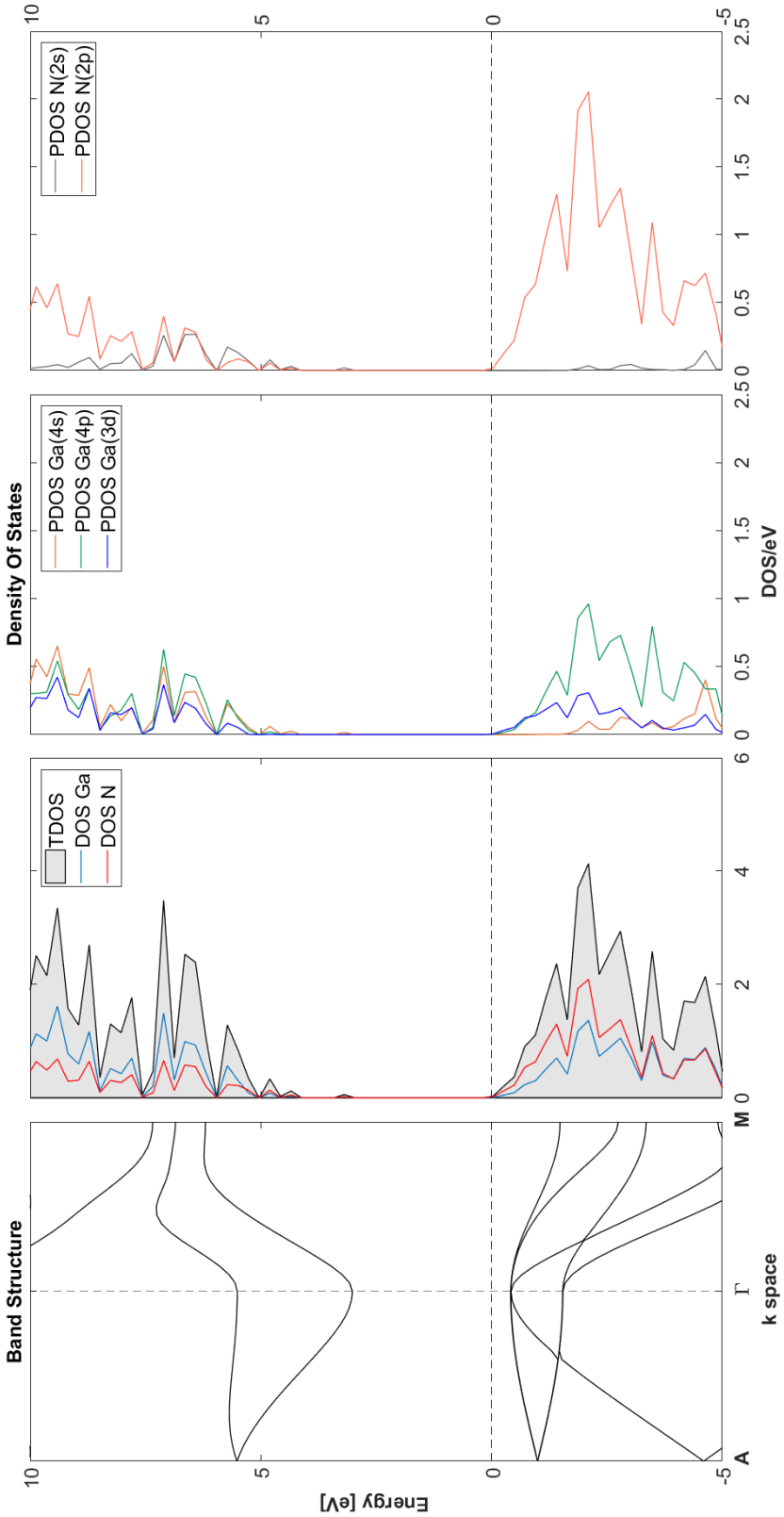

ZB GaN

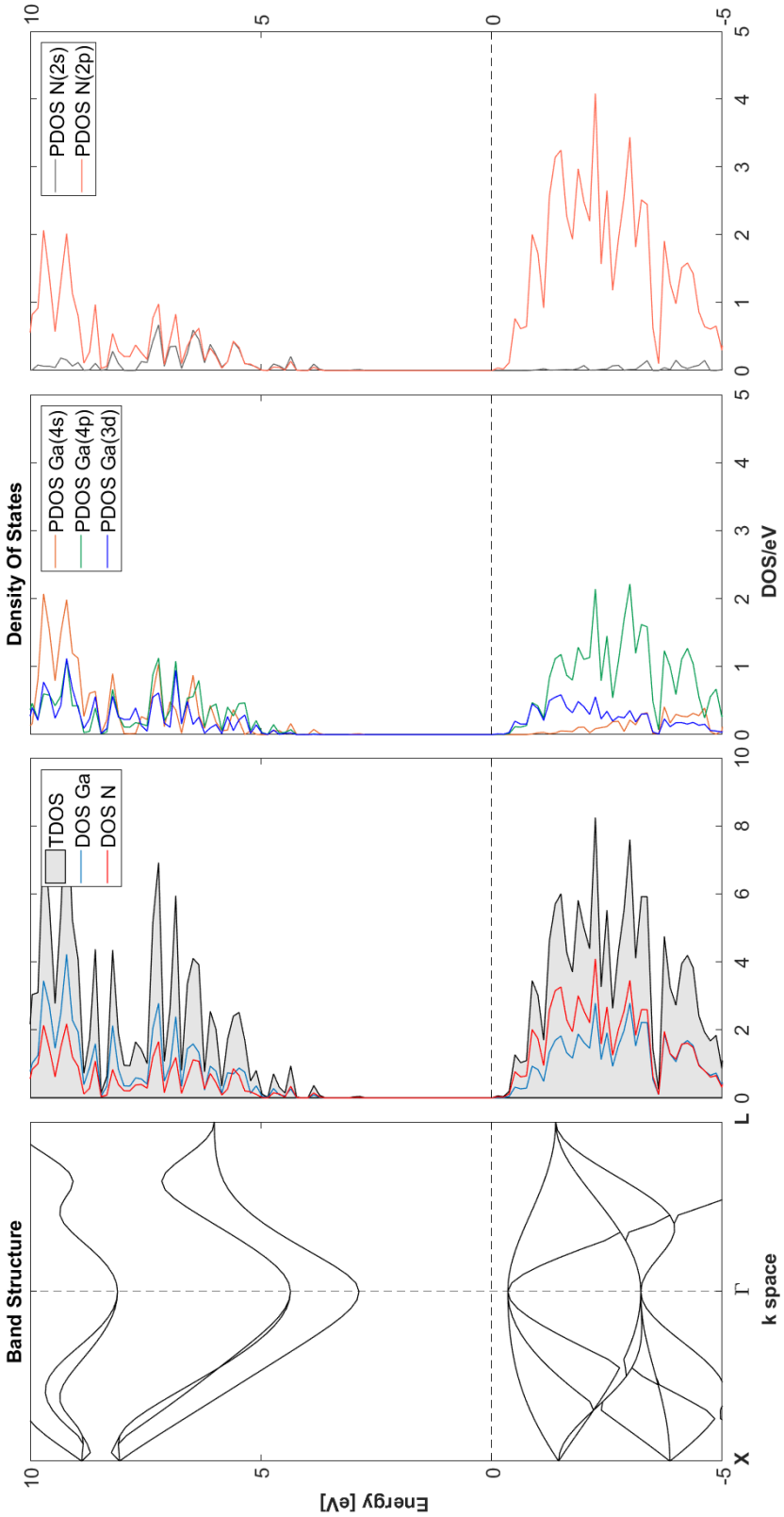
Band Structure
Density Of States
Energy [eV]
k space
DOS/eV
PDOS N(2s)
PDOS N(2p)
PDOS Ga(4s)
PDOS Ga(4p)
PDOS Ga(3d)
TDOS
DOS Ga
DOS N
X
Γ
L

ZB-(111) GaN

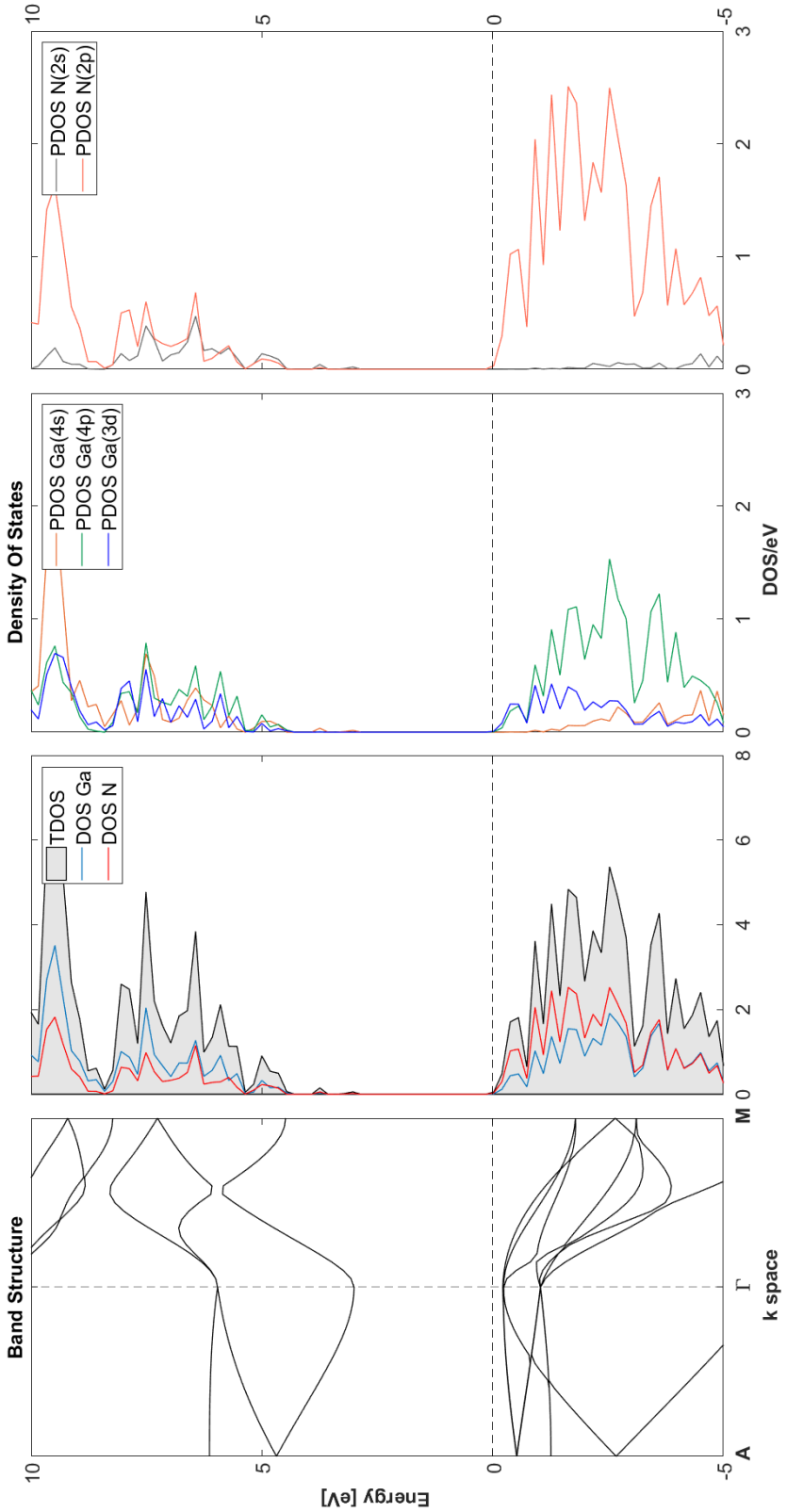
PDOS N(2s)
PDOS N(2p)
PDOS Ga(4s)
PDOS Ga(4p)
PDOS Ga(3d)
TDOS
DOS Ga
DOS N
Density Of States
DOS/eV
Band Structure
k space
Energy [eV]
M
Γ
A

9.3.3 GaSb

WZ GaSb

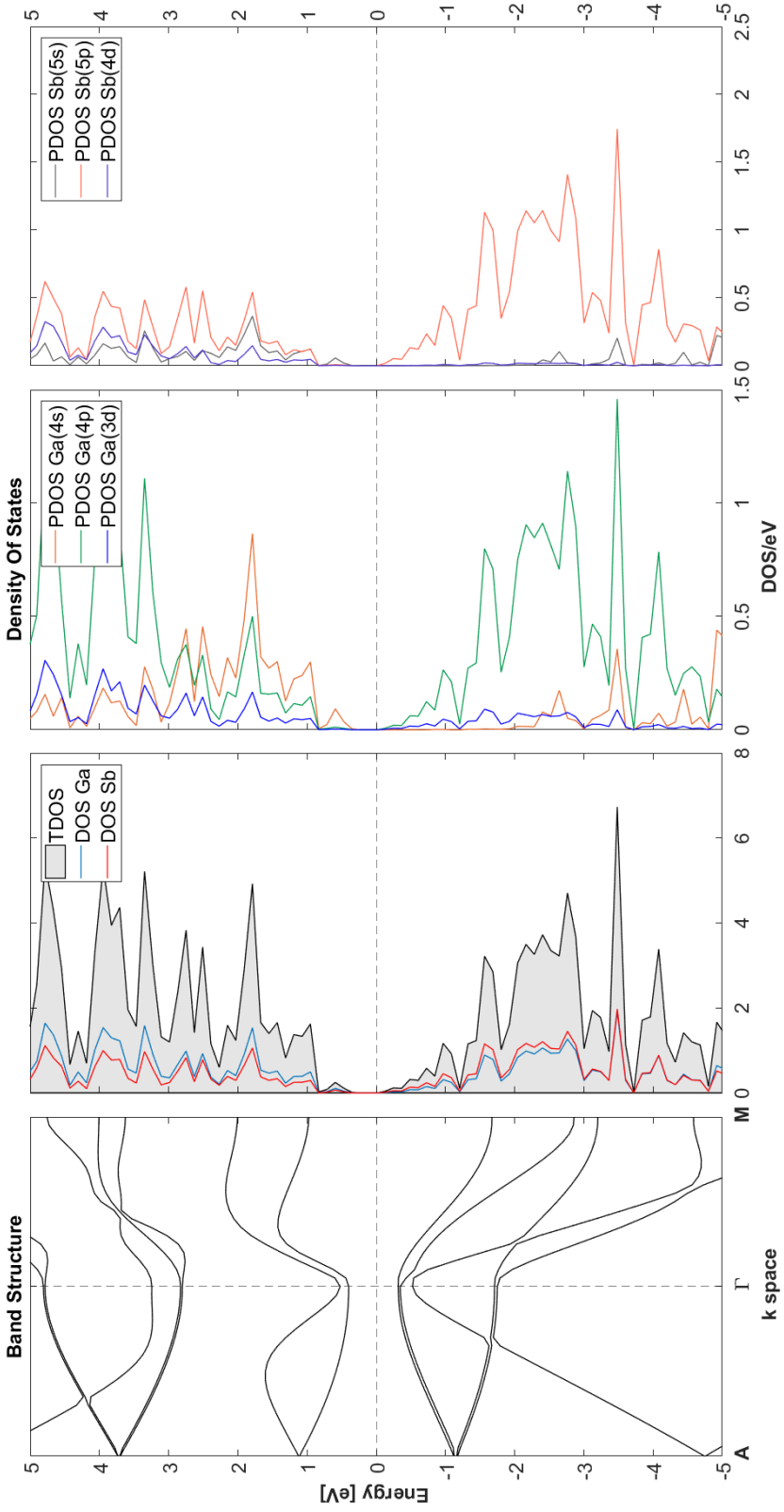

ZB GaSb

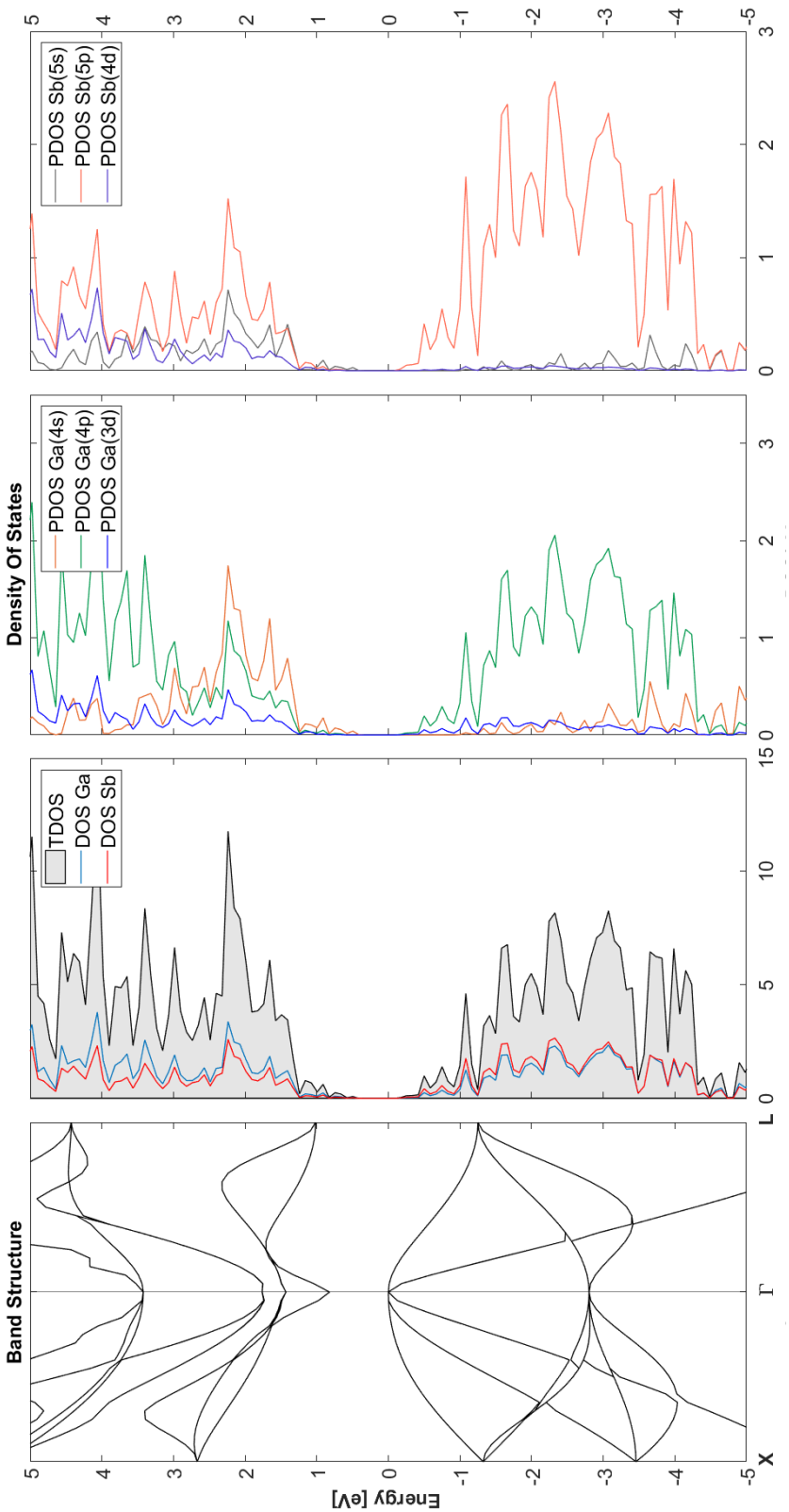
Band Structure
Density Of States
Energy [eV]
PDOS Sb(5s)
PDOS Sb(5p)
PDOS Sb(4d)
PDOS Ga(4s)
PDOS Ga(4p)
PDOS Ga(3d)
TDOS
DOS Ga
DOS Sb
X
Γ
L

ZB-(111) GaSb

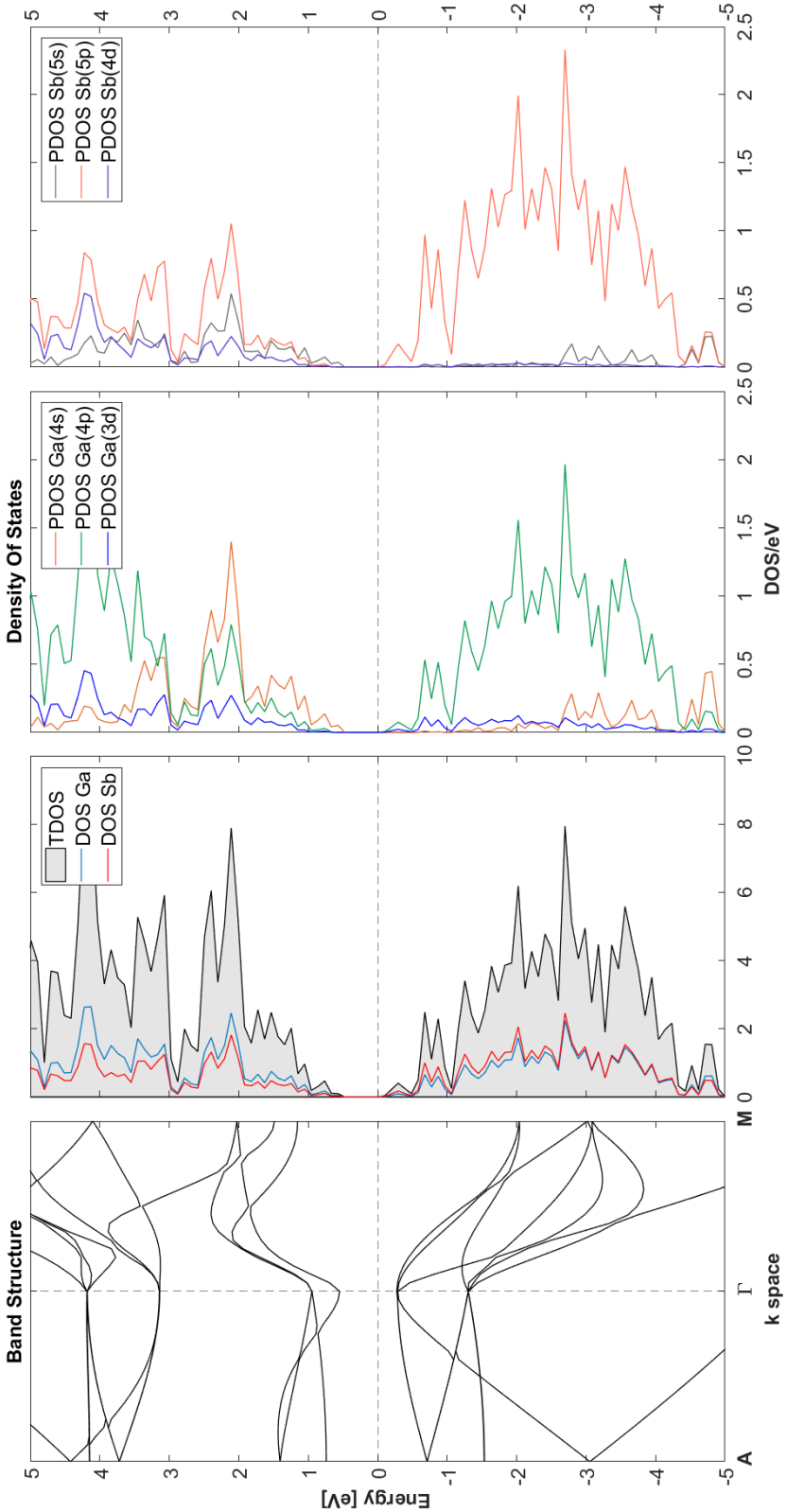
Band Structure
Density Of States
Energy [eV]
k space
A
Γ
M
DOS/eV
PDOS Sb(5s)
PDOS Sb(5p)
PDOS Sb(4d)
PDOS Ga(4s)
PDOS Ga(4p)
PDOS Ga(3d)
TDOS
DOS Ga
DOS Sb

9.3.4 InAs

WZ InAs

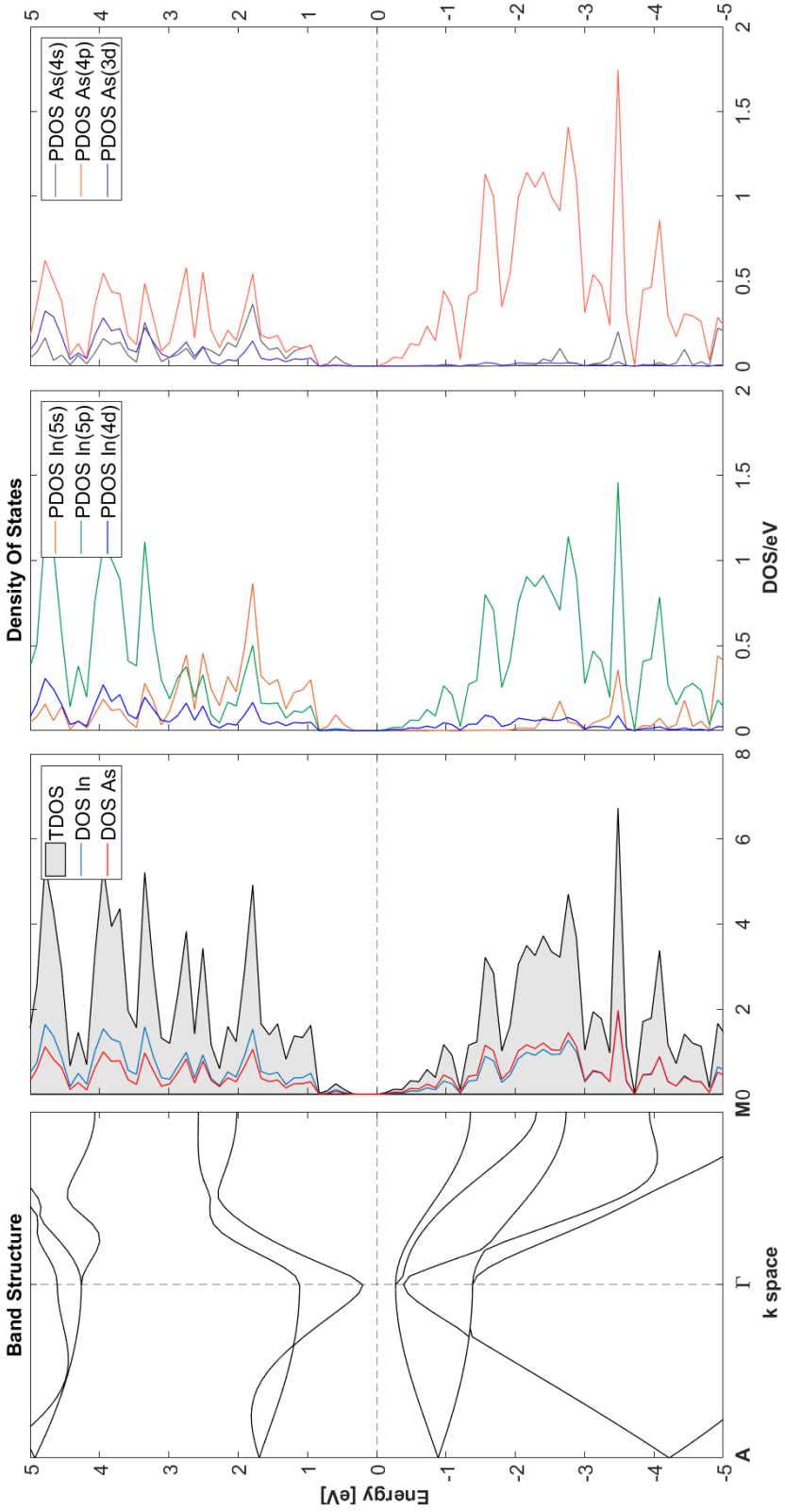

ZB InAs

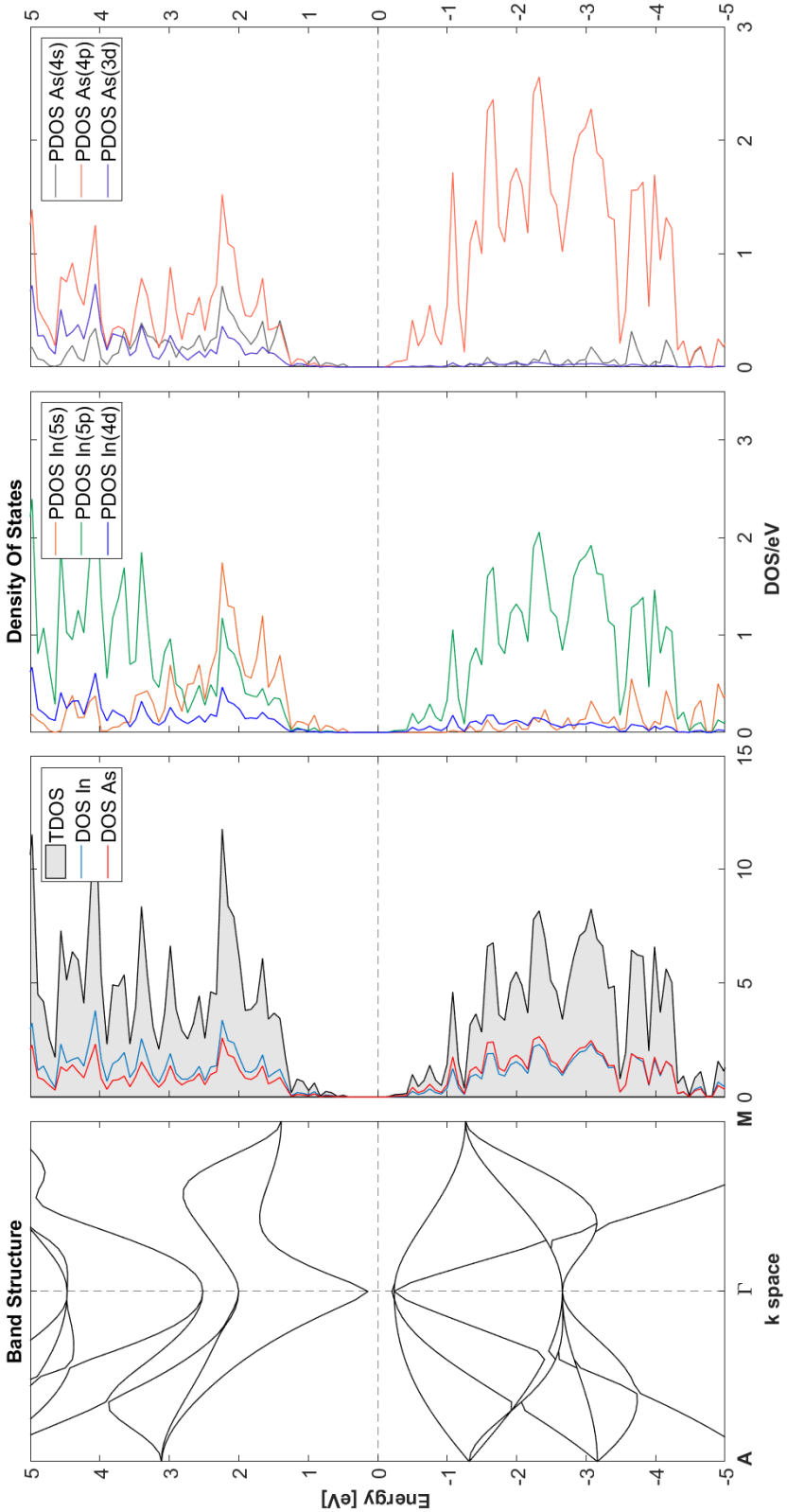
Band Structure
Density Of States
Energy [eV]
k space
DOS/eV
PDOS As(4s)
PDOS As(4p)
PDOS As(3d)
PDOS In(5s)
PDOS In(5p)
PDOS In(4d)
TDOS
DOS In
DOS As
A
Γ
M

ZB-(111) InAs

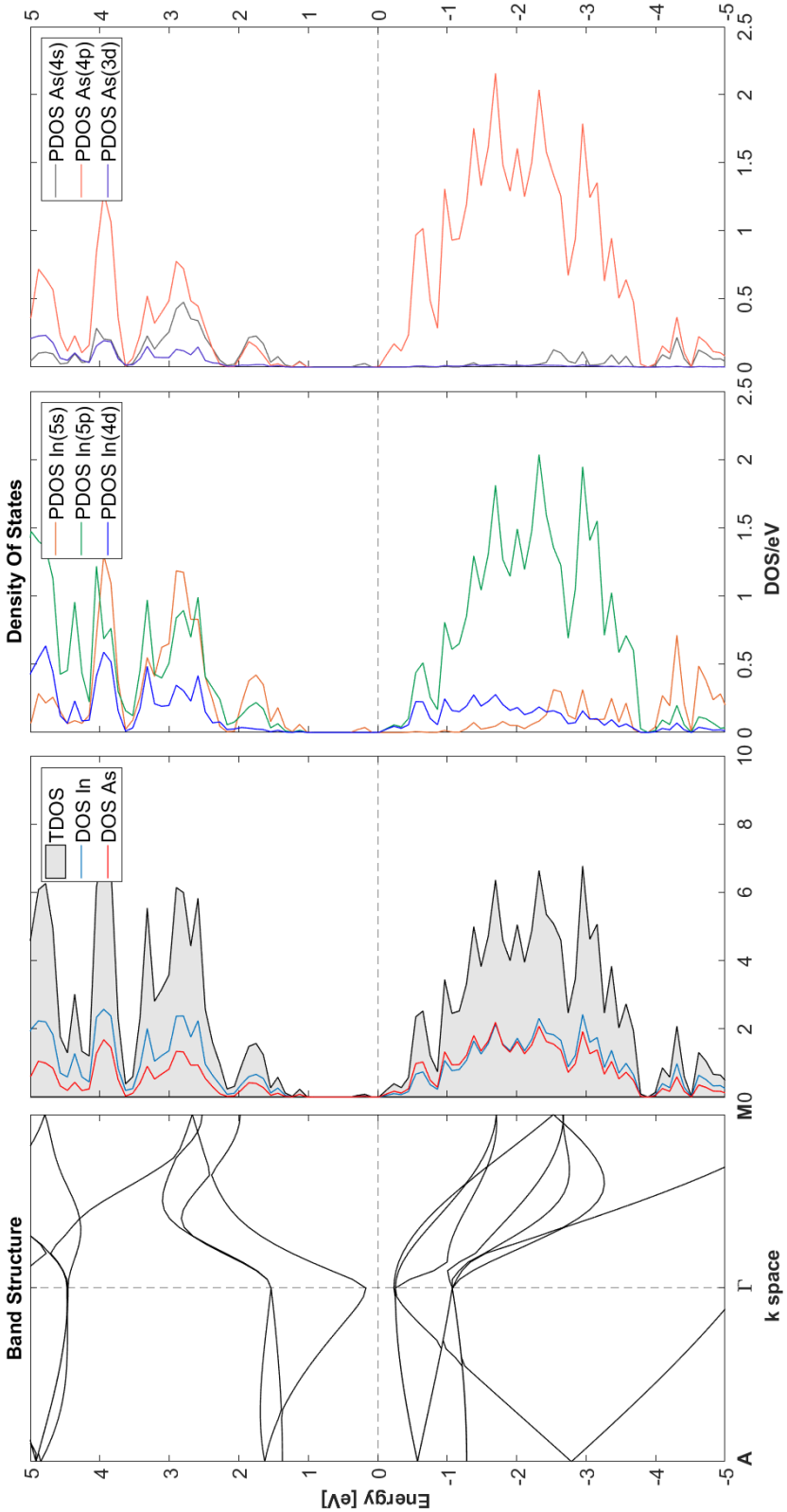
PDOS As(4s)
PDOS As(4p)
PDOS As(3d)
PDOS In(5s)
PDOS In(5p)
PDOS In(4d)
TDOS
DOS In
DOS As
Density Of States
DOS/eV
Band Structure
k space
Γ
M0
A
Energy [eV]

9.3.5 InP

WZ InP

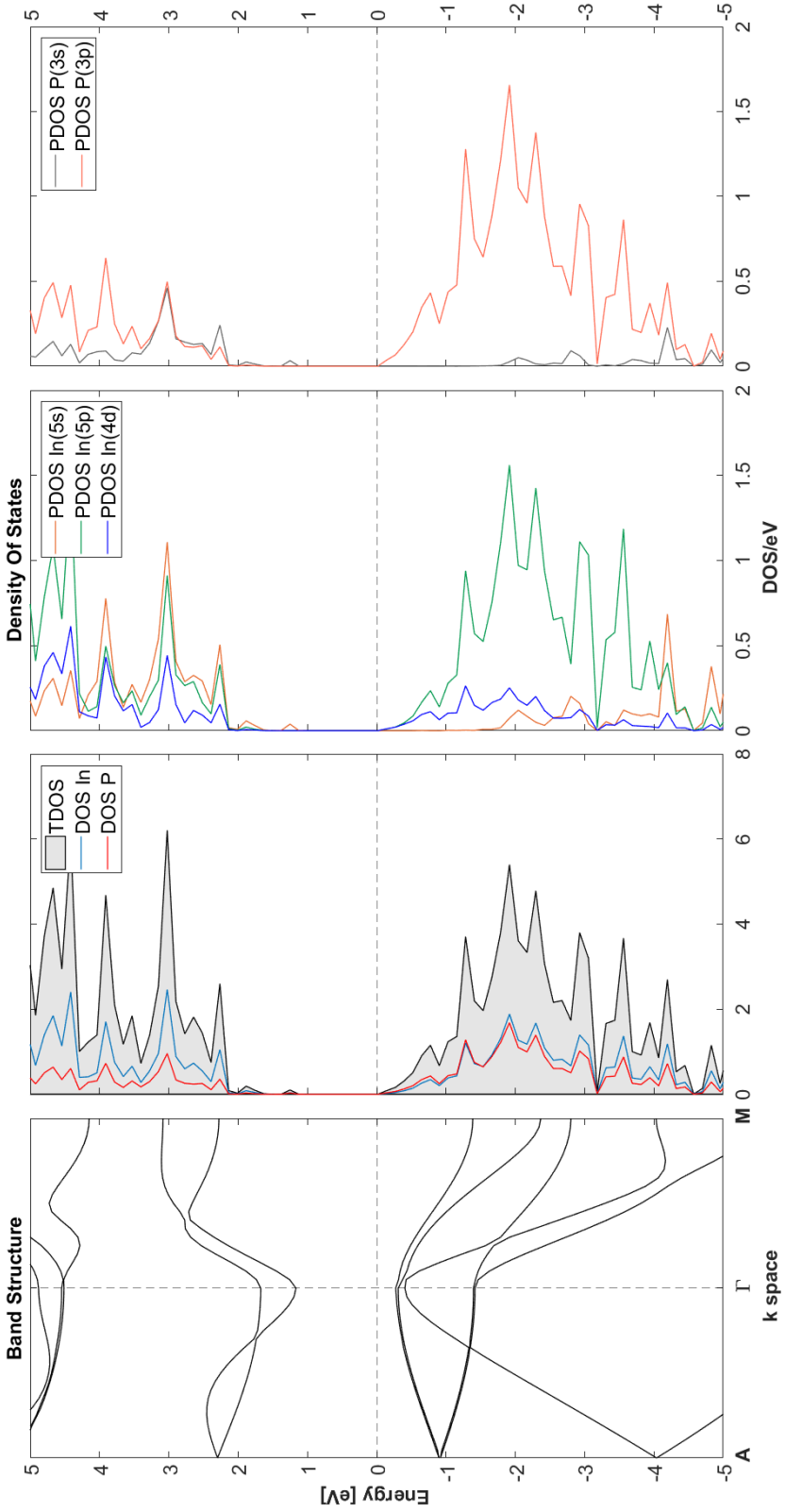

ZB InP

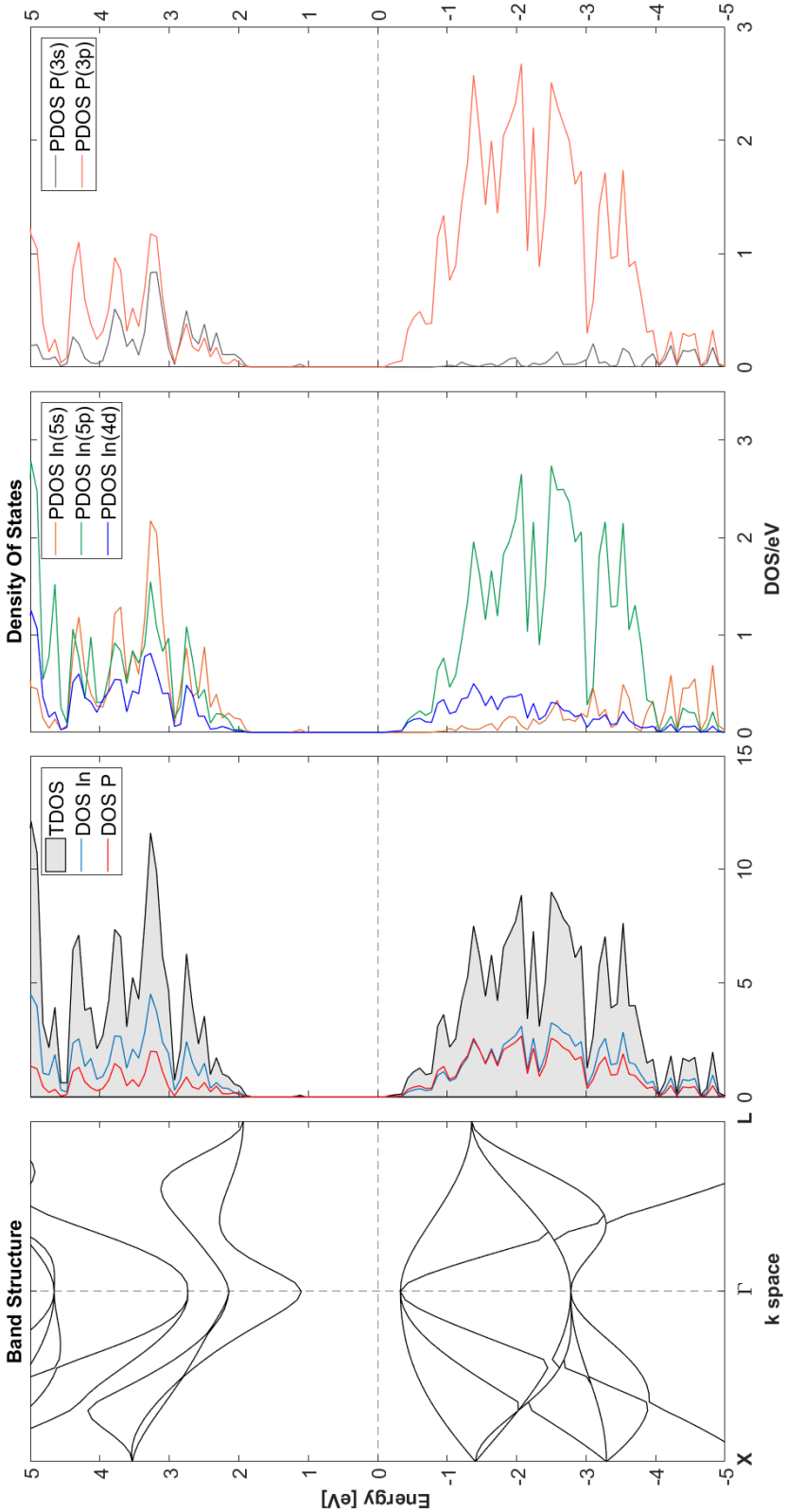
PDOS P(3s)
PDOS P(3p)
PDOS In(5s)
PDOS In(5p)
PDOS In(4d)
TDOS
DOS In
DOS P
Density Of States
DOS/eV
Band Structure
Energy [eV]
k space
X
Γ
L

ZB-(111) InP

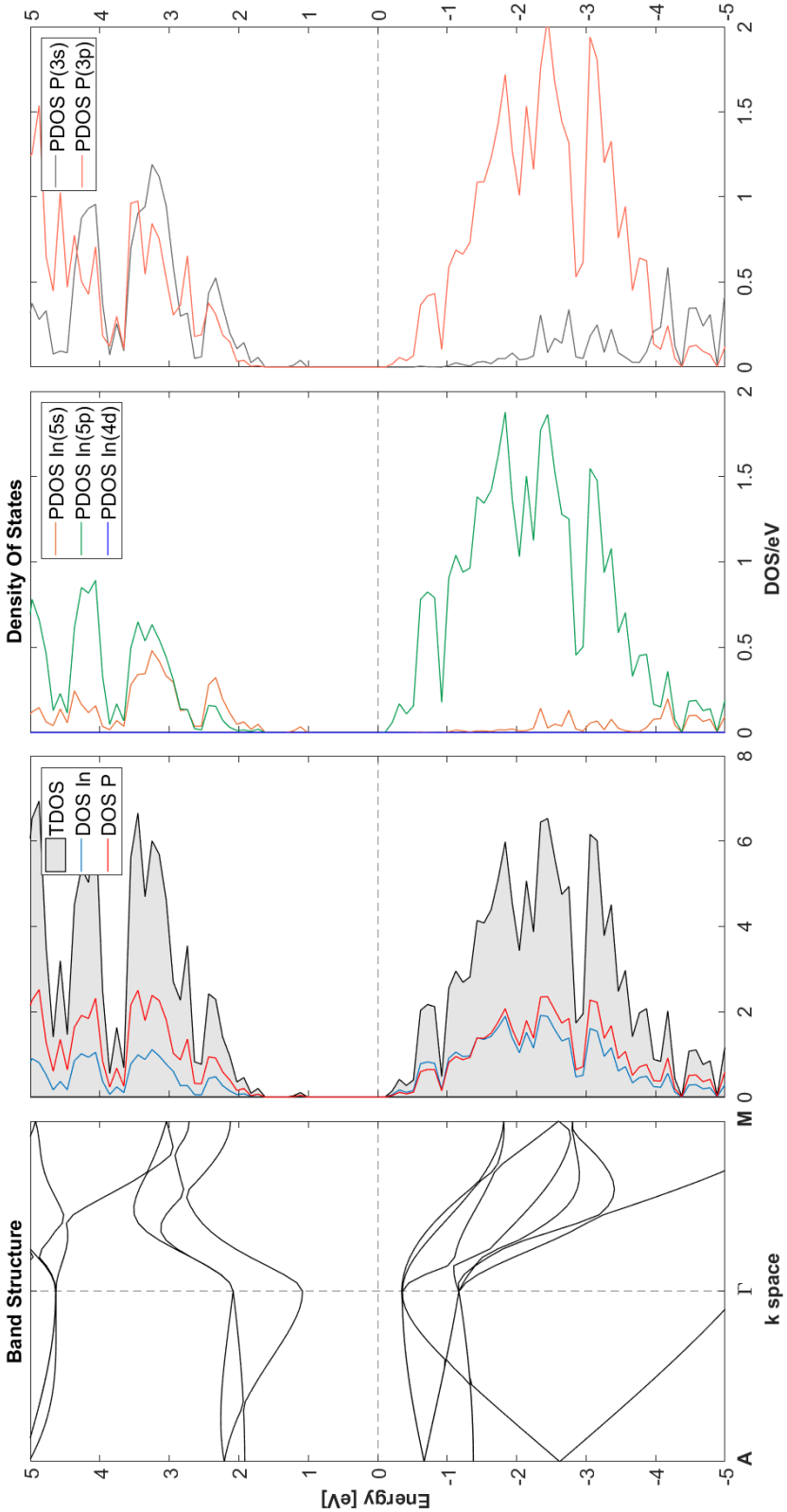
PDOS P(3s)
PDOS P(3p)
PDOS In(5s)
PDOS In(5p)
PDOS In(4d)
TDOS
DOS In
DOS P
Density Of States
DOS/eV
Band Structure
k space
Energy [eV]
A
Γ
M

9.3.6 ZnO

WZ ZnO

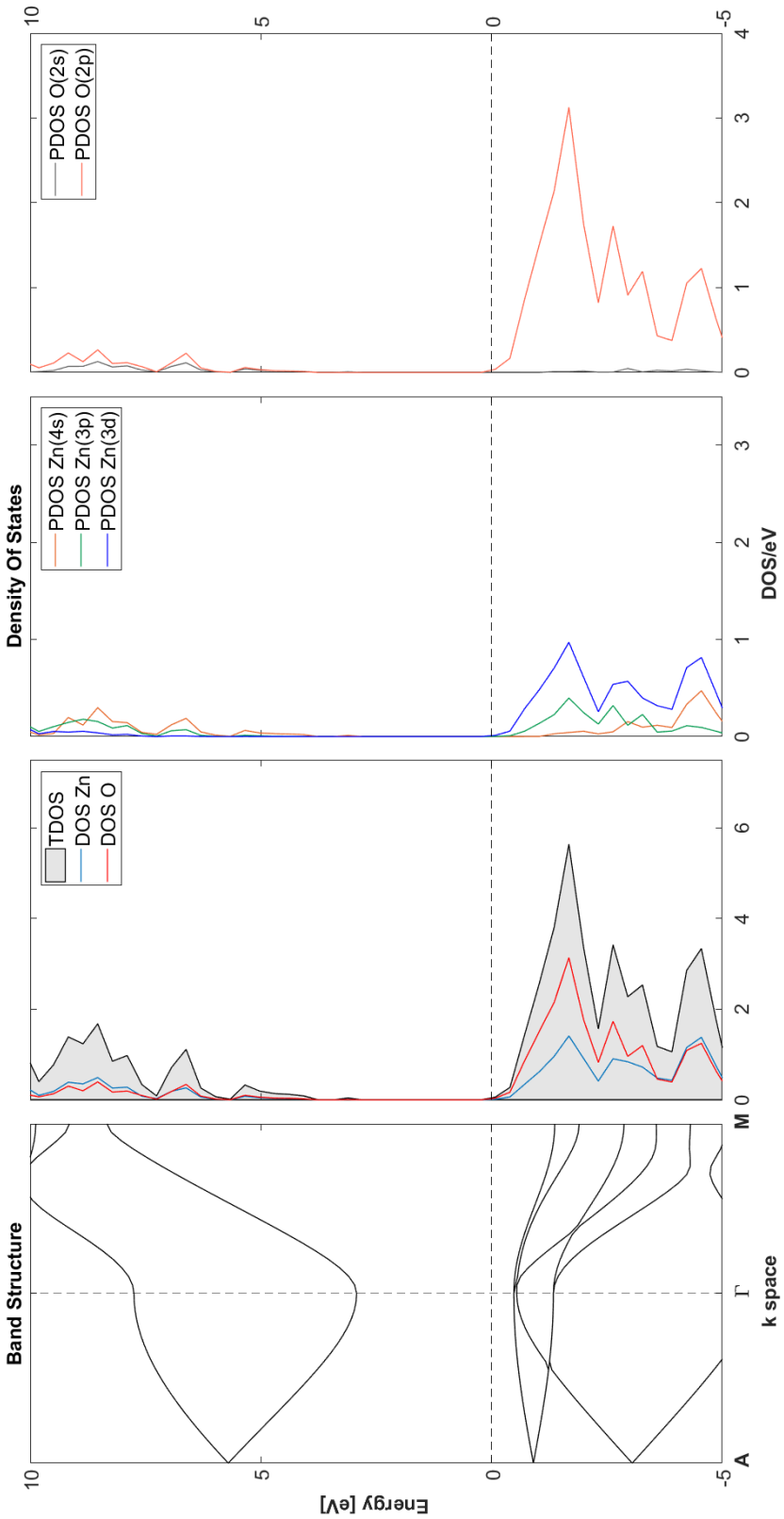

ZB ZnO

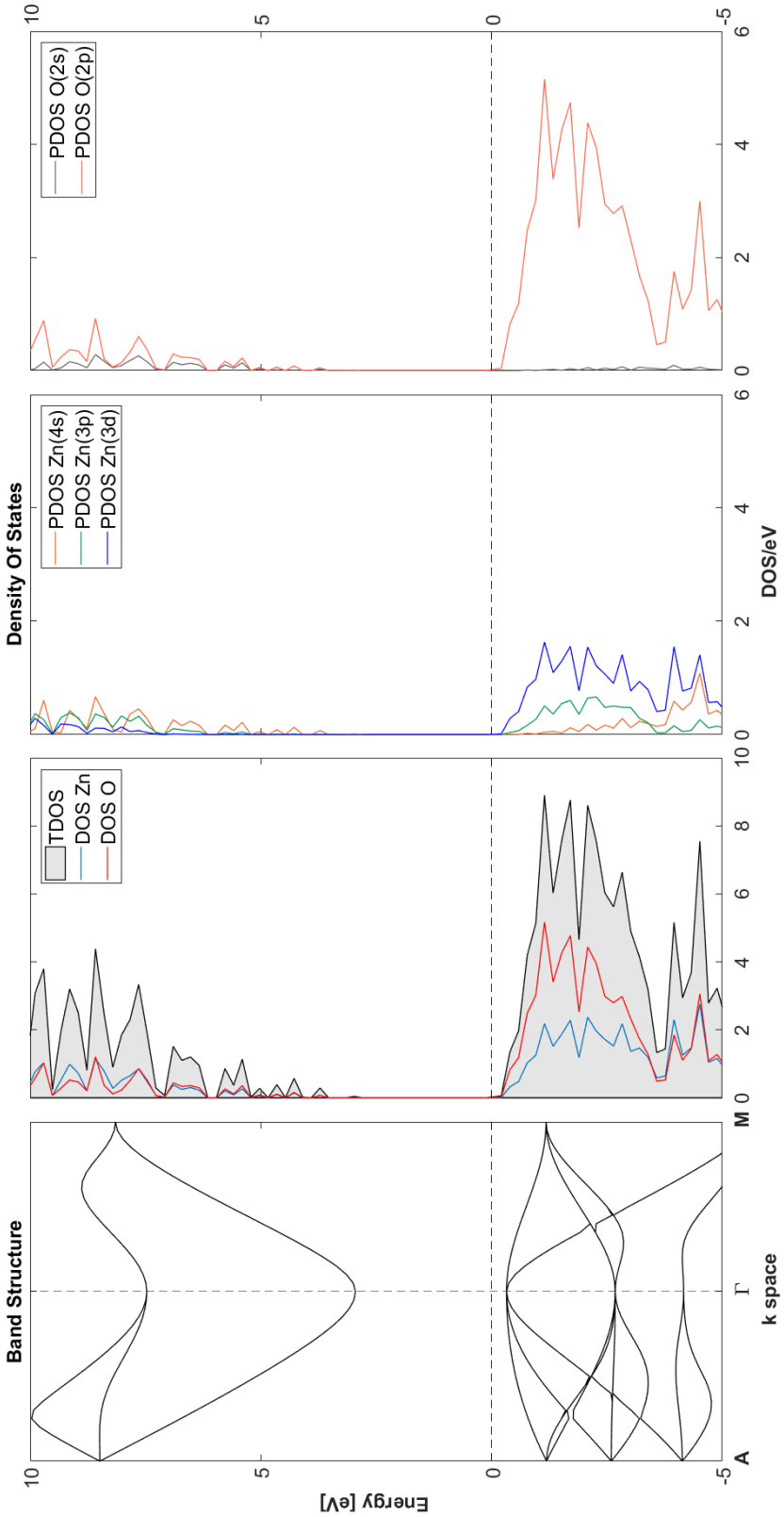
PDOS O(2s)
PDOS O(2p)
PDOS Zn(4s)
PDOS Zn(3p)
PDOS Zn(3d)
TDOS
DOS Zn
DOS O
Density Of States
DOS/eV
Band Structure
k space
Energy [eV]
A
Γ
M

ZB-(111) ZnO

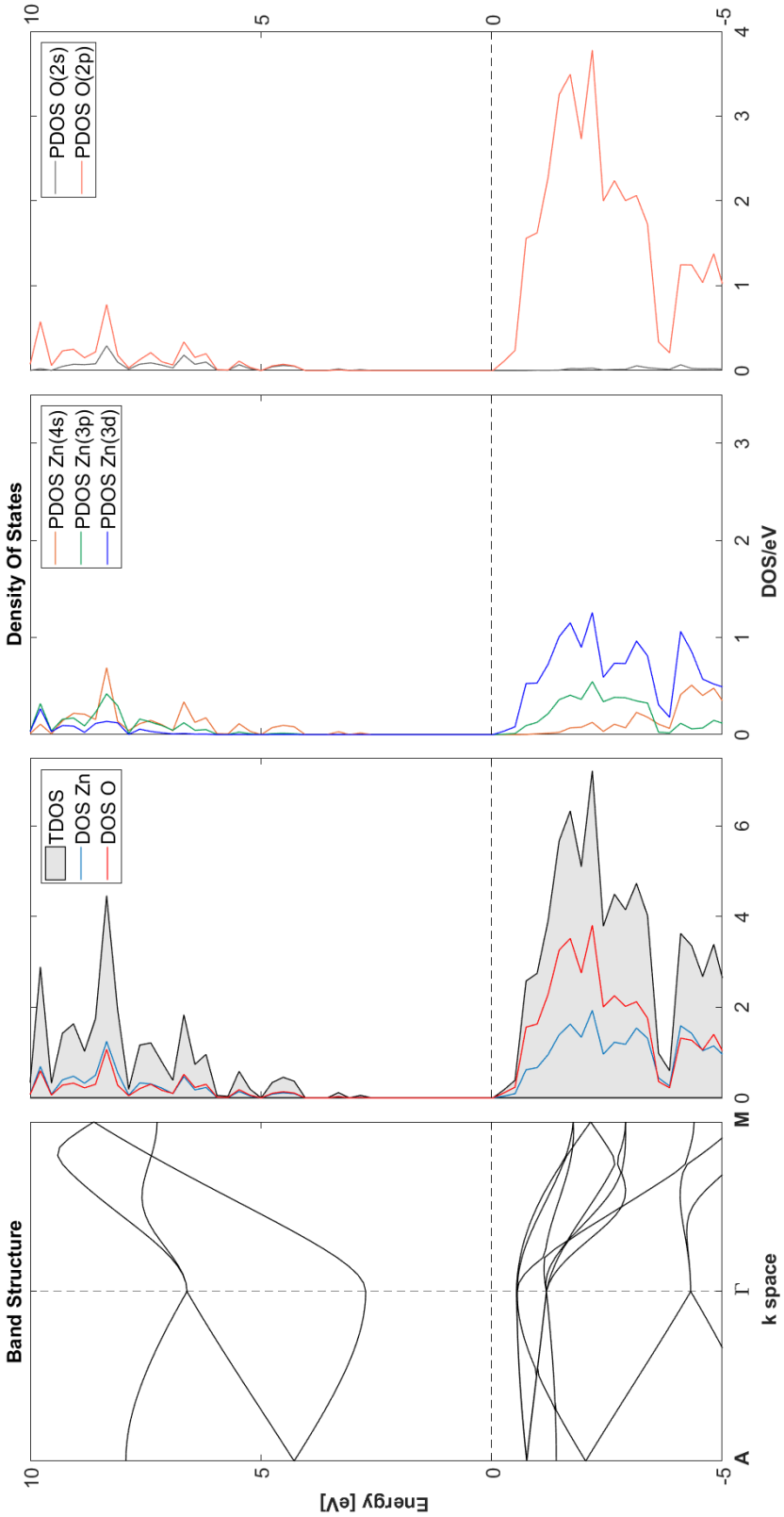
Band Structure
Density Of States
Energy [eV]
k space
DOS/eV
A
Γ
M
PDOS O(2s)
PDOS O(2p)
PDOS Zn(4s)
PDOS Zn(3p)
PDOS Zn(3d)
TDOS
DOS Zn
DOS O

9.3.7 ZnS

WZ ZnS

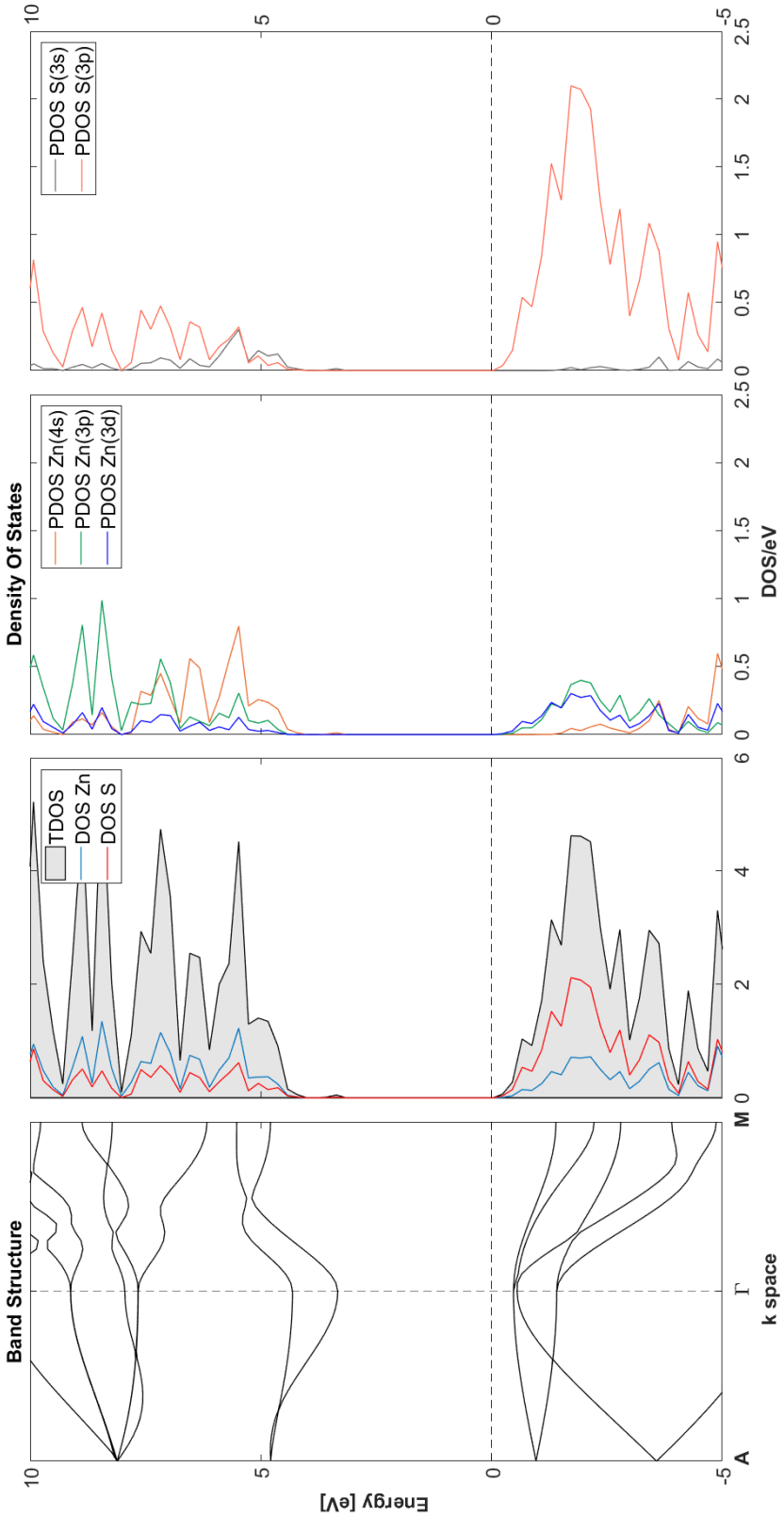

ZB ZnS

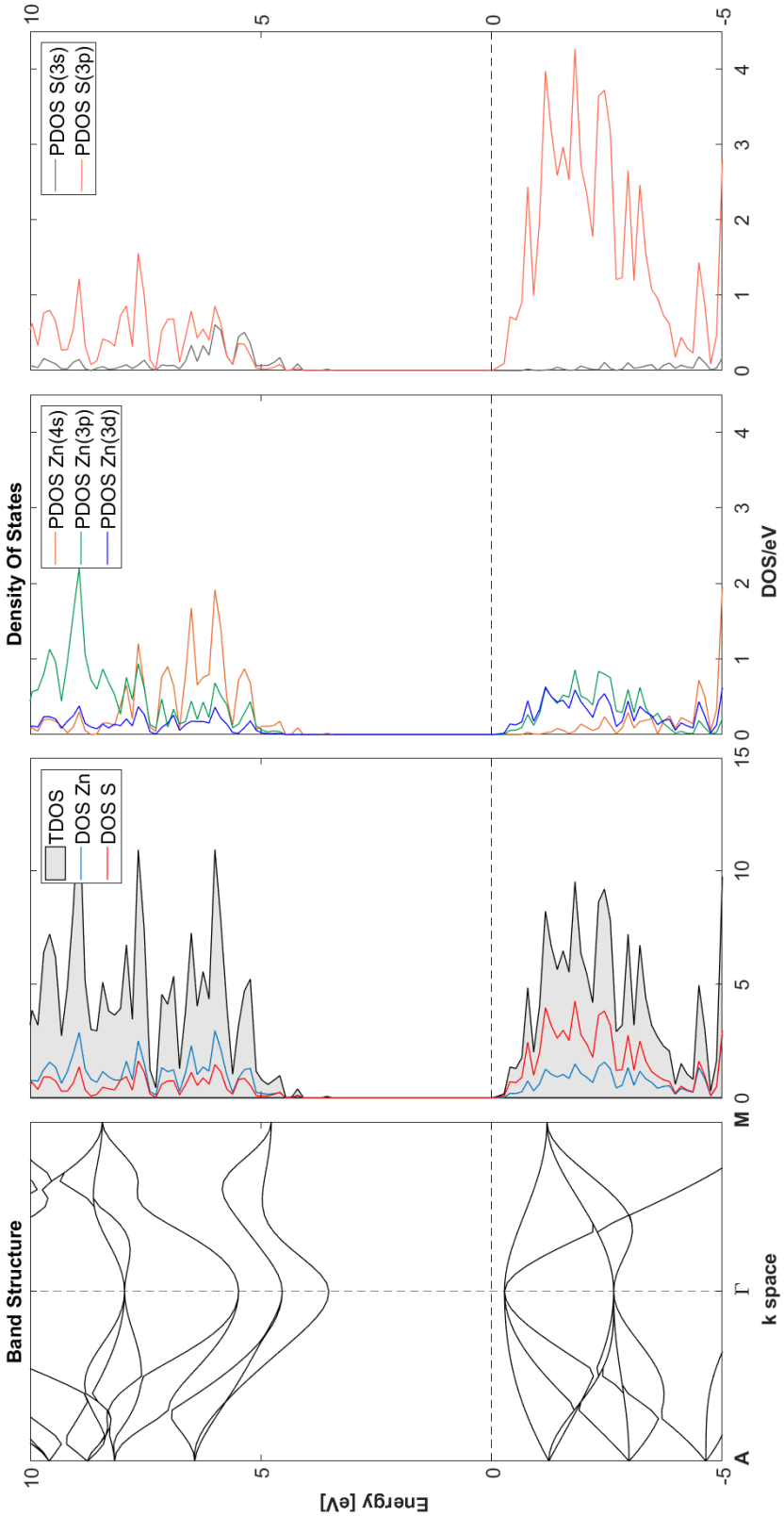
Band Structure
Density Of States
DOS/eV
k space
Energy [eV]
PDOS S(3s)
PDOS S(3p)
PDOS Zn(4s)
PDOS Zn(3p)
PDOS Zn(3d)
TDOS
DOS Zn
DOS S
A
Γ
M

ZB-(111) ZnS

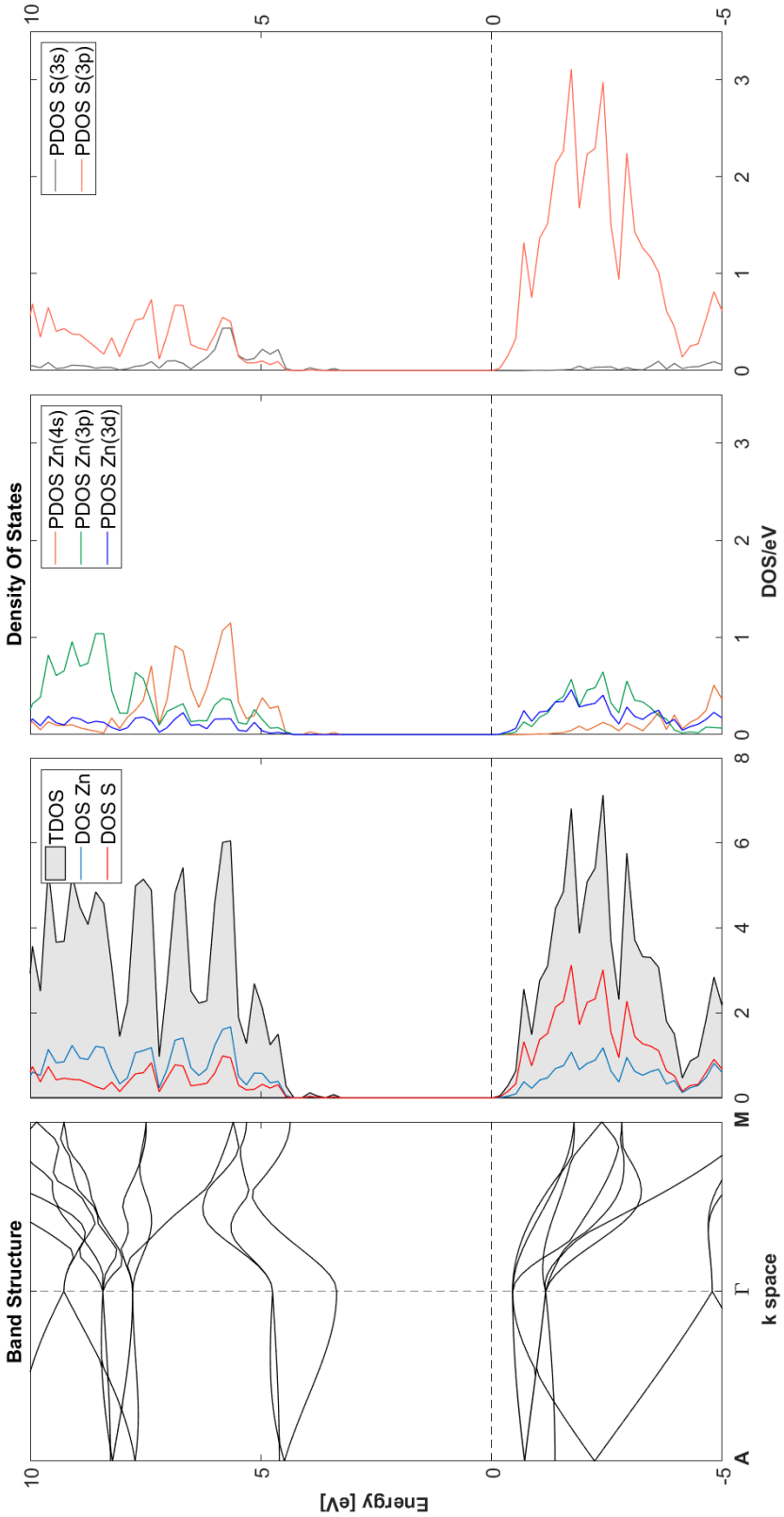
Band Structure
Density Of States
Energy [eV]
k space
DOS/eV
A
Γ
M
PDOS S(3s)
PDOS S(3p)
PDOS Zn(4s)
PDOS Zn(3p)
PDOS Zn(3d)
TDOS
DOS Zn
DOS S

9.4 Strain-Mediated Band Structures

The following figures show the electronic band structures of WZ & ZB-(111) structures upon application of strain. **k** points were plotting along the path $\mathbf{A} \rightarrow \mathbf{\Gamma} \rightarrow \mathbf{M}$ for the resultant band structures. Positive strains represent tensions & negative strains represent compression. The Fermi-level for all band structures was shifted to 0eV. Relevant data is also tabulated preceding the band structures.

9.4.1 GaAs

WZ GaAs

ε	a (Å)	c (Å)	A_{VBM} (eV)	A_{CBM} (eV)	Γ_{VBM} (eV)	Γ_{CBM} (eV)	M_{VBM} (eV)	M_{CBM} (eV)
-6%	4.046	6.180	-1.311	1.735	-0.261	0.628	-1.449	1.376
-4%	4.028	6.312	-1.230	1.811	-0.277	0.819	-1.516	1.491
-2%	4.015	6.443	-1.128	1.905	-0.265	1.014	-1.544	1.622
0	3.981	6.575	-1.118	1.979	-0.341	1.132	-1.689	1.666
2%	3.992	6.706	-0.956	2.067	-0.251	0.951	-1.598	1.841
4%	3.981	6.837	-0.883	2.137	-0.246	0.756	-1.621	1.933
6%	3.974	6.969	-0.823	2.185	-0.248	0.551	-1.643	2.008

ZB-(111) GaAs

ε	a (Å)	c (Å)	A_{VBM} (eV)	A_{CBM} (eV)	Γ_{VBM} (eV)	Γ_{CBM} (eV)	M_{VBM} (eV)	M_{CBM} (eV)
-6%	4.067	9.205	-0.876	1.008	-0.205	1.280	-2.092	1.596
-4%	4.048	9.401	-0.879	1.097	-0.279	1.189	-2.142	1.634
-2%	4.031	9.597	-0.722	1.343	-0.204	1.224	-2.025	1.823
0	3.998	9.792	-0.709	1.505	-0.295	1.158	-2.076	1.818
2%	4.003	9.988	-0.643	1.587	-0.282	0.963	-2.015	1.847
4%	3.991	10.184	-0.636	1.668	-0.312	0.763	-2.034	1.755
6%	3.982	10.380	-0.526	1.843	-0.235	0.658	-1.946	1.758

WZ GaAs

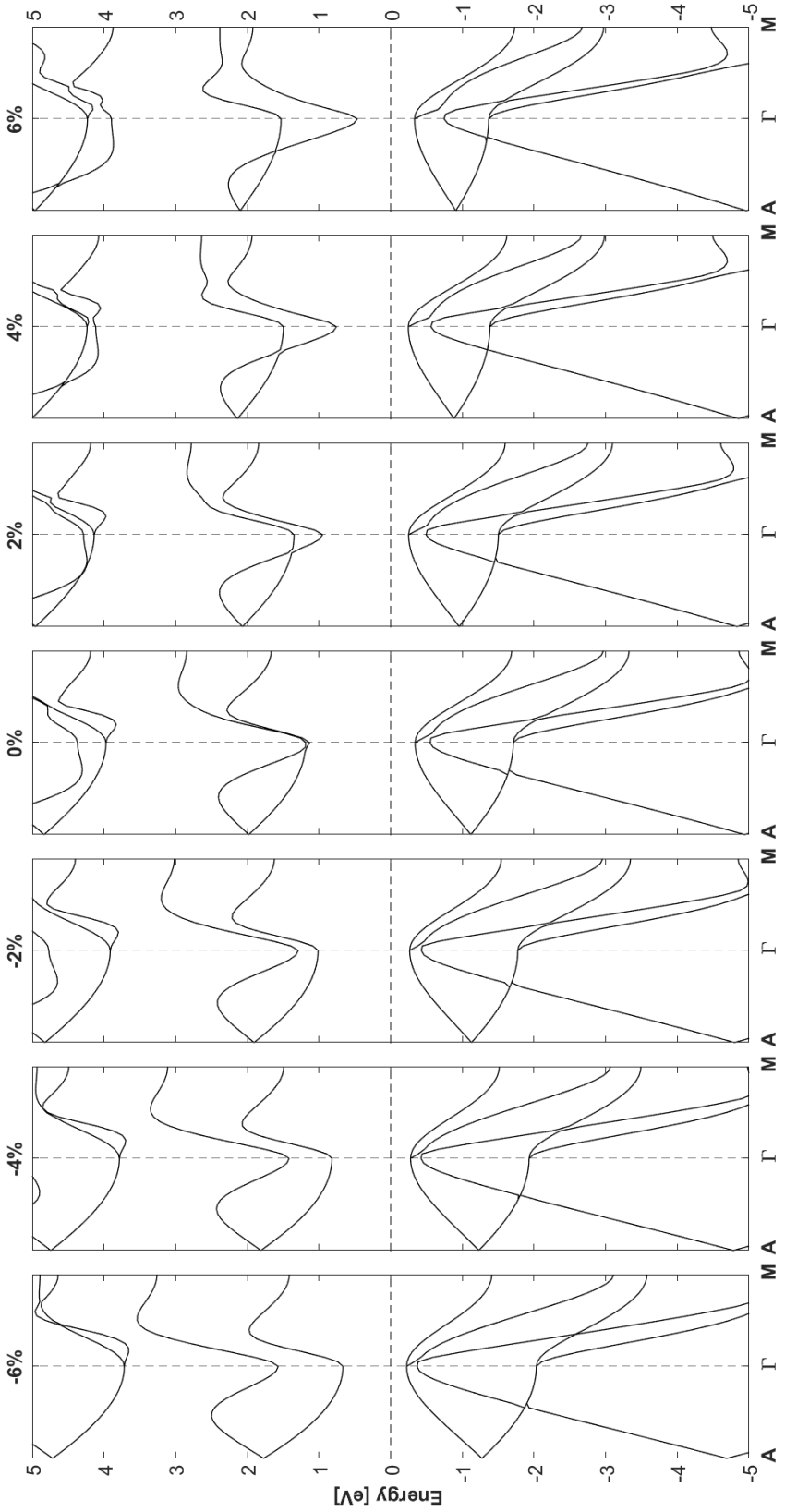

ZB-(111) GaAs

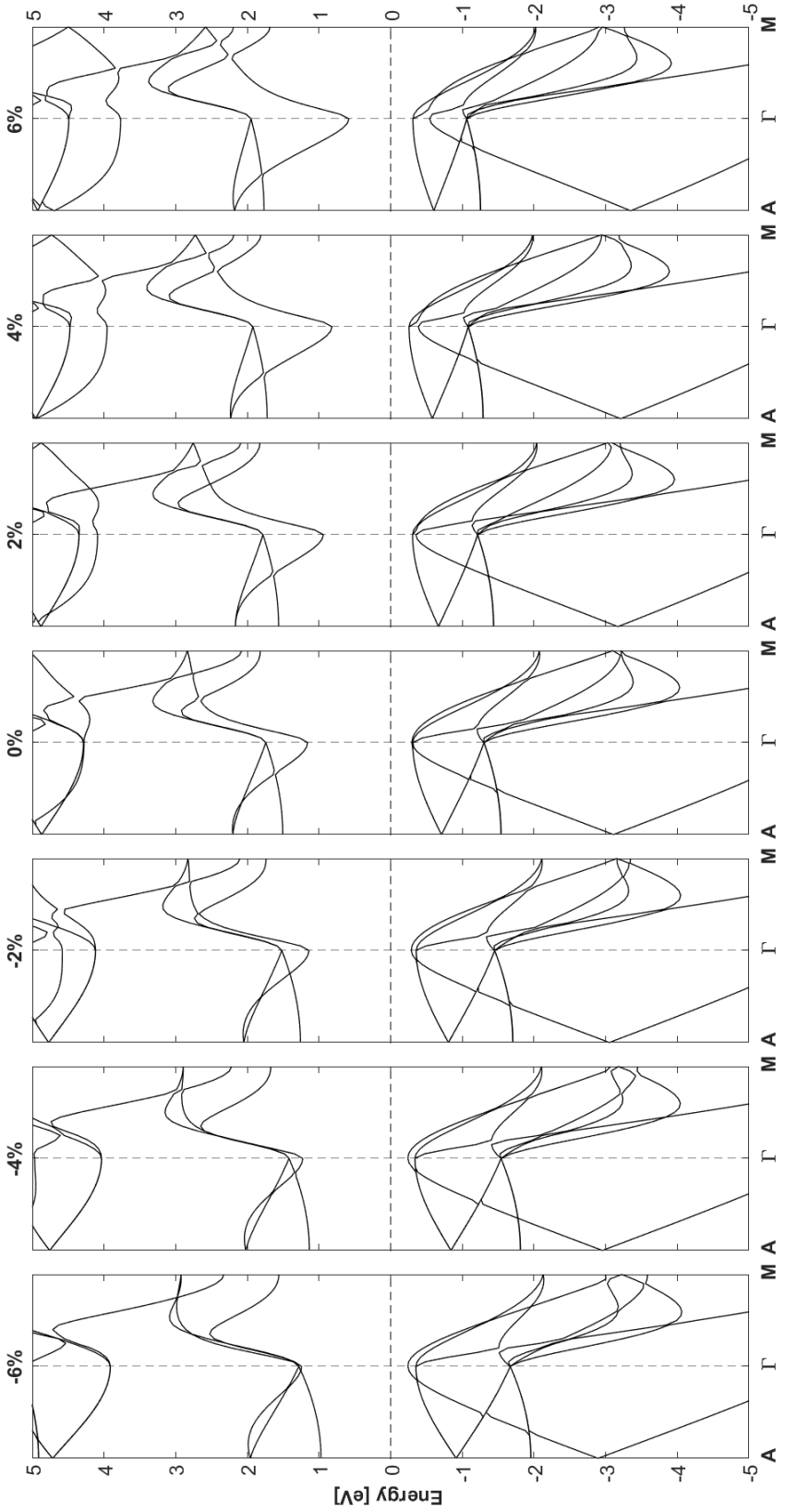

9.4.2 GaN

WZ GaN

ε	a (Å)	c (Å)	A_{VBM} (eV)	A_{CBM} (eV)	Γ_{VBM} (eV)	Γ_{CBM} (eV)	M_{VBM} (eV)	M_{CBM} (eV)
-10%	3.283	4.679	-1.336	5.508	-0.308	3.490	-1.165	5.576
-8%	3.261	4.783	-1.289	5.502	-0.329	3.423	-1.279	5.702
-6%	3.241	4.887	-1.235	5.507	-0.358	3.344	-1.372	5.829
-4%	3.223	4.991	-1.119	5.571	-0.338	3.306	-1.391	6.009
-2%	3.208	5.095	-1.056	5.581	-0.378	3.202	-1.448	6.133
0	3.203	5.199	-1.104	5.409	-0.520	2.907	-1.593	6.093
2%	3.181	5.303	-0.863	5.631	-0.339	2.981	-1.464	6.418
4%	3.170	5.407	-0.869	5.523	-0.390	2.720	-1.562	6.436
6%	3.161	5.511	-0.760	5.520	-0.328	2.574	-1.529	6.566

ZB-(111) GaN

ε	a (Å)	c (Å)	A_{VBM} (eV)	A_{CBM} (eV)	Γ_{VBM} (eV)	Γ_{CBM} (eV)	M_{VBM} (eV)	M_{CBM} (eV)
-10%	3.265	7.049	-1.134	4.263	-0.369	2.833	-2.226	4.009
-8%	3.248	7.205	-1.017	4.377	-0.339	2.921	-2.158	4.133
-6%	3.231	7.362	-0.815	4.566	-0.229	3.071	-2.000	4.325
-4%	3.216	7.519	-0.770	4.585	-0.281	3.038	-1.993	4.344
-2%	3.201	7.675	-0.740	4.572	-0.353	2.962	-1.999	4.328
0	3.197	7.832	-0.763	4.441	-0.464	2.760	-2.038	4.242
2%	3.176	7.989	-0.581	4.581	-0.320	2.811	-1.896	4.349
4%	3.166	8.145	-0.526	4.523	-0.291	2.664	-1.862	4.315
6%	3.158	8.302	-0.455	4.456	-0.243	2.505	-1.809	4.287

WZ GaN

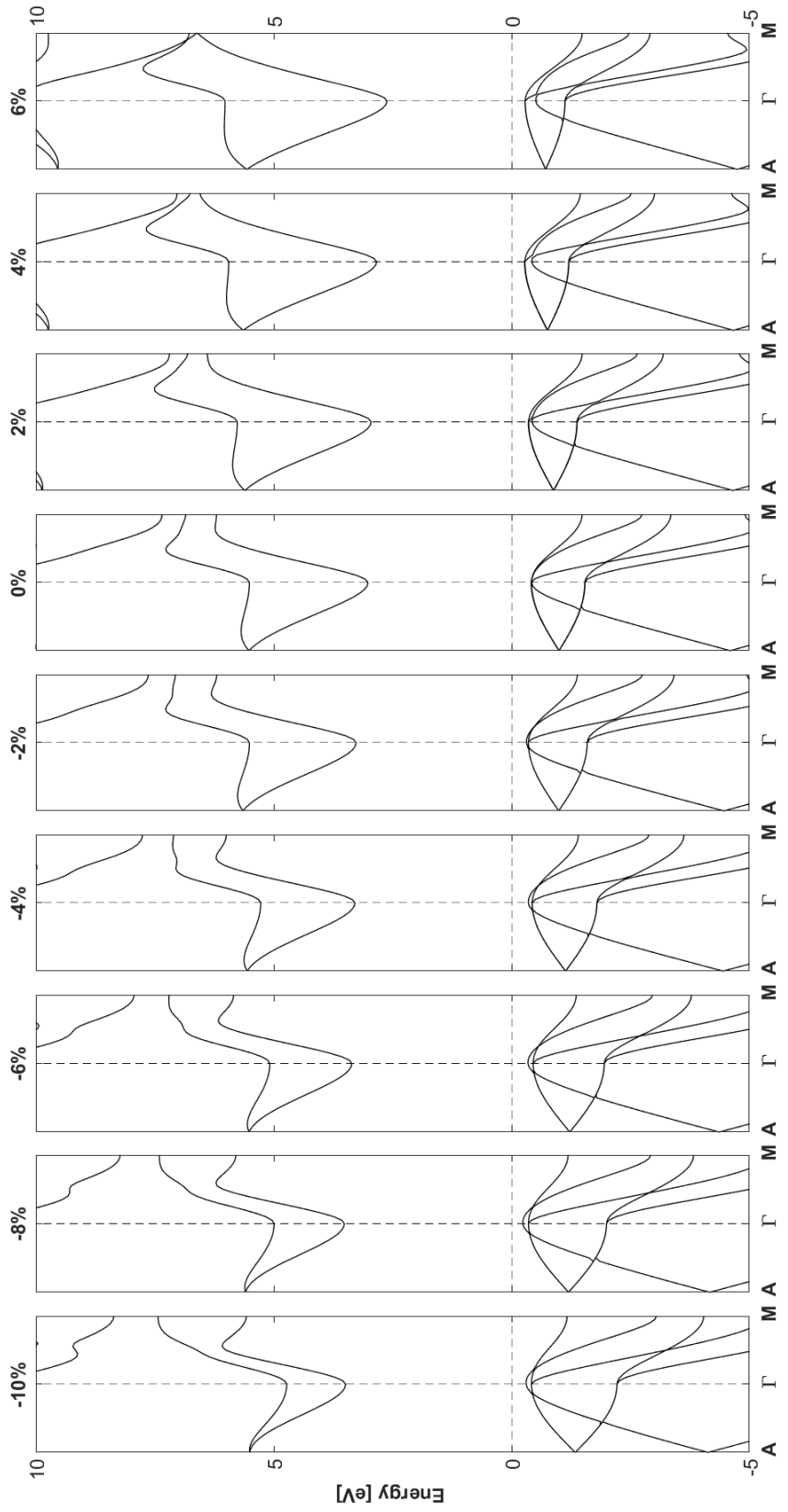

ZB-(111) GaN

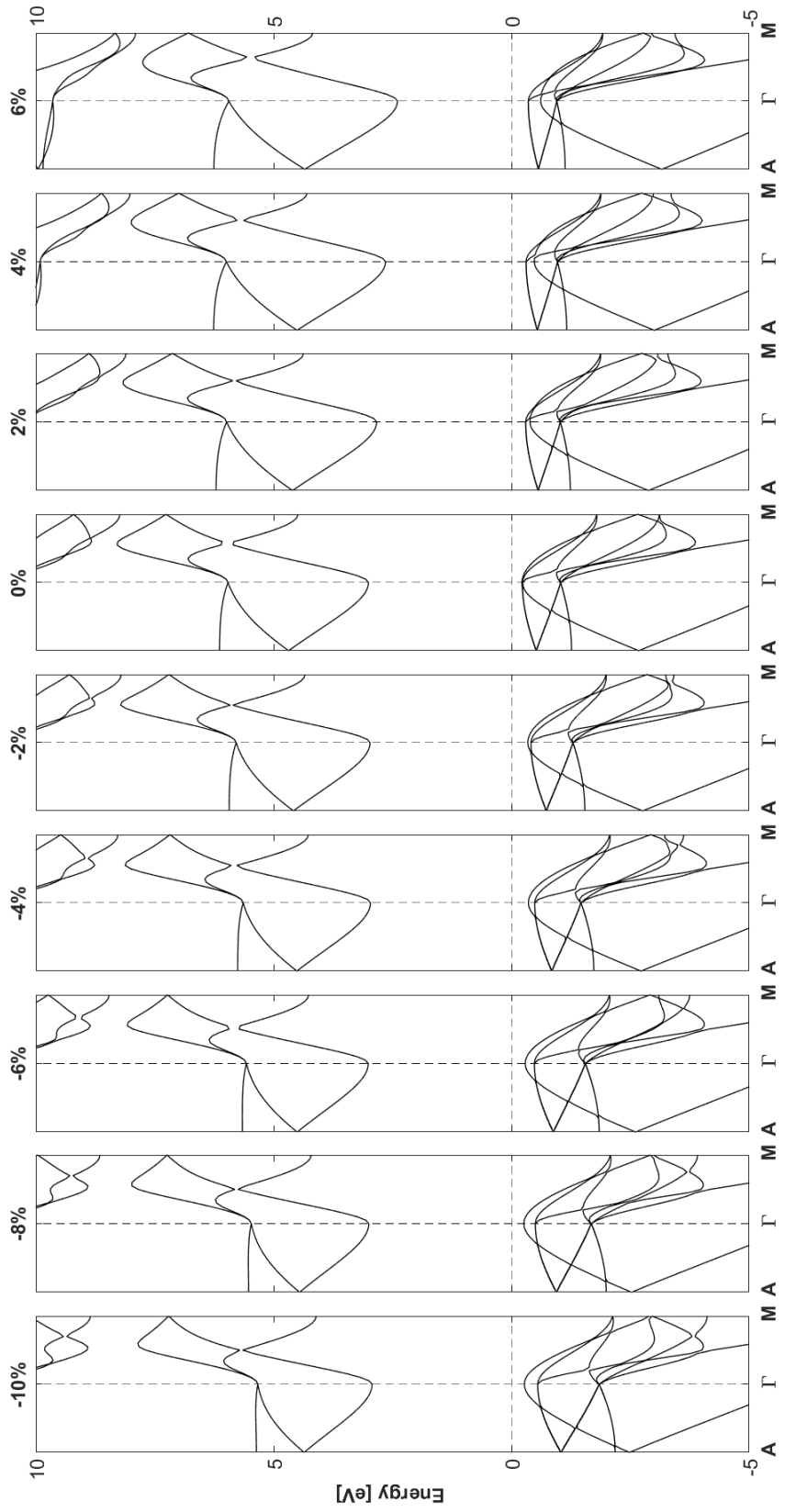

9.4.3 GaSb

WZ GaSb

ε	a (Å)	c (Å)	A_{VBM} (eV)	A_{CBM} (eV)	Γ_{VBM} (eV)	Γ_{CBM} (eV)	M_{VBM} (eV)	M_{CBM} (eV)
-6%	4.382	6.655	-1.131	1.028	-0.038	0.035	-1.251	0.883
-4%	4.358	6.796	-1.134	1.032	-0.145	0.144	-1.403	0.910
-2%	4.333	6.938	-1.147	1.040	-0.255	0.244	-1.558	0.923
0	4.303	7.079	-1.073	1.159	-0.269	0.447	-1.623	1.021
2%	4.309	7.221	-0.939	1.300	-0.180	0.382	-1.534	1.189
4%	4.303	7.363	-0.829	1.419	-0.127	0.196	-1.488	1.308
6%	4.299	7.504	-0.696	1.544	-0.050	0.045	-1.418	1.442

ZB-(111) GaSb

ε	a (Å)	c (Å)	A_{VBM} (eV)	A_{CBM} (eV)	Γ_{VBM} (eV)	Γ_{CBM} (eV)	M_{VBM} (eV)	M_{CBM} (eV)
-6%	4.396	9.935	-0.839	0.299	-0.199	0.631	-2.008	1.040
-4%	4.373	10.147	-0.800	0.430	-0.213	0.741	-2.019	1.099
-2%	4.353	10.358	-0.809	0.505	-0.284	0.529	-2.071	1.093
0	4.315	10.569	-0.692	0.759	-0.256	0.566	-2.019	1.172
2%	4.322	10.781	-0.625	0.841	-0.244	0.380	-1.954	1.194
4%	4.313	10.992	-0.560	0.966	-0.219	0.264	-1.912	1.183
6%	4.304	11.204	-0.490	1.094	-0.184	0.179	-1.862	1.169

WZ GaSb

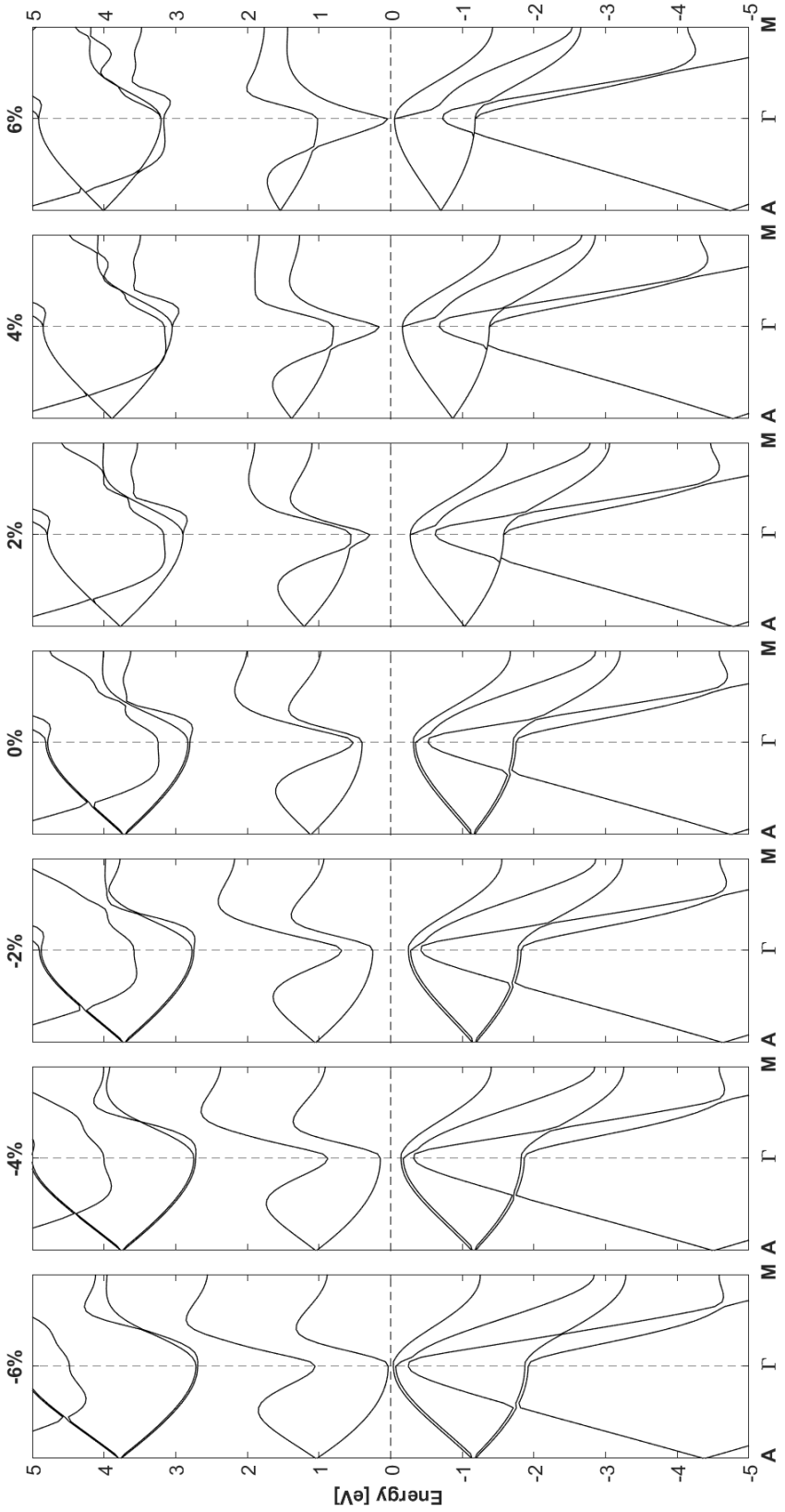

ZB-(111) GaSb

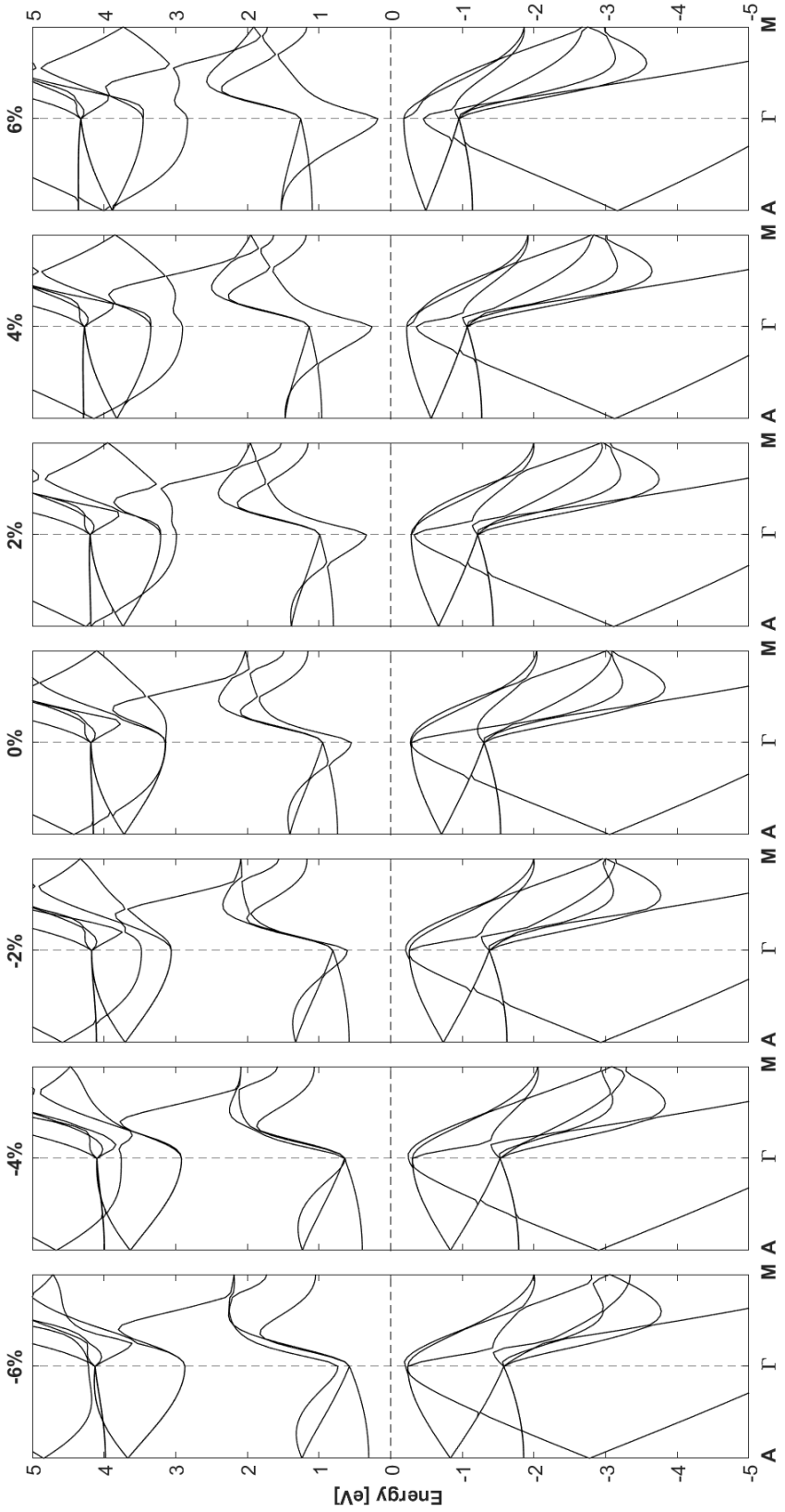

9.4.4 InAs

WZ InAs

ε	a (Å)	c (Å)	A_{VBM} (eV)	A_{CBM} (eV)	Γ_{VBM} (eV)	Γ_{CBM} (eV)	M_{VBM} (eV)	M_{CBM} (eV)
-6%	4.375	6.650	-1.162	1.482	-0.283	0.374	-1.290	1.649
-4%	4.353	6.791	-1.087	1.526	-0.259	0.302	-1.338	1.759
-2%	4.333	6.933	-0.960	1.629	-0.243	0.272	-1.323	1.915
0	4.312	7.074	-0.841	1.741	-0.226	0.245	-1.308	2.065
2%	4.297	7.216	-0.731	1.822	-0.140	0.180	-1.287	2.194
4%	4.286	7.357	-0.629	1.896	-0.091	0.129	-1.261	2.312
6%	4.274	7.499	-0.542	1.956	-0.047	0.090	-1.245	2.343

ZB-(111) InAs

ε	a (Å)	c (Å)	A_{VBM} (eV)	A_{CBM} (eV)	Γ_{VBM} (eV)	Γ_{CBM} (eV)	M_{VBM} (eV)	M_{CBM} (eV)
-6%	4.387	9.935	-0.825	0.907	-0.284	0.234	-1.850	1.729
-4%	4.363	10.147	-0.702	1.102	-0.224	0.267	-1.769	1.868
-2%	4.341	10.358	-0.643	1.233	-0.231	0.219	-1.748	1.927
0	4.321	10.569	-0.570	1.373	-0.230	0.171	-1.706	1.980
2%	4.301	10.781	-0.460	1.554	-0.172	0.169	-1.626	2.043
4%	4.285	10.992	-0.393	1.682	-0.136	0.131	-1.585	2.043
6%	4.273	11.204	-0.336	1.749	-0.105	0.098	-1.544	2.027

WZ InAs

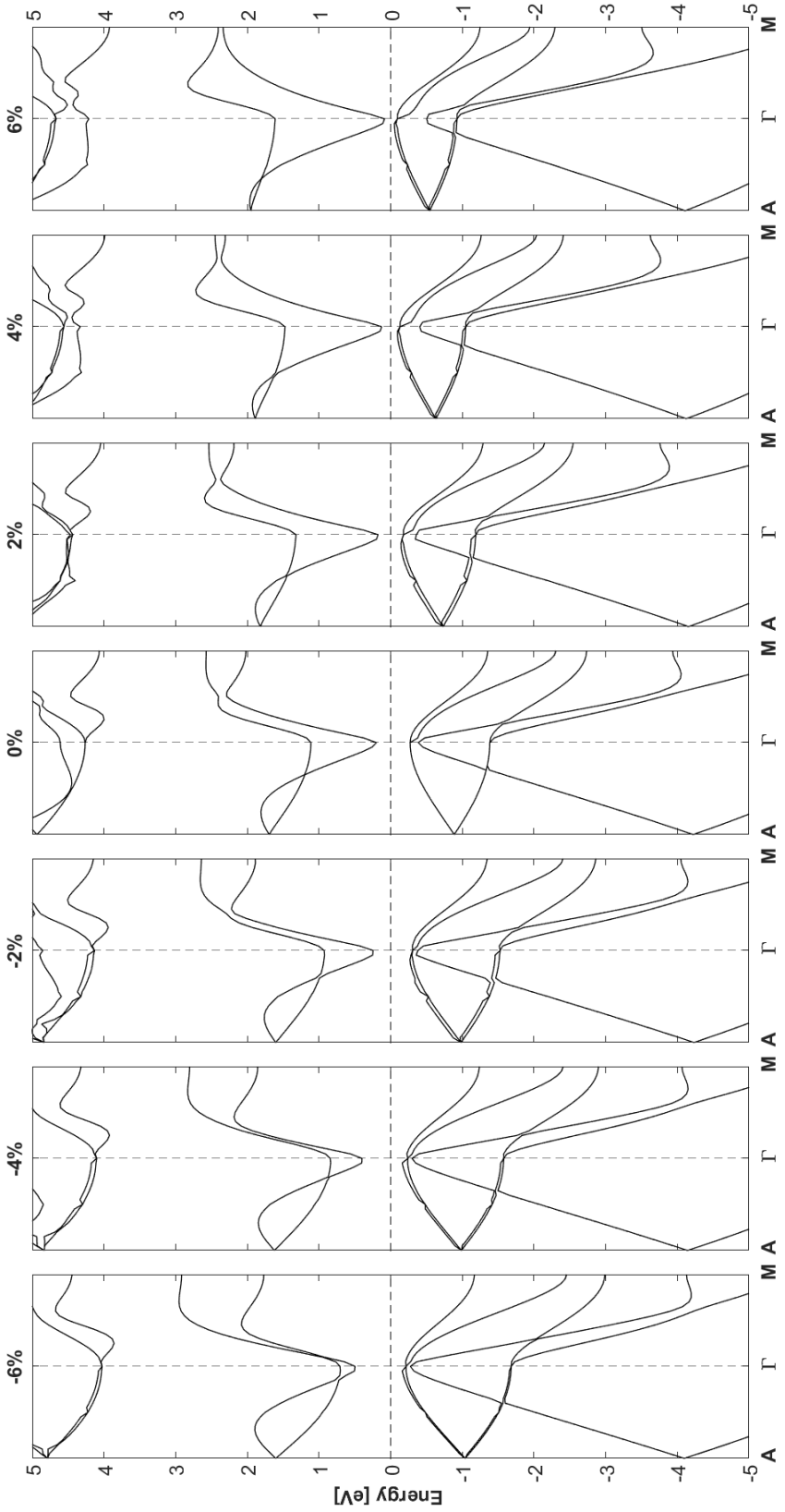

ZB-(111) InAs

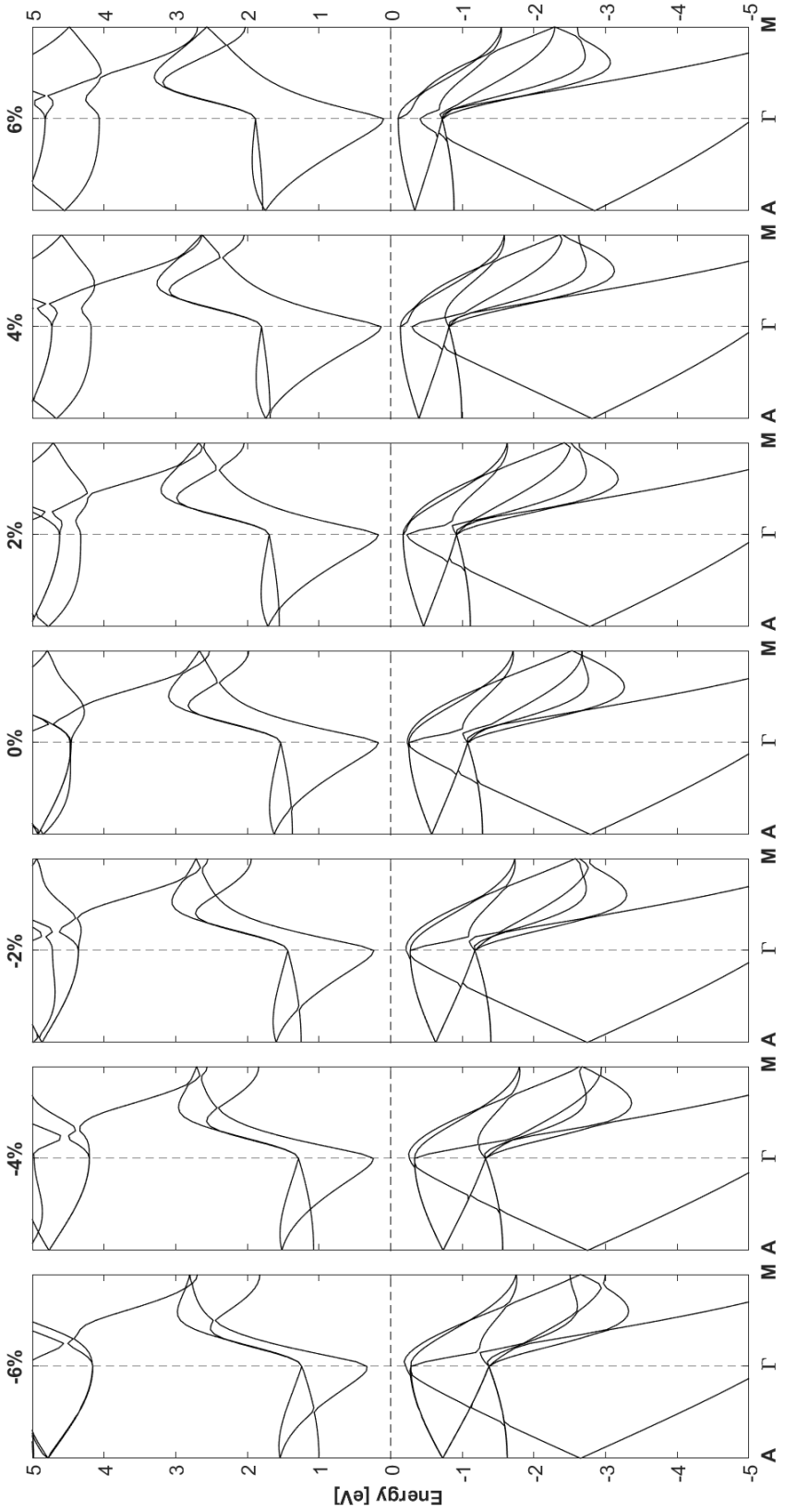

9.4.5 InP

WZ InP

ε	a (Å)	c (Å)	A_{VBM} (eV)	A_{CBM} (eV)	Γ_{VBM} (eV)	Γ_{CBM} (eV)	M_{VBM} (eV)	M_{CBM} (eV)
-10%	4.299	6.154	-1.249	1.980	-0.269	0.776	-1.077	1.733
-8%	4.271	6.291	-1.156	2.043	-0.262	0.988	-1.135	1.875
-6%	4.238	6.428	-1.040	2.155	-0.217	1.232	-1.172	2.037
-4%	4.216	6.564	-0.985	2.203	-0.237	1.390	-1.241	2.131
-2%	4.196	6.701	-0.985	2.193	-0.293	1.243	-1.364	2.156
0	4.172	6.838	-0.914	2.281	-0.290	1.150	-1.402	2.262
2%	4.159	6.975	-0.849	2.351	-0.300	1.061	-1.406	2.376
4%	4.143	7.111	-0.722	2.480	-0.226	0.990	-1.361	2.529
6%	4.130	7.248	-0.760	2.473	-0.252	0.571	-1.393	2.487

ZB-(111) InP

ε	a (Å)	c (Å)	A_{VBM} (eV)	A_{CBM} (eV)	Γ_{VBM} (eV)	Γ_{CBM} (eV)	M_{VBM} (eV)	M_{CBM} (eV)
-6%	4.258	9.619	-1.127	1.008	-0.251	0.859	-2.213	1.596
-4%	4.235	9.824	-1.014	1.265	-0.302	0.911	-2.118	1.776
-2%	4.213	10.028	-0.752	1.660	-0.223	1.081	-1.870	2.070
0	4.178	10.233	-0.597	1.984	-0.274	1.152	-1.744	2.189
2%	4.174	10.438	-0.594	2.046	-0.303	0.955	-1.735	2.126
4%	4.157	10.642	-0.512	2.223	-0.241	0.847	-1.662	2.080
6%	4.142	10.847	-0.487	2.233	-0.237	0.656	-1.645	1.959

WZ InP

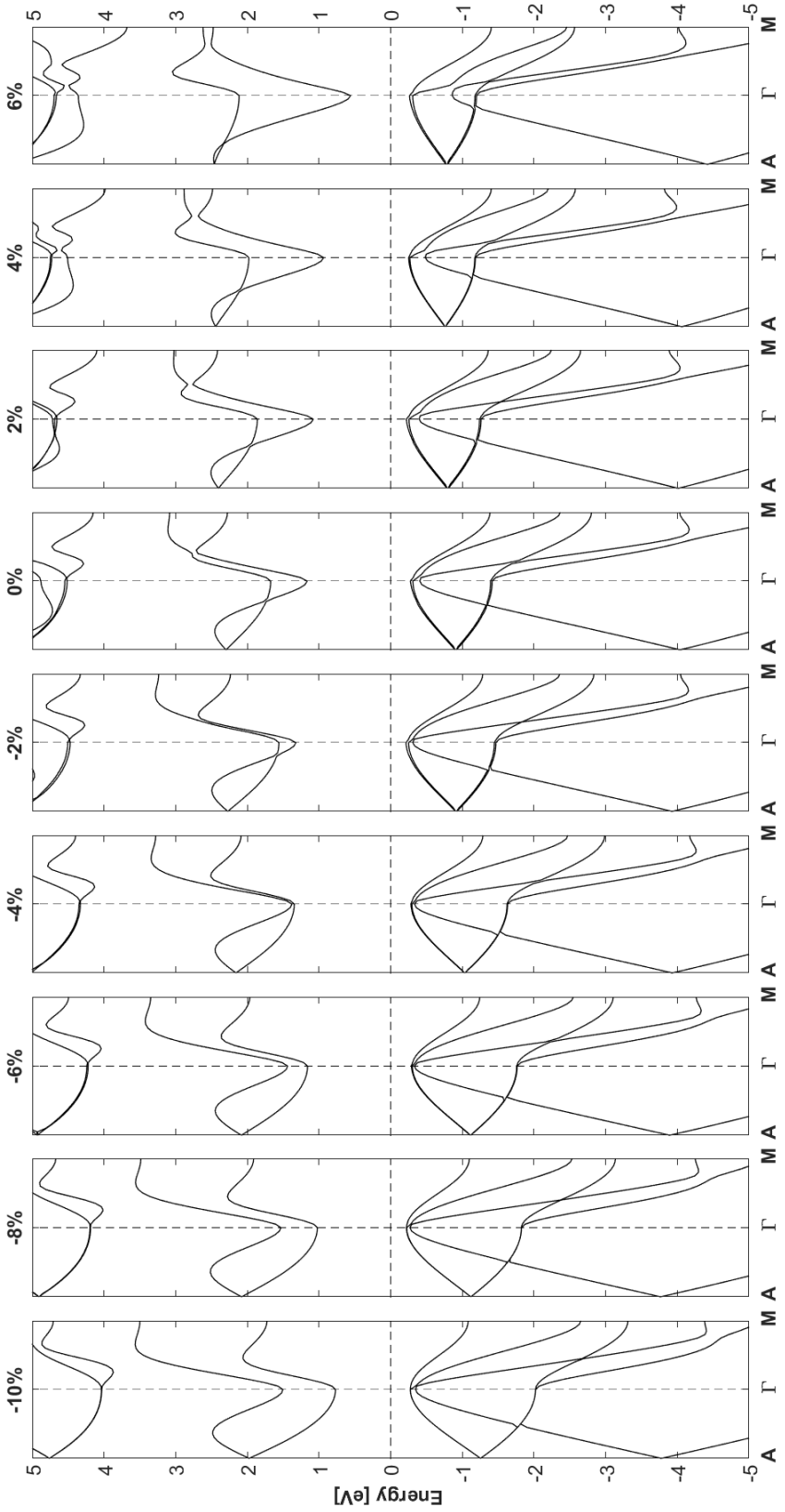

ZB-(111) InP

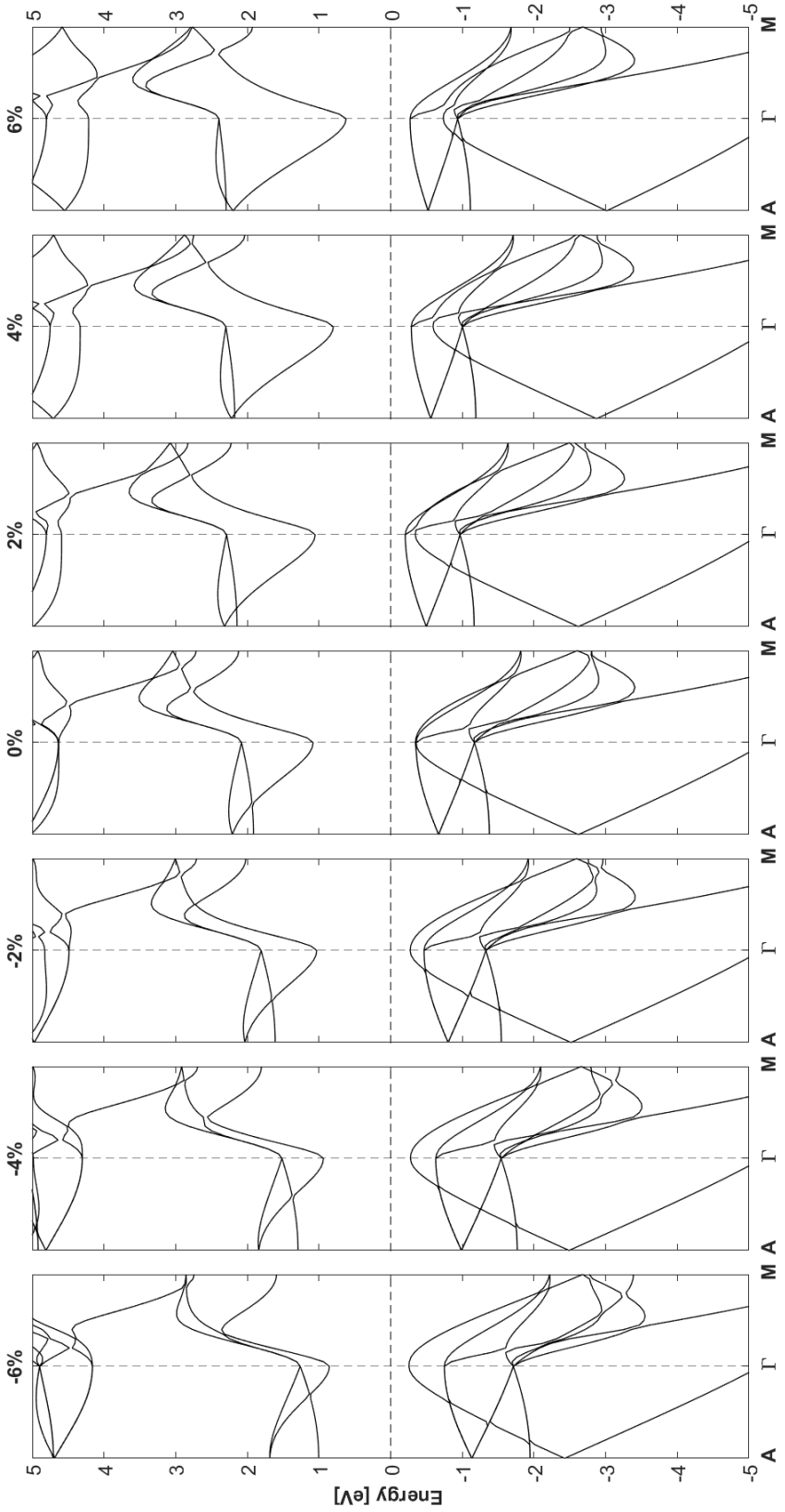

9.4.6 ZnO

WZ ZnO

ε	a (Å)	c (Å)	A_{VBM} (eV)	A_{CBM} (eV)	Γ_{VBM} (eV)	Γ_{CBM} (eV)	M_{VBM} (eV)	M_{CBM} (eV)
-10%	3.315	4.713	-0.935	6.360	-0.205	3.386	-1.031	8.794
-8%	3.298	4.817	-0.899	6.258	-0.239	3.336	-1.086	8.750
-6%	3.283	4.922	-0.977	6.047	-0.390	3.168	-1.246	8.589
-4%	3.269	5.027	-0.726	6.168	-0.216	3.325	-1.074	8.752
-2%	3.264	5.132	-0.737	6.015	-0.274	3.206	-1.144	8.620
0	3.258	5.236	-0.867	5.746	-0.442	2.964	-1.330	8.374
2%	3.233	5.341	-0.649	5.860	-0.262	3.094	-1.189	8.538
4%	3.223	5.446	-0.710	5.669	-0.357	2.922	-1.303	8.371
6%	3.212	5.550	-0.730	5.519	-0.409	2.789	-1.371	8.242

ZB-(111) ZnO

ε	a (Å)	c (Å)	A_{VBM} (eV)	A_{CBM} (eV)	Γ_{VBM} (eV)	Γ_{CBM} (eV)	M_{VBM} (eV)	M_{CBM} (eV)
-6%	3.275	7.458	-0.857	4.397	-0.396	2.809	-1.817	7.263
-4%	3.258	7.617	-0.770	4.427	-0.395	2.854	-1.756	7.326
-2%	3.243	7.776	-0.644	4.486	-0.353	2.924	-1.650	7.416
0	3.239	7.934	-0.601	4.439	-0.380	2.887	-1.609	7.408
2%	3.218	8.093	-0.541	4.430	-0.347	2.881	-1.573	7.413
4%	3.190	8.252	-0.532	4.333	-0.356	2.792	-1.557	7.358
6%	3.174	8.410	-0.480	4.326	-0.321	2.773	-1.557	7.333

WZ ZnO

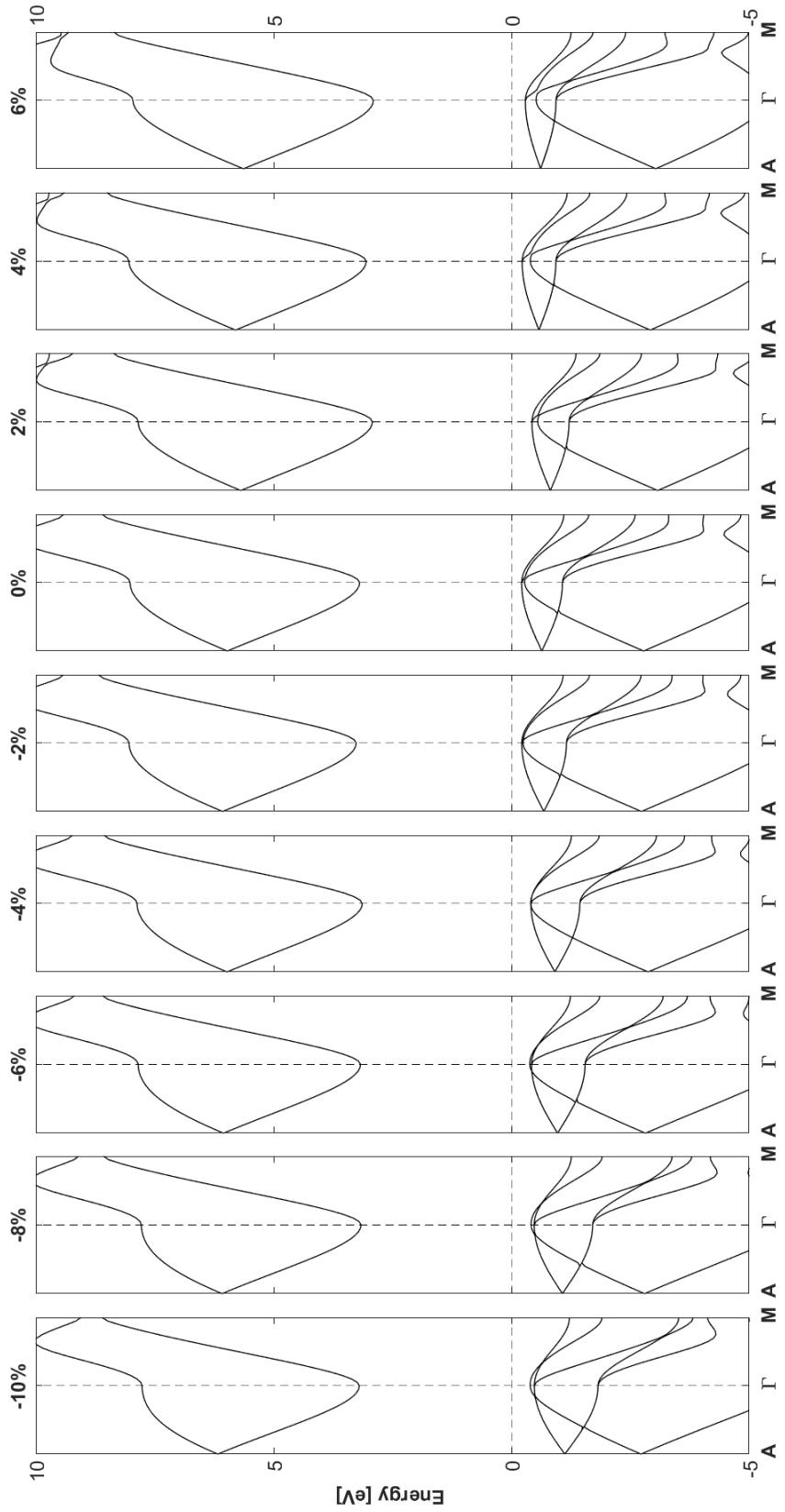

ZB-(111) ZnO

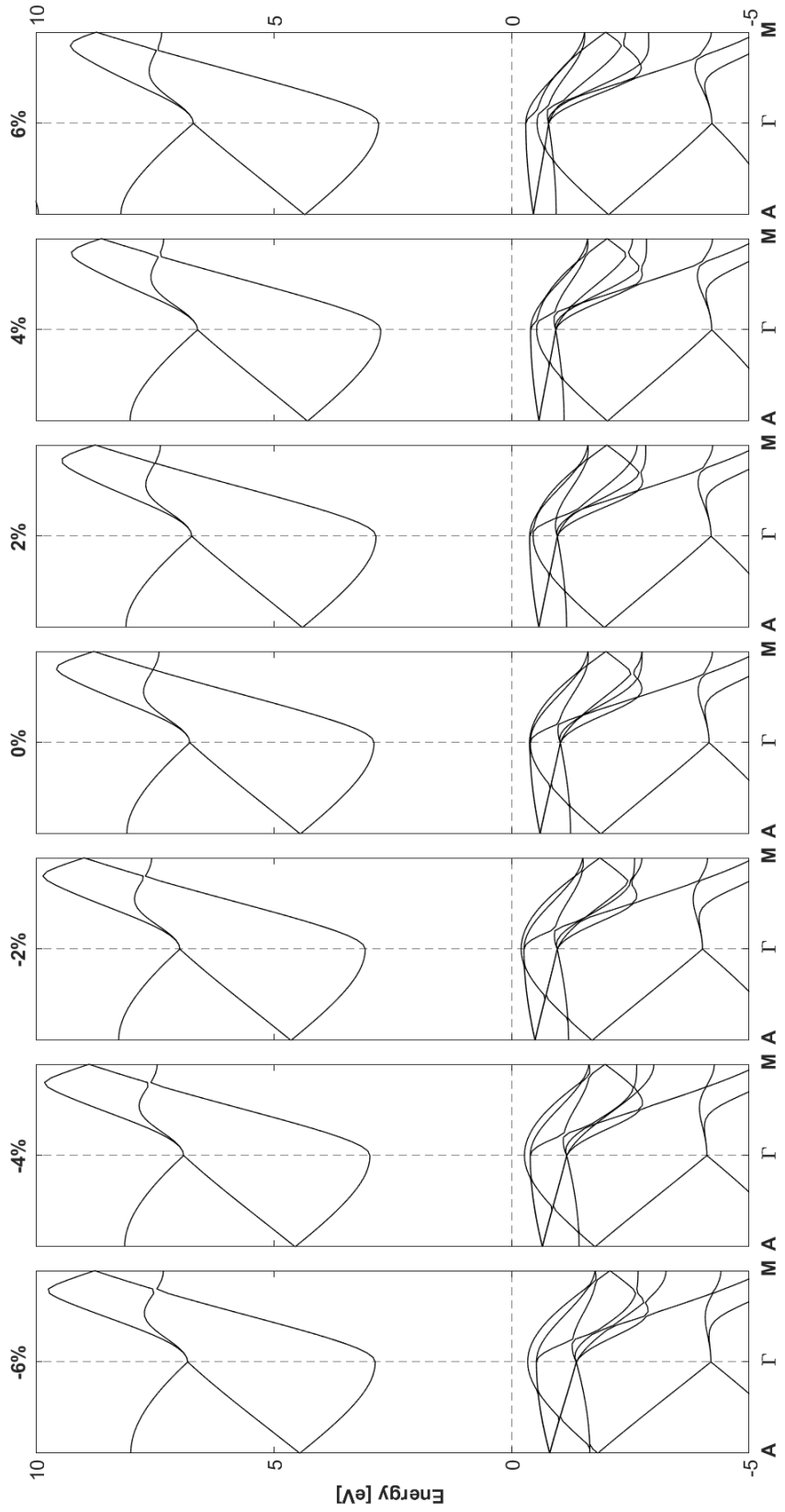

9.4.7 ZnS

WZ ZnS

ε	a (Å)	c (Å)	A_{VBM} (eV)	A_{CBM} (eV)	Γ_{VBM} (eV)	Γ_{CBM} (eV)	M_{VBM} (eV)	M_{CBM} (eV)
-10%	3.940	5.673	-1.255	4.621	-0.317	3.558	-1.146	4.264
-8%	3.919	5.799	-1.055	4.786	-0.205	3.786	-1.073	4.521
-6%	3.892	5.925	-0.996	4.832	-0.244	3.745	-1.140	4.635
-4%	3.869	6.051	-0.870	4.948	-0.228	3.752	-1.127	4.811
-2%	3.849	6.177	-0.797	5.006	-0.256	3.684	-1.157	4.926
0	3.845	6.303	-0.832	4.919	-0.343	3.465	-1.264	4.923
2%	3.818	6.429	-0.651	5.108	-0.209	3.501	-1.180	5.144
4%	3.798	6.555	-0.673	5.071	-0.275	3.306	-1.283	5.154
6%	3.785	6.681	-0.644	5.062	-0.286	3.147	-1.319	5.209

ZB-(111) ZnS

ε	a (Å)	c (Å)	A_{VBM} (eV)	A_{CBM} (eV)	Γ_{VBM} (eV)	Γ_{CBM} (eV)	M_{VBM} (eV)	M_{CBM} (eV)
-6%	3.895	8.823	-1.054	3.901	-0.343	3.233	-2.115	3.954
-4%	3.879	9.011	-0.806	4.328	-0.326	3.418	-1.804	4.297
-2%	3.856	9.199	-0.724	4.498	-0.349	3.432	-1.760	4.380
0	3.832	9.386	-0.508	4.697	-0.244	3.562	-1.580	4.569
2%	3.822	9.574	-0.478	4.659	-0.246	3.458	-1.564	4.567
4%	3.804	9.762	-0.497	4.582	-0.290	3.307	-1.610	4.480
6%	3.790	9.950	-0.431	4.566	-0.245	3.222	-1.563	4.471

WZ ZnS

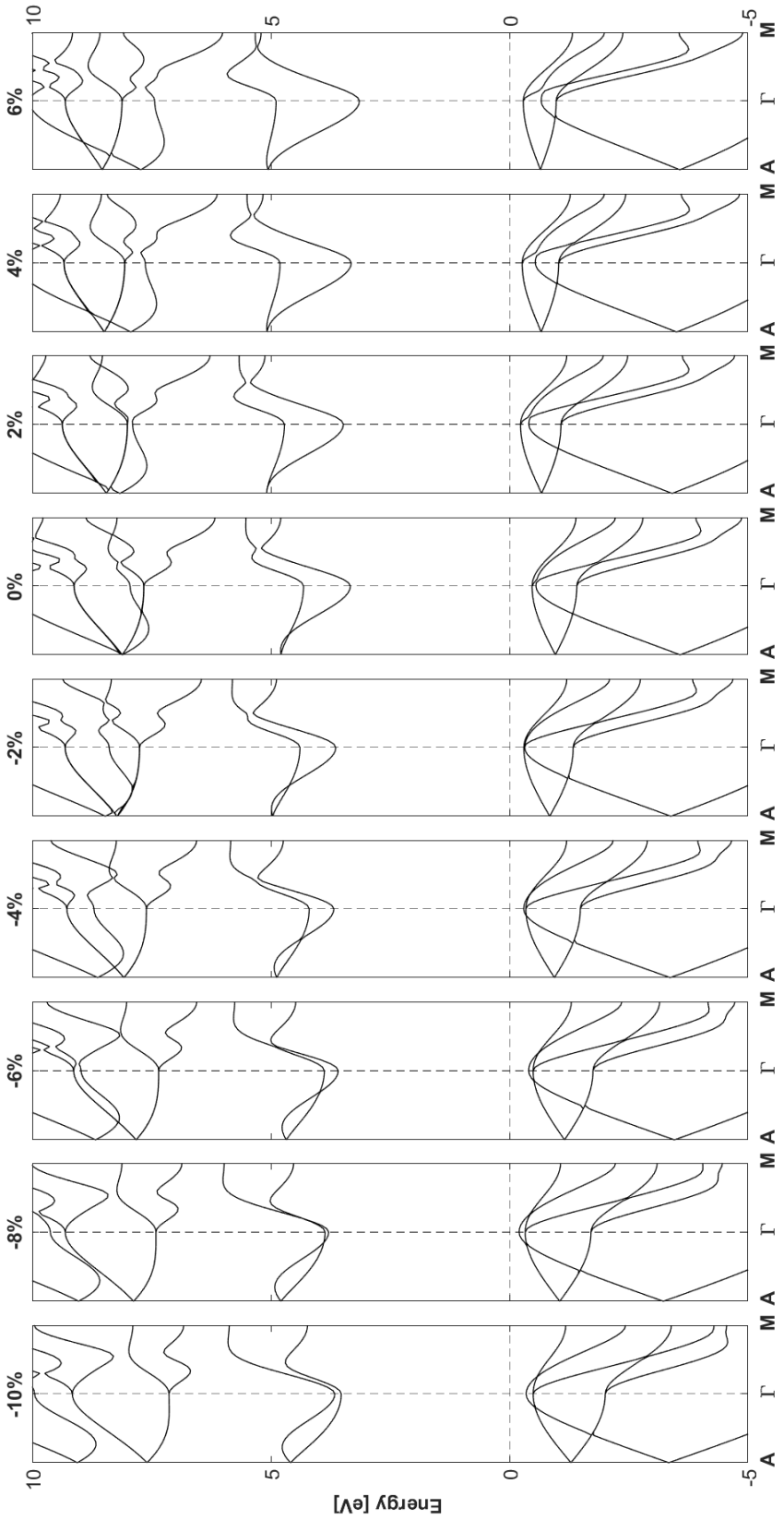

ZB-(111) ZnS